Dynamics, Noise Properties, and Spectral Characteristics of Semiconductor Lasers with External Coupling

Thesis By

Lun-Tseng Lu

In Partial Fulfillment of the Requirements

for the Degree of

Doctor of Philosophy

California Institute of Technology

Pasadena, California

1989

(Submitted August 1, 1988)

©1989

Lun-Tseng Lu

All Rights Reserved

This thesis is dedicated

to my mother

and

to the memory of my father

Acknowledgements

I would like to thank my advisor, Professor Amnon Yariv, for his encouragement and support. His extraordinary scientific intuition has been a source of inspiration. To be a member of his quantum electronics group and to have the use of his super facilities have made my stay at Caltech an invaluable experience.

Many thanks go to Desmond Armstrong for his technical assistance, to my fellow students for their friendship, and to Jana Mecado for her administrative help. My appreciation goes also to Professor Yuk L. Yung for his friendship and to Mr. Koichi Sayano for his careful reading of this thesis.

I also wish to acknowledge the following people for discussions and collaborations in areas not treated in this thesis. Colloborations with Professor M. B. Yi, Drs. S. Margalit, E. Kapon, Z. Rav-Noy, S. Mukai, K. Lau, and H. Blauvelt contributed to my graduate work in the area of InP/InGaAsP optoelectronic devices. Discussions with Dr. S. Mukai on the crystal growth and device fabrications have been very fruitful. I am also indebted to Dr. K.-L. Yu who introduced me to the fields of liquid phase epitaxial crystal growth and device fabrications and to Dr. Nadav Bar-Chaim of Ortel Corporation for his generosity of providing the diode lasers for the projects of experimental investigations.

Finally, I would like to express my appreciation to my brother Chung-Hsin for his constant encouragement. I am especially thankful to my wife Lily and my daughter Eunice for their constant support and love.

Abstract

This thesis is a study of the dynamics, noise properties, and linewidth of semiconductor lasers with external coupling. In Chapter 2, a general formalism is developed for obtaining the optical-field equations of semiconductor lasers with external coupling. This formalism is applied to three different types of semiconductor lasers: (1) a diode laser coupled to an external mirror, (2) an injection-locked diode laser, and (3) an axially coupled two-section diode laser. The resulting equations are the basis for the studies and discussions given in Chapters 3, 4, and 5.

The third chapter considers, using a small-signal analysis, a single-mode semiconducor laser coupled to an external mirror. Light trapped for many round trips inside the external cavity is taken into account. Analytical expressions for the frequency and relative-intensity fluctuation spectra, the laser linewidth and the small-signal current modulation response are obtained. The fundamental mechanism that prevents the mode locking in semiconductor lasers with an external feedback is identified. The observed data on the intensity noise and the current modulation response are elucidated.

An injection-locked semiconductor laser is studied in Chapter 4. The origin and importance of the facet's amplitude reflectivities are described. The instability occurring in the high-frequency side of the locked range is fully explored. A detailed study of the locking bandwidth is presented. It is shown that, depending on the detuning of the lasing frequency, the relative-intensity noise can be reduced or increased. It is also demonstrated on a general basis that the locked laser linewidth is the same as that of the injected field.

The dynamics and laser linewidth of an axially coupled two-section semicon-

ductor laser are scrutinized in the last chapter. The relative-intensity and frequency fluctuation spectra can be obtained from the results given in this chapter. A formula is obtained for the laser linewidth. This formula explains the experimental observations that the linewidth is nearly inversely proportional to the power with a nonzero intercept. Finally, the contribution to the reduction in dynamic frequency chirping of two-section lasers is clarified.

Table of Contents

Acknowledgements iv

Abstract v

Table of Contents vii

List of Figures x

Chapter 1 Introduction

1.1 Why Semiconductor Lasers with External Coupling 1

1.2 Outline of the Thesis 11

References 14

Chapter 2 Optical-Field Equation for Semiconductor Lasers with External Coupling

2.1 Introduction 17

2.2 Effective Mirror 19

2.3 General Theory 24

2.3-A. The Optical-Field Equation of Solitary Diode Lasers 24

2.3-B. Effective Photon Lifetime $\tau_{eff}(t)$ 27

2.3-C. Spatial Mode Expansions of the Optical Field Inside Cavities Formed by One Facet Mirror and One Effective Mirror 29

2.3-D. Relation Between $\tau_p^{eff}(t)$ *and* $r_{eff}(t)$ 40

2.3-E. Steady-State Characteristics 42

2.4 Application of the Theory 43

2.4-A. A Diode Laser Coupled to An External Mirror 44

2.4-B. An Injection-Locked Diode Laser 45

2.4-C. An Axially Coupled Two-Section Diode Laser 49

2.5 Conclusion 53

References 54

Chapter 3 Dynamics, Noise Properties, and Linewidth of Single-Mode Semiconductor Lasers Coupled to an External Mirror

3.1 Introduction 55

3.2 Small-Signal Equations for the Optical Field and Carrier Density 57

3.3 Relative-Intensity and Frequency Fluctuation Spectra 64

3.4 Laser Linewidth 74

3.5 Small-Signal Current Modulation Response 78

3.6 Conclusion 80

References 83

Chapter 4 Instability, Locking Bandwidth, Noise Properties, and Linewidth of Injection-Locked Semiconductor Lasers

4.1 Introduction 85

4.2 Small-Signal Equations for the Optical Field and Carrier Density 87

4.3 $1/r_2$, Locking Bandwidth and Instability 92

4.3-A. Origin of the Factor $1/r_2$ 92

4.3-B. The Maximum Locking Range and $1/r_2$ 93

4.3-C. Locking Bandwidth and Instability 98

4.4 Frequency and Relative-Intensity Fluctuation Spectra 110

4.5 Linewidth of the Injection-Locked Laser 117

4.6 Conclusion 120

Appendix 121

References 127

Chapter 5 Dynamics and Linewidth of Axially Coupled Two-Section Semiconductor Lasers

5.1 Introduction 130

5.2 Small-Signal Equations for the Optical Fields and the Carrier Densities 132

5.3 Relative-Intensity and Frequency Fluctuation Spectra 140

5.4 Laser Linewidth 146

5.5 Small-Signal Current Modulation Response and Frequency Chirping 153

5.6 Conclusion 161

References 163

List of Figures

Figure 1.1 2

Band gap and lattice constant for $In_{1-x}Ga_xAs_{1-y}P_y$.

Figure 1.2 3

Measured loss in a single-mode silica fiber as a function of wavelength.

Figure 1.3 4

Measured material dispersion for typical single-mode silica fibers.

Figure 1.4 7

Schematic cross section of a surface-emitting laser.

Figure 1.5 9

Theoretical curves of the maximum transmission bandwidth of a conventional single-mode fiber 100-km long.

Figure 1.6 10

Block diagram of an optical transmitter.

Figure 2.1 20

(a) Schematic of a semiconductor laser with an external coupling. (b) The composite laser is equivalent to a diode laser with an effective mirror.

Figure 2.2 23

(a) Schematic of a single-mode semiconductor laser coupled to an external mirror. (b) A single-mode semiconductor laser coupled to an external mirror is equivalent to a diode laser with an effective mirror.

Figure 2.3 31

Optical field spectrum of a semiconductor laser with an external coupling.

Figure 2.4 46

(a) Schematic of an in-jection-locked semiconductor laser. (b) An injection-locked semiconductor laser is equivalent to a diode laser with an effective mirror.

Figure 2.5 48

(a) Schematic of an axially coupled two-section semiconductor laser. (b) Each cavity of the two-section semiconductor laser is equivalent to a diode laser with an effective mirror.

Figure 3.1 59

(a) Schematic of a single-mode semiconductor laser coupled to an external mirror. (b) A single-mode semiconductor laser coupled to an external mirror is equivalent to a diode laser with an effective mirror.

Figure 3.2 71

(a) The calculated relative-intensity noise spectrum at $p_o = 1\times10^{14}\text{cm}^{-3}$; (b) The experimental intensity noise spectrum of Temkin et al.

Figure 3.3 73

(a) The calculated first-harmonic frequency of the relative-intensity noise spectra versus photon density p_o inside the active region; (b) The experimental results on the biased current dependence of the first harmonic of the high- and the low- frequency noise components.

Figure 3.4 81

(a) Small-signal modulation response of a window BH on SI laser; (b) The simulated small-signal modulation response A_{mod} for different r_3.

Figure 4.1 88

(a) Schematic of an injection-locked semiconductor laser. (b) The injection-locked semiconductor laser is equivalent to a solitary laser with one of its two facet mirrors replaced by an effective mirror which has a time-dependent effective reflectivity $r_{eff}(t)$.

Figure 4.2 95

Schematic representation of the injection-locking mechanism.

Figure 4.3 103

The locked phase ϕ_o versus $(t_2/r_2)^2 I_{in,o}/I_o$.

Figure 4.4 104

The locking bandwidth versus $(t_2/r_2)^2 I_{in,o}/I_o$.

Figure 4.5 107

(a) The calculated locking bandwidth versus $(t_2/r_2)^2 I_{in,o}/I_o$. (b) The experimental results of the locking bandwidth versus $(t_2/r_2)^2 I_{in,o}/I_o$ by Goldberg et al.

Figure 4.6 115

Relative-intensity noise spectra for different values of frequency detuning.

Figure 4.7 116

Relative-intensity noise spectra for different values of frequency detuning.

Figure 4.8 119

Free-running and injection-locked linewidth versus reciprocal output power.

Figure 5.1 133

(a) Schematic of an axially coupled two-section semiconductor laser. (b) Each cavity of the two-section semiconductor laser is equivalent to a diode laser with an effective mirror.

Figure 5.2 139

(a) Calculated light-current characteristics of two-section lasers when the right section is pumped and the other section is passive. (b) Light-current characteristics measured from each side of a cleaved-couple-cavity laser fabricated from 1.3 μm wavelength InP/InGaAsP crescent laser wafer when the right section is pumped.

Figure 5.3 141

(a) Calculated light-current characteristics of two-section lasers when the right section is pumped and the other section is biased at different current levels. (b) Light-current characteristics measured from the right side of a cleaved-couple-cavity laser fabricated from 1.5 μm wavelength InP/InGaAsP crescent laser wafer when the left section is pumped and the right section is biased at different current levels.

Figure 5.4 151

(a) Two different current paths used in calculating the linewidth of a two-section laser. (b) Calculated laser linewidth as a function of reciprocal photon number $(p_1 V_1)^{-1}$ for two different current paths shown in (a).

Figure 5.5 152

(a) Constant-power contours (solid lines) and mode-hopping boundaries (dotted line) for a C^3 laser. (b) Linewidth against inverse power for two distinct modes as indicated in (a).

Figure 5.6 158

(a) Calculated wavelength chirpings as a function of the modulation current at 100 MHz for 1.3 μm lasers. (b) Measured wavelength chirpings vs modulation current at 100 MHz for 1.3 and 1.55 μm lasers.

Figure 5.7 159

Calculated chirping ratio $\Delta\Omega/(\Delta\Omega)_{sl}$ as a function of the coupling strength t_{21}/r_{11}.

Figure 5.8 160

Calculated chirping ratio $\Delta\Omega/(\Delta\Omega)_{sl}$ as a function of the coupling strength t_{21}/r_{11} with $p_{1o} = p_{2o} = 1 \times 10^{14} cm^{-3}$.

Chapter 1

Introduction

1.1 Why Semiconductor Lasers with External Coupling?

The semiconductor diode laser was invented twenty six years ago. Since then, through continuous, extensive, and interdisciplinary efforts around the world, the properties of the laser have been greatly improved.

By adjusting the composition of the semiconductor crystal, scientists and engineers are able to make semiconductor lasers emit in the region from visible to near infrared (Figure 1.1). Two major material systems have dominated research activities. The GaAs/GaAlAs system with a lasing wavelength from 0.7 μm to 0.9 μm was the first to be developed and the first to mature in the semiconductor laser industry. The lasers grown in the InP/InGaAsP system emit light in the wavelength range from 1.1 μm to 1.7 μm. Because modern optical fibers exhibit low loss and minimal material dispersion in this range (Figures 1.2 and 1.3), the second system has been studied more intensively than the GaAs/GaAlAs system in past years.

The characteristics of common semiconductor lasers are given below. With a junction turn on voltage of 1.4 volts, the threshold current is 15 mA. The size of the active region is $3.0\mu m \times 0.2\mu m \times 300\mu m$. The cavity formed by the two facet mirrors on each side is 300 μm long. The output power is 5-10 mW. Single devices with CW powers up to 100 mW are commercially available. Extrapolated room-temperature lifetime is in excess of 10^7 hours. By modulating the pumping current, the light output of the laser can be modulated at frequencies beyond 10 GHz [4].

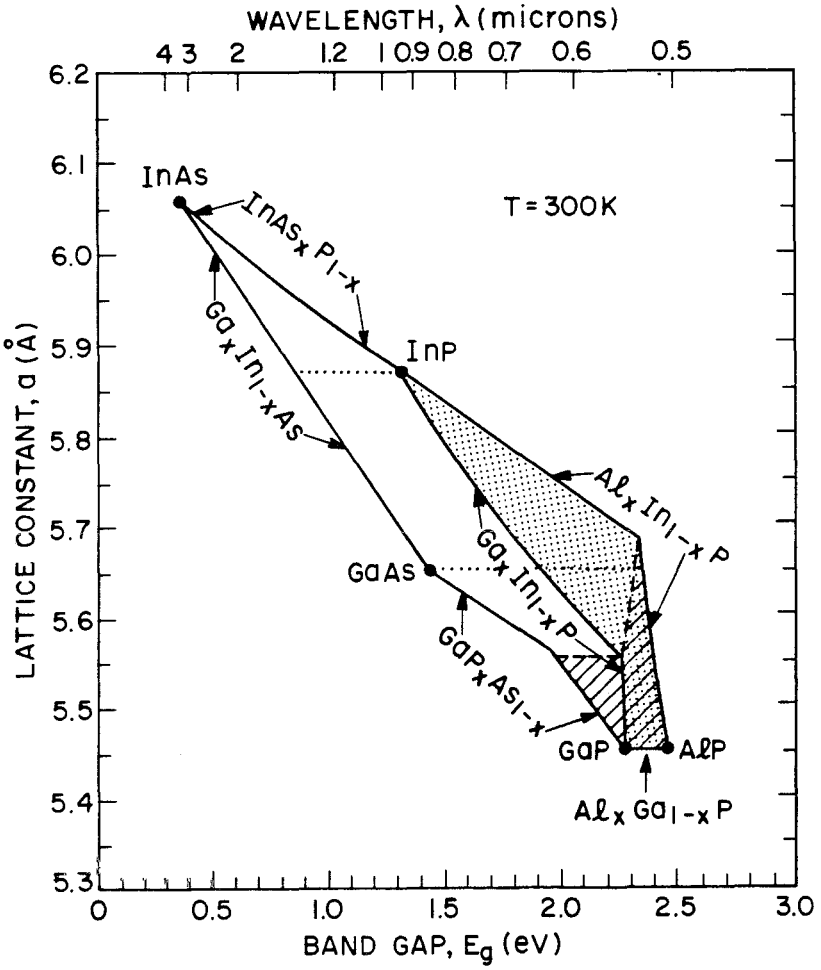

Figure 1.1 Band gap and lattice constant for $In_{1-x}Ga_xAs_{1-y}P_y$ (clear region) and $(Al_xGa_{1-x})_yIn_{1-y}P$ (shaded regions) obtained by varying compositions x and y. Dashed lines separate indirect-band-gap regions (shown hatched). Dotted lines show the wavelength range (top scale) for a semiconductor laser, whose quaternary active layer is lattice-matched to the binary compound. [1]

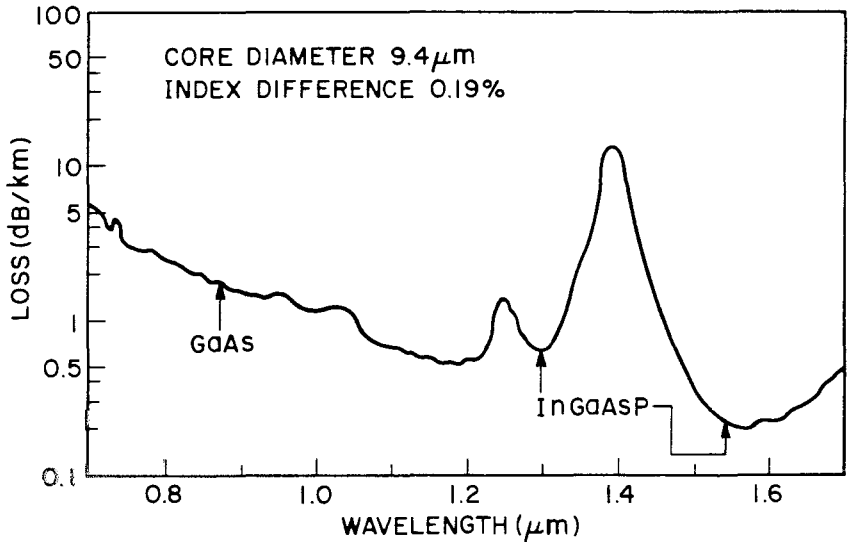

Figure 1.2 Measured loss in a single-mode silica fiber as a function of wavelength. Arrows indicate wavelength regions used for optical fiber communications. Minimum loss occurs around the 1.55 μm wavelength. [2]

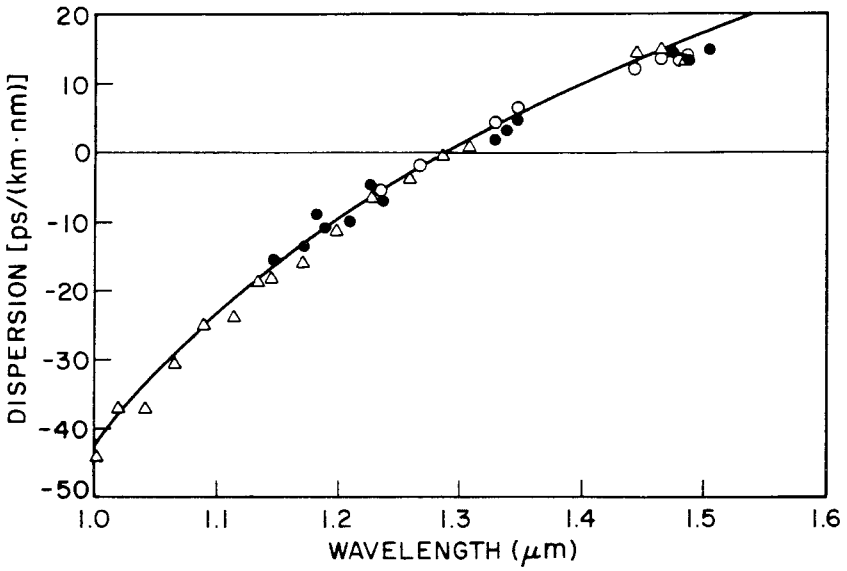

Figure 1.3 Measured material dispersion for typical single-mode silica fibers. Data points for three fibers are shown. [3]

Because of its small size, high efficiency, low cost, long life, high reliability, low power consumption, and versatility in performance, the laser plays an important role in modern technology. In the past years, millions of semiconductor lasers have been used in optical communication systems, laser scanning printers, compact audio disks, and many other applications.

Many books give comprehensive coverage to the fundamentals of semiconductor lasers [1] [2] [5] [6] [7]. In this thesis, a basic familiarity with this topic is assumed.

Because of the carrier density dependence of the refractive index in the active region, there is a strong coupling between intensity and phase of the optical field. A variation in intensity will change the carrier density, which, in turn, will change the phase. This coupling results in an enhancement of the linewidth broadening caused by spontaneous emission events. Thus, the conventional diode laser has an excessively large linewidth on the order of 10 MHz. Through the same effect, a single longitudinal mode laser under direct current modulation displays phase modulation and may have multilongitudinal modes. These make the conventional laser unsuitable for many important applications.

Nevertheless, the demand for semiconductor lasers with special qualities at lower cost is increasing. For example, many fiber-optical sensors require a laser source with narrow linewidth and stable phase. Optical communication systems require lasers which, under pulsed current pumping, have fast response, small dynamic frequency chirping, single mode with large side mode suppression, narrow linewidth, and low power fluctuation noise.

Consequently, the search for high-quality lasers is going on. It can be roughly divided into two directions. The first is to invent and fabricate solitary lasers

with specific properties. The efforts involved include growing high-quality crystals, inventing new structures, and improving the production yield with innovative chemical processing techniques. All these require the collaboration of scientists and engineers from all scientific disciplines. In the following, some of the important advances made in this direction will be highlighted.

A conventional semiconductor laser has two cleaved facets and its light is emitted parallel to the surface of the wafer. For integrated optoelectronic circuits, conventional lasers are not appropriate, and lasers with output normal to the wafer surface are highly desired. Figure 1.4 shows the schematic cross section of a surface emitting laser fabricated by Soda et al. [8].

The typical thickness of the active region in a conventional laser is 0.2 μm. By using the chemical vapor deposition technique or molecular-beam-epitaxy technique, lasers with one or more thin active layer regions with thickness comparable to the carrier de Broglie wavelength have been grown. Electrons confined in the thin layer exhibit the quantum effect. Laser with such thin active regions are called quantum well lasers. When compared to conventional lasers, the reduction of the CW linewidth was predicted [9] and demonstrated [10].

The second direction employs different methods to couple light externally to the solitary lasers. Through external coupling, the laser can be pushed to perform beyond its intrinsic limits. This will be clear after reviewing the following examples.

The typical linewidth of semiconductor lasers is on the order of 10 MHz. After coupling to an external mirror, a linewidth of 10 KHz was demonstrated [11]. Lasers with such high spectral purity will not only enable new applications but also improve existing ones. Many new kinds of optical fiber sensors can

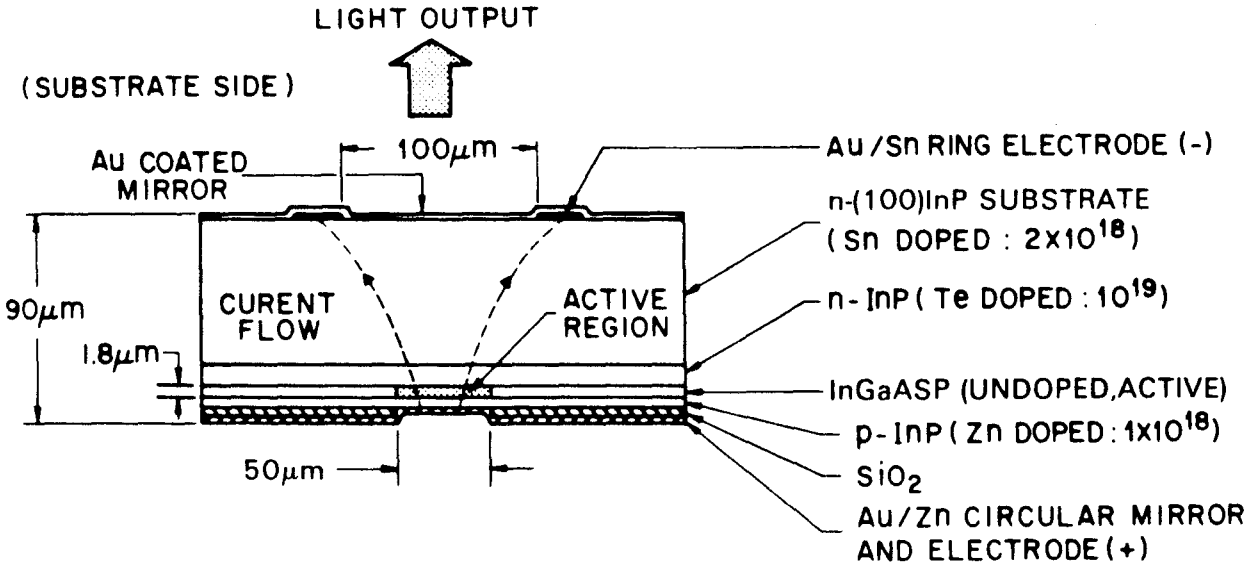

Figure 1.4 Schematic cross section of a surface-emitting laser. Surfaces of the wafer from the Fabry-Perot cavity. [8]

be developed, and the maximum transmission distance or the bandwidth of the signal in a light wave transmission system will increase substantially. For example, for a single-mode fiber lightwave channel of 100 km long, Figure 1.5 shows the maximum bit rates as a function of wavelength for sources of various linewidths $\Delta\lambda$. Figure 1.6 shows a block diagram of an optical transmitter.

The modulation bandwidth of solitary lasers is dictated by the photon lifetime, photon density and the differential optical gain constant [4]. This basic understanding has led to the development of advanced laser structures that can be directly modulated beyond 10 GHz [4]. On the other hand, Lau and Yariv [14] reported that the laser can be directly modulated in a narrow band with center frequency equal to twice its intrinsic modulation bandwidth. Laser transmitters operating at such high speeds will be ideal for transmitting microwave signals.

When the frequency difference between a solitary laser and an incident field falls in a certain locking bandwidth, the frequency of the solitary laser can be locked to the frequency of the incident field. In addition, locked by the narrow-linewidth injected field, the excessively large linewidth of solitary laser was reduced to that of the incident field [15]. In a coherent transmission system, injection locking may be used to synchronize the local oscillator [16].

From the examples given above, it is evident that the progress made in the second direction is as impressive as in the first one. Although both directions are equally important, this thesis will focus only on some important problems in the dynamics, noise properties, and spectral characteristics of semiconductor lasers with external coupling.

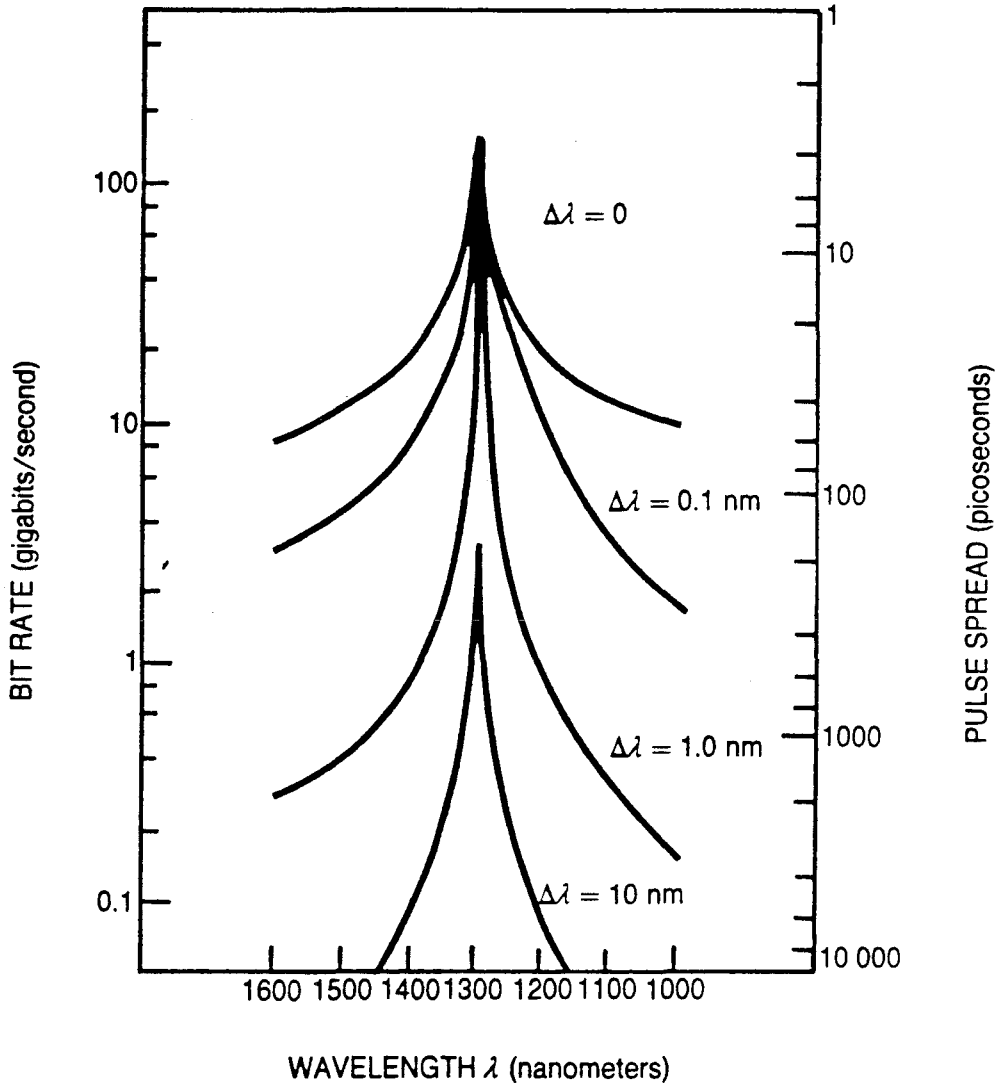

Figure 1.5 These theoretical curves show the maximum transmission bandwidth of a conventional single-mode fiber 100-km long. The four curves are for sources of different spectral widths $\Delta\lambda$. The fiber's dispersion minimum is at 1300 nm. [12]

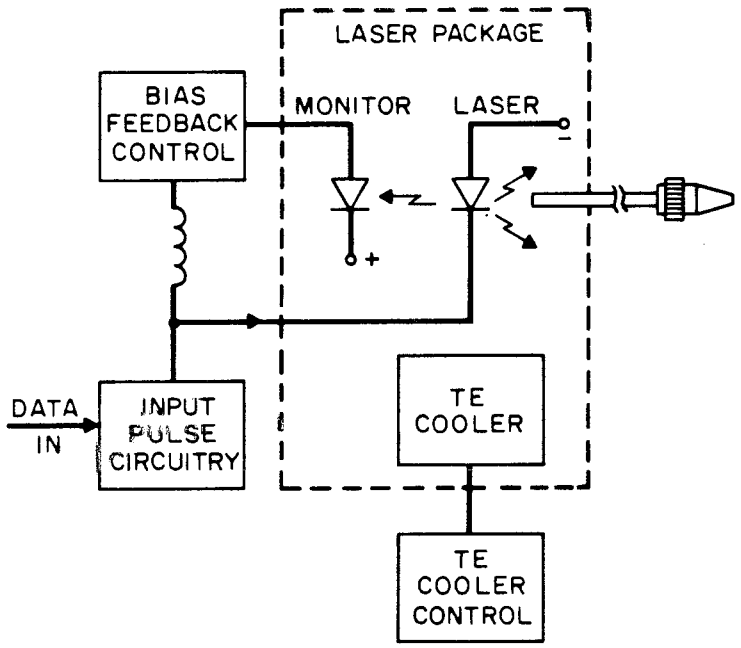

Figure 1.6 Block diagram of an optical transmitter. [13]

1.2 Outline of the Thesis

Many studies were devoted to the understanding of how the laser's properties were affected by the external coupling. In general, equations for the optical field and carrier density will be the basis for analysis and discussion. For each coupling scheme, the optical field equation was often derived heuristically [17] [18] or by using the mode expansions [19]. There has been a lack of a coherent and general approach to find the optical field equation. In addition, the optical field equations of References 17 and 19 have drawbacks and limitations. In Reference 17, the equation for lasers with external feedback is valid only under special conditions. In Reference 19, a set of coupled, first-order differential equations for two-section lasers are too complicated and difficult to apply.

Under these situations, it is essential to have a rigorous formalism for obtaining optical field equations. To this end, semiconductor lasers with external optical coupling through one of their two facet mirrors will be considered in Chapter 2. New concepts will be introduced and explained, and a general formalism will be developed directly from Maxwell's wave equation. This formalism will be applied to obtain optical field equations for semiconductor lasers coupled to an external mirror, injection-locked semiconductor lasers, and axially coupled two-section semiconductor lasers. After inspecting these equations, their major achievements will be described.

Since Chapter 2 will be devoted mainly to deriving the optical field equations for composite lasers, the importance and significance of the general formalism and these equations can be fully recognized only after detailed studies are carried out in all of the above mentioned three different types of lasers in Chapters 3, 4, and 5. Because the frequency and relative intensity fluctuation spectra, laser linewidth,

small-signal current modulation response, and dynamic frequency shift are major considerations in industrial applications and laboratory researches, these subjects will be the main concerns for each type of laser. The treatments on noise follow closely to that of Reference [20].

In Chapter 3, a single-mode semiconducor laser coupled to an external mirror will be considered. Light trapped for many round trips inside the external cavity will be taken into account. A method for obtaining the Lorentzian linewidth will be established in Chapter 3. This method will be employed to derive linewidth formulas in this chapter and Chapters 4 and 5. For lasers with external feedback, the modulation response reported by Lau and Yariv [14] and the intensity noise data of Temkin et al. [21] will be examined. The fundamental limiting mechanism in the mode-locking phenomena will be clarified.

In Chapter 4, the importance of diode-facet amplitude reflectivity of an injection-locked diode laser will be emphasized. Analytical expressions will be derived to describe the instability condition and stability locking bandwidth. The key role played by the linewidth enhancement factor in the instability nature of injection-locked lasers will be explained. The possible increase of the laser noise by a noise-free, injected field will be described. It will be shown, on a general basis, that the linewidth is dictated by that of the injected field. In the appendix to this chapter, an important and as yet unexplored aspect of the linewidth enhancement factor will be clarified.

Finally, in Chapter 5, an axially coupled two-section diode laser will be considered. The steady-state current-light characteristic will first be studied. The linewidth behavior will be investigated. The reduction of dynamic frequency chirping of this laser will be explained.

Results obtained in other areas, not covered in this thesis, are presented in [22], [23], [24], [25], [26], and [27].

References

[1] H. C. Casey and M. B. Panish, *Heterostructure Lasers*, Academic Press, New York, 1978.

[2] G. P. Agrawal and N. K. Dutta, *Long-wavelength Semicondutor Lasers*, Nan Nostrand Reinhold Company, New York, 1986.

[3] A. Sugimura, K. Daikoku, N. Imoto, and T. Miya, *IEEE J. Quantum Electron.*, **QE-16**, 215, 1980.

[4] For a review, see K. Y. Lau and A. Yariv, *IEEE J. Quantum Electron.*, **21**, 121, 1985.

[5] H. Kressel and J. K. Butler, *Semiconductor Lasers and Heterojunction LEDs*, Academic Press, New York, 1977.

[6] G.H.B. Thompson, *Physics of Semiconductor Laser Devices*, John Wiley and Sons, Chichester, England, 1980.

[7] W. T. Tsang, ed., *Semiconductor Injection Lasers, I, Semiconductors and Semi-metals*, **vol. 22**, Part B, Academic Press, New York, 1985.

[8] H. Soda, K. Iga, C. Kitahara, and Y. Suematsu, *Jpn. J. Appl. Phys.* **18**, 2329, 1979.

[9] Y. Arakawa and A. Yariv, *IEEE J. Quantum Electron.*, **QE-21**, 1666, 1985.

[10] P. L. Derry, T. R. Chen, Y. H. Zhuang, J. Paslaski, M. Mittelstein, K. Vahala, and A. Yariv, "Spectral and dynamic characteristics of buried heterostructure single quantum well (Al, Ga)As lasers," unpublished.

[11] R. Wyatt and W. J. Devlin, *Electron. Lett.*, **19**, 110, 1983.

[12] T. Li, *Phys. Today*, **38**, 24, 1985.

[13] J. J. Mcnulty, In *Undersea Lightwave Communications* (P. K. Runge and P. R. Trischitta, editors), Chapter 11, IEEE Press, New York, 1986.

[14] K. Y. Lau and A. Yariv, *Appl. Phys. Lett.*, **46**, 326, 1985.

[15] P. Gallion, H. Nakajima, G. Debarge, and C. Chabran, *Electron. Lett.*, **21**, 626, 1985.

[16] Y. Yamamoto, T. Kimura, *IEEE J. Quantum Electron.*, **QE-17**, 919, 1981.

[17] R. Lang and K. Kobayashi, *IEEE J. Quantum Electron.*, **QE-16**, 347, 1980.

[18] R. Lang, *IEEE J. Quantum Electron.*, **QE-18**, 976, 1980.

[19] D. Marcuse, *IEEE J. Quantum Electron.*, **QE-21**, 1819, 1985.

[20] K. Vahala and A. Yariv, *IEEE J. Quantum Electron.*, **QE-19**, 1102, 1983.

[21] H. Temkin, N. A. Olsson, J. H. Abeles, R. A. Logan, and M. B. Panish, *IEEE J. Quantum Electron.*, **QE-22**, 286, 1986.

[22] Z. Rav-Noy, L.-T. Lu, E. Kapon, S. Mukai, S. Margalit, and A. Yariv, *Appl. Phys. Lett.*, **45**, 258, 1984.

[23] E. Kapon, Z. Rav-Noy, L.-T. Lu, M. Yi, S. Margalit, and A. Yariv, *Appl. Phys. Lett.*, **45**, 1159, 1984.

[24] E. Kapon, L.-T. Lu, Z. Rav-Noy, M. Yi, S. Margalit, and A. Yariv, *Appl. Phys. Lett.*, **46**, 136, 1985.

[25] M. B. Yi, L.-T. Lu, E. Kapon, Z. Rav-Noy, S. Margalit, and A. Yariv, *Appl. Phys. Lett.*, **46**, 328, 1985.

[26] M. B. Yi, J. Paslaski, L.-T. Lu, S. Margalit, A. Yariv, H. Blauvelt, and K. Lau, *J. Appl. Phys.*, **58**, 4730, 1985.

[27] L.-T. Lu and A. Yariv, "Large signal analysis of mode-hopping phenomena in semiconductor lasers," unpublished.

Chapter 2

Optical-Field Equation for Semiconductor Lasers with External Coupling

2.1 Introduction

As discussed in Chapter 1, the performance of diode lasers can be improved substantially by external feedback, external light injection, or coupling with other external resonant cavities. Because of their great potential in pratical applications, these three types of lasers have attracted considerable attention.

The fundamental problem in analyzing the externally coupled laser is developing the time-dependent optical-field equation, and several approaches have been used in the past. In one of these, the optical-field equation is obtained heuristically [1] [2], while another approach is based on modal expansions [3]. The modal-expansion approach is based on either the longitudinal modes of the composite resonator or the modes of the individual cavities. However, lasers with different coupling schemes were treated differently, and there has been a lack of a general and coherent treatment for solving this fundamental and important problem.

Furthermore, the equations derived in References 1 and 3 have drawbacks and limitations. For lasers coupled to an external mirror, the light with multi-reflection in the external cavity is not included in the optical-field equation which was introduced by Lang and Kobayashi [1] and which has been widely adopted. This equation is valid only in the weak external-feedback regime. Since many

interesting and important characteristics were observed in the strong external-feedback regime, the multiple reflections from the external mirror can no longer be overlooked. An optical-field equation that takes into account the strong external feedback is a prerequisite for further exploration. For the case of two coupled resonant cavities, because of the lack of the appropriate optical-field equations, their dynamic characteristics such as laser linewidth remain unclear. The coupled mode theory of Marcuse [3], for example, requires the evaluation of the coupling coefficients, which is difficult or impossible to carry out.

Under these circumstances, it is highly desirable to have a unified theory for semiconductor lasers with external coupling, and through the applications of this theory, the appropriate optical-field equations can be obtained. To fulfill this need, this chapter will be presented in the following way.

Two new concepts, the time-dependent effective amplitude reflectivity and the time-dependent effective photon lifetime, will be introduced first. The concept of time-dependent effective amplitude reflectivity will be based on physical arguments. After reviewing the semiclassical laser theory [4], another new and important concept, the complex, time-dependent photon lifetime will be introduced in Section 2.3-B. To account for this effective photon lifetime, a time-dependent effective conductivity will be included in Maxwell's wave equation. Based on modal expansion in terms of the composite cavity modes, the general optical-field equation will be derived directly from Maxwell's wave equation in Section 2.3-C.

The time-dependent effective photon lifetime, which describes the effects of external coupling, will be expressed as a function of the time-dependent effective reflectivity. In developing the general theory, the crucial role played by both

effective reflectivity and effective photon lifetime will become clear at the end of Section 2.3-D. In Section 2.3-E, it will be shown that the newly derived general optical-field equation gives the oscillation condition of Reference 5, and in the limit of no external coupling, is reduced to the well-known optical-field equation of solitary semiconductor lasers [4]. At the end of Section 2.3-E, this theory will be established with all of its key ingredients.

In Section 2.4, this theory will be applied to lasers with specific external coupling. Lasers considered will be injection-locked diode lasers, axially coupled two-section lasers, and lasers coupled to an external mirror. After inspecting these equations, the major achievements of these equations as compared to those derived by different approaches will be given. Because this chapter will be devoted mainly to deriving the optical-field equations for composite lasers, the analysis for special cases will start with Chapter 3.

2.2 Effective Mirror

In the following sections, lasers with external coupling will be referred to as composite lasers and their cavities as composite cavities. The schematic representation of the composite laser is shown in Figure 2.1a, where l is the cavity length of the solitary diode laser. The constants r_1 and r_2 denote the amplitude reflectivities of the two facet mirrors. As shown in Figure 2.1b, a semiconductor diode laser with external coupling is equivalent to a solitary semiconductor laser with its original facet mirror, facing the external coupling, replaced by an effective mirror. The amplitude reflectivity of this effective mirror is designated as $r_{eff}(t)$.

Koch and Coldren [6] used an effective mirror formalism to study the mode

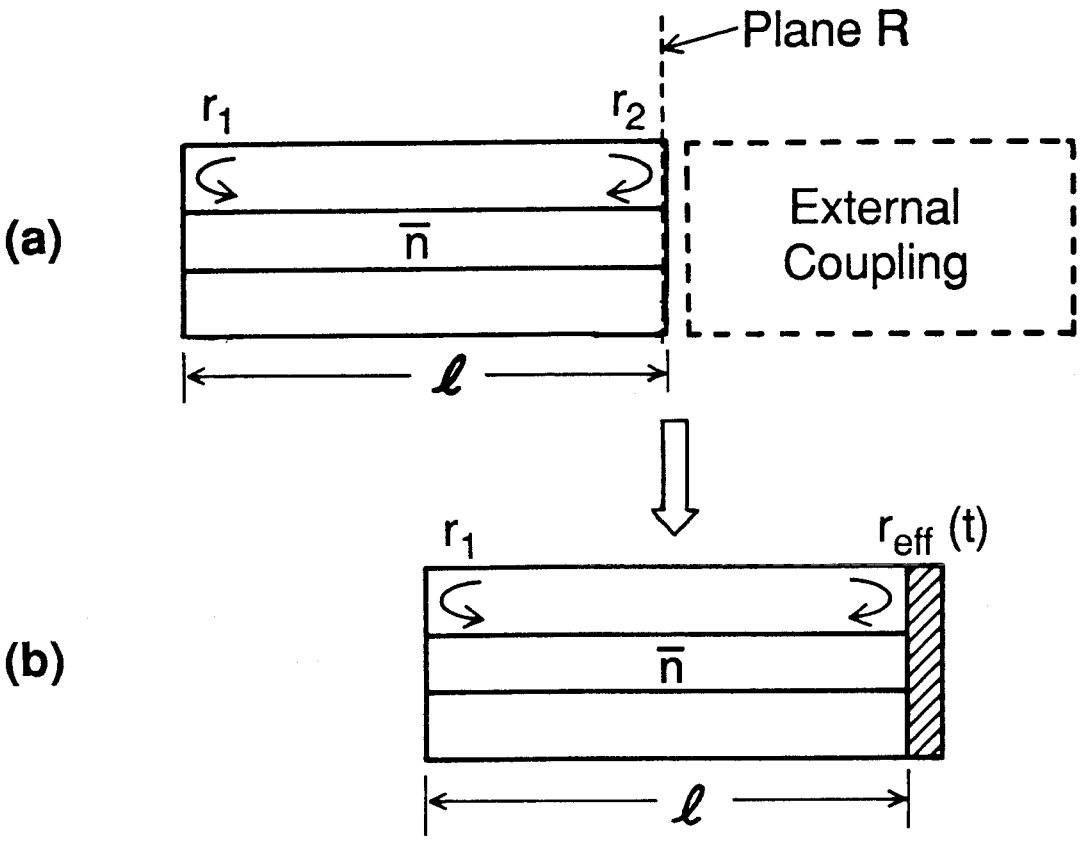

Figure 2.1 (a) Schematic of a semiconductor laser with an external coupling. The laser is called the composite laser and its cavity is called composite cavity. (b) The composite laser is equivalent to a diode laser with an effective mirror.

behavior in coupled-cavity semiconductor lasers. But their formalism is valid only in the steady-state regime. The effective mirror introduced in this section can be applied to any kind of external coupling, and its effective reflectivity $r_{eff}(t)$ is time-dependent. Later, it will be shown that this time-dependent $r_{eff}(t)$ plays an important role in both dynamic and steady-state characteristics of semiconductor lasers with external coupling.

Next, the $r_{eff}(t)$ will be defined and derived for a laser coupled to an external mirror. Because of the popularity and simplicity of this laser, its $r_{eff}(t)$ will provide a good and concrete example of the abstract concept of time-dependent effective reflectivity.

In the semiclassical theory [4] of solitary semiconductor lasers, the average optical field inside the diode cavity is $E(t)e^{i\Omega_m t}$, where Ω_m is the average lasing frequency, and the time evolution of $E(t)e^{i\Omega_m t}$ is governed by an optical-field equation. In this chapter, it is assumed that these features can also be applied to semiconductor lasers with external coupling. On the other hand, at any point inside this resonator, the optical field has two counterpropagating components. For lasers with an effective mirror (Figure 2.1b), when the field travelling from the left at plane R is $E_i(t)e^{i\Omega_m t}$ and the total field travelling to the left at plane R is $E_r(t)e^{i\Omega_m t}$, the effective reflectivity of this effective mirror is defined as

$$r_{eff}(t) = \frac{E_r(t)}{E_i(t)}. \tag{2.1}$$

Assuming that $E_i(t)e^{i\Omega_m t}$ is linearly proportional to $E(t)e^{i\Omega_m t}$, i.e.,

$$E_i(t)e^{i\Omega_m t} = aE(t)e^{i\Omega_m t}, \tag{2.2}$$

according to Equation (2.1), one obtains

$$E_r(t)e^{i\Omega_m t} = ar_{eff}(t)E(t)e^{i\Omega_m t}.$$

In other words, $E_r(t)e^{i\Omega_m t}$ is also linearly proportional to $E(t)e^{i\Omega_m t}$.

Equation (2.1) is a general statement for the $r_{eff}(t)$. Lasers with different external coupling will possess different $r_{eff}(t)$. Consider, for example, a diode laser coupled to an external mirror (Figures 2.2a and 2.2b). The incident wave from the left on the effective mirror is

$$E_i(t)e^{i\Omega_m t} = aE(t)e^{i\Omega_m t}, \tag{2.3a}$$

and the wave travelling to the left at the same plane is

$$\begin{aligned} E_r(t)e^{i\Omega_m t} =& ae^{i\Omega_m t} \\ &\times[r_2E(t) + r_3(1-r_2^2)e^{-i\Omega_m\tau}E(t-\tau) \\ &\quad - r_3(1-r_2^2)(r_2r_3)e^{-2i\Omega_m\tau}E(t-2\tau) \\ &\quad + r_3(1-r_2^2)(r_2r_3)^2e^{-3i\Omega_m\tau}E(t-3\tau) + \cdots], \end{aligned} \tag{2.3b}$$

where $\tau = 2L/c$ is the external-cavity round-trip time of the optical field. In arriving at (2.3b), it is assumed that a is time-independent. The amplitude reflectivity r_3 of the external mirror includes all coupling, absorption, and diffraction losses during each round trip in the external cavity. Substituting Equations (2.3a) and (2.3b) into (2.1) leads to

$$\begin{aligned} r_{eff}(t) = r_2 &+ r_3(1-r_2^2)e^{-i\Omega_m\tau}\frac{E(t-\tau)}{E(t)} \\ &- r_3(1-r_2^2)(r_2r_3)e^{-2i\Omega_m\tau}\frac{E(t-2\tau)}{E(t)} \\ &+ r_3(1-r_2^2)(r_2r_3)^2e^{-3i\Omega_m\tau}\frac{E(t-3\tau)}{E(t)} + \cdots. \end{aligned} \tag{2.3c}$$

For this laser, the optical-field round-trip time in the external cavity may be on the order of 10^{-9} sec. Lasers with modulation bandwidth 1 GHz or higher

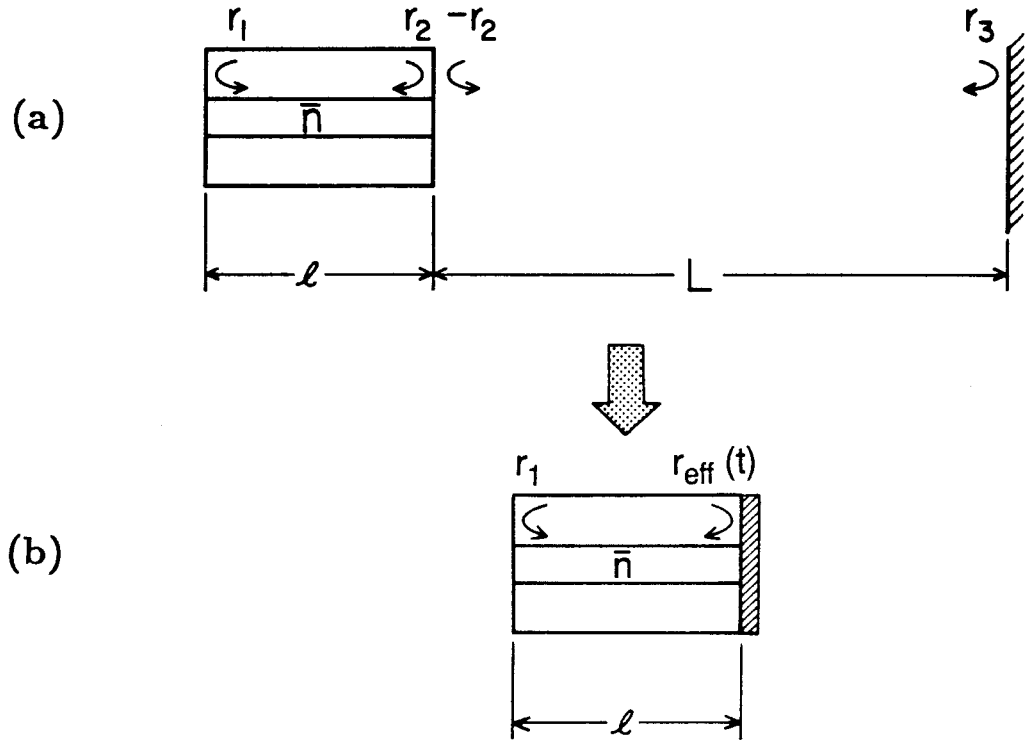

Figure 2.2 (a) Schematic of a single-mode semiconductor laser coupled to an external mirror. (b) A single-mode semiconductor laser coupled to an external mirror is equivalent to a diode laser with an effective mirror.

will show a strong time-dependence in terms such as

$$\frac{E(t-N\tau)}{E(t)} \qquad\qquad N=1,2,\cdots.$$

Since $r_{eff}(t)$ depends on these terms, it is obvious that a laser coupled to an external mirror has a time-dependent effective reflectivity. Therefore, in general, diode lasers with an effective mirror or external coupling have an instantaneous effective reflectivity $r_{eff}(t)$. More examples of diode lasers with time-dependent effective reflectivities will be given in Section 2.4.

2.3 General Theory

Before deriving the optical-field equation for the semiconductor laser with an effective mirror, the derivation of the solitary diode laser's optical-field equation will be reviewed briefly. This review will provide guidelines for the derivation presented later in Section 2.3-C. In addition, following the results of this review, the concept of the complex, time-dependent effective photon lifetime will be developed in Section 2.3-B.

2.3-A. The Optical Field Equation of Solitary Diode Lasers

Inside the resonator of solitary diode lasers, the optical field $\mathcal{E}(t)$ is given by

$$[\nabla^2-\kappa\sigma\frac{\partial}{\partial t}-\kappa\epsilon\frac{\partial^2}{\partial t^2}]\vec{\mathcal{E}}(\vec{r},t)=\kappa\frac{\partial^2}{\partial t^2}[\vec{P}(\vec{r},t)+\vec{p}(\vec{r},t)], \tag{2.4}$$

where κ is the magnetic permeability, σ is the medium conductivity accounting for the distributed waveguide losses and the losses through facet mirrors, ϵ is the nonresonant dielectric constant, $\vec{P}(\vec{r},t)$ is the induced polarization, and $\vec{p}(\vec{r},t)$ is the random component of polarization causing spontaneous emissions. The

resonator field quantities can be expanded in terms of any complete orthonormal set $\{\vec{e}_m(\vec{r})\}$:

$$\vec{\mathcal{E}}(\vec{r},t) = \sum_m \mathcal{E}_m(t)\vec{e}_m(\vec{r}) \tag{2.5a}$$

$$\vec{P}(\vec{r},t) = \sum_m P_m(t)\vec{e}_m(\vec{r}) \tag{2.5b}$$

$$\vec{p}(\vec{r},t) = \sum_m p_m(t)\vec{e}_m(\vec{r}), \tag{2.5c}$$

where $\vec{e}_m(\vec{r})$ will be chosen as the dimensionless eigenfunction of the mth spatial mode of the unpumped and lossless cavity. Accordingly, $\mathcal{E}_m(t)$ has the same dimensions as $\vec{\mathcal{E}}(\vec{r},t)$, and $P_m(t)$ and $p_m(t)$ have the same dimensions as $\vec{P}(\vec{r},t)$. The $\vec{e}_m(\vec{r})$ satisfy

$$\nabla^2\vec{e}_m(\vec{r}) + \kappa\epsilon\omega_m^2\vec{e}_m(\vec{r}) = 0 \tag{2.5d}$$

with appropriate boundary conditions of the resonator, and ω_m is the eigenfrequency of the mth mode $\vec{e}_m(\vec{r})$.

After substituting expansions (2.5a)-(2.5c) into Equation (2.4), using (2.5d), and employing the orthonormality of $\{\vec{e}_m(\vec{r})\}$, one obtains

$$\ddot{\mathcal{E}}_m(t) + \frac{1}{\tau_p}\dot{\mathcal{E}}_m(t) + \omega_m^2\mathcal{E}_m(t) = -\frac{1}{\epsilon_0\mu^2}\ddot{P}_m(t) + \Delta(t)e^{i\Omega_m t} \tag{2.6}$$

with

$$\Delta(t)e^{i\Omega_m t} = -\frac{1}{\epsilon\mu^2}\ddot{p}_m(t),$$

where the dots indicate differentiation with respect to time, $\tau_p \equiv \epsilon/\sigma$ is the photon lifetime, μ is the nonresonant index, Ω_m is the lasing frequency, and $\Delta(t)$ is the slowly varying complex amplitude of the Langevin force term. The polarization $P_m(t)$ induced by stimulated emissions is given by:

$$P_m(t) = \epsilon_0\Gamma\chi(n)\mathcal{E}_m(t), \tag{2.6a}$$

where Γ is the filling factor that accounts for the partial confinement of the mode energy in the active region, $\chi(n)$ is the susceptibility, and n is the carrier density in the active region. The complex susceptibility is assumed to be an instantaneous function of carrier density. (This is true when the intraband electron-electron and electron-phonon scatterings occur at a time scale of $\sim 10^{-12}$ sec.)

The temporal part of the mth mode can be expressed as

$$\mathcal{E}_m(t) = E_m(t)e^{i\Omega_m t} = \beta(t)e^{i(\Omega_m t+\phi(t))}, \tag{2.7}$$

where $E_m(t)$ is the complex amplitude, $\beta(t)$ is the real amplitude, and $\phi(t)$ is the slowly varying phase. There are two different time regimes for the optical field and carrier density. One is for the rapidly varying phase $e^{i\Omega_m t}$, and the other is for the slowly varying $\beta(t)$, $e^{i\phi(t)}$, and $n(t)$. In other words,

$$|\ddot{\beta}| \ll \Omega_m^2|\beta|, \qquad |\dot{\beta}| \ll \Omega_m|\beta| \tag{2.8a}$$

$$\left|\frac{\Gamma\dot{\chi}(n)}{\mu^2}\right| \ll \Omega_m, \qquad \left|\frac{\Gamma\chi(n)}{\mu^2}\right| \ll 1, \qquad \left(\frac{1}{\tau_p}\right) \ll \Omega_m. \tag{2.8b}$$

Substituting Equations (2.6a)-(2.8b) into Equation (2.6) yields the first-order differential equation of the optical field:

$$\frac{d}{dt}E_m(t) - \left[i\left(\omega_m - \Omega_m - \frac{\Gamma\chi_r(n)\Omega_m}{2\mu^2}\right) + \frac{1}{2}\left(\frac{\Gamma\chi_i(n)\Omega_m}{\mu^2} - \frac{1}{\tau_p}\right)\right]E_m(t) = \frac{\Delta(t)}{2i\Omega_m}, \tag{2.9}$$

where $\chi_r(n)$ and $\chi_i(n)$ are the real and imaginary parts of $\chi(n)$, respectively. Equation (2.9) is the well-known optical-field equation for solitary semiconductor lasers.

2.3-B. Effective Photon Lifetime $\tau_{eff}(t)$

In this section, the photon lifetime of solitary diode lasers will be expressed in terms of the amplitude reflectivities of diode facet mirrors and the distributed passive losses of the medium between the two facet mirrors. This close examination will set the stage for introducing the complex, time-dependent effective photon lifetime which, as will be seen in Section 2.3-C, is indispensable in the semiclassical theory of semiconductor lasers with external coupling.

Imposing steady state ($d/dt = 0$) on the optical-field Equation (2.9) yields

$$i\left(\omega_m - \Omega_m - \frac{\Gamma\chi_r(n)\Omega_m}{2\mu^2}\right) + \frac{1}{2}\left(\frac{\Gamma\chi_i(n)\Omega_m}{\mu^2} - \frac{1}{\tau_p^{sl}}\right) = 0, \tag{2.10}$$

where the superscript *sl* stands for solitary diode lasers. Since, for the lossless cavity with carrier density n_o, the mth resonant frequency is

$$\omega_m(n_o) = \frac{m\pi c}{\bar{n}(n_o)l}$$

with

$$\bar{n}(n_o) \simeq \bar{n}(n_o = 0)\left(1 + \frac{\Gamma\chi_r(n_o)}{2\mu^2}\right),$$

where l is the cavity length of the diode laser and $\bar{n}(n_o)$ is the spatially averaged index of refraction of the lossless resonator with carrier density n_o. Equation (2.10) can be rewritten as

$$i\left(\omega_m(n_o) - \Omega_m\right) + \frac{1}{2}\left(\frac{\Gamma\chi_i(n)\Omega_m}{\mu^2} - \frac{1}{\tau_p^{sl}}\right) = 0, \tag{2.11a}$$

or, in the exponential form,

$$e^{(g(n_o) - 1/\tau_p^{sl})\bar{n}(n_o)l/c} e^{-2i\Omega_m\bar{n}(n_o)l/c} = 1, \tag{2.11b}$$

where

$$g(n_o) = \frac{\Gamma\chi_i(n_o)\Omega_m}{\mu^2}$$

is the optical gain provided by the gain medium.

On the other hand, as explained in Reference 5, a laser oscillator is basically a Fabry-Perot etalon containing a gain medium. It is also shown in [5] that, when a plane wave of complex amplitude E_I incident on one side of this etalon, the total outgoing wave E_T received on the other side is

$$E_T \propto E_I \frac{1}{1 - r_1 r_2 e^{(g(n_o)-\alpha_0)\bar{n}(n_o)l/c} e^{-2i\Omega_m \bar{n}(n_o)l/c}},$$

where α_o is the distributed waveguide loss constant inside the diode cavity. Notice that the unit of α_o is sec^{-1}. If

$$r_1 r_2 e^{(g(n_o)-\alpha_0)\bar{n}(n_o)l/c} e^{-2i\Omega_m \bar{n}(n_o)l/c} = 1, \tag{2.12}$$

then the ratio E_T/E_I becomes infinite. Physically, this means that the oscillation occurs inside the resonator and Equation (2.12) is referred to as the oscillation condition. Since Equations (2.11b) and (2.12) apply to the same system, according to these two equations, the photon lifetime τ_p^{sl} is given by

$$\frac{1}{\tau_p^{sl}} = \alpha_0 - \frac{c}{\bar{n}l} \ln r_1 r_2. \tag{2.13}$$

Equation (2.13) indicates that the photon lifetime is indeed an indicator of the distributed waveguide losses and the losses through the facet mirrors.

For solitary diode lasers without facet mirror coatings, r_1 and r_2 are real numbers, and according to Equation (2.13), the photon lifetime τ_p^{sl} is a real-number quantity. However, after one applies mirror coatings such that r_1 and r_2 are complex numbers, τ_p^{sl} of (2.13) is complex and can be viewed formally as a physical parameter having both amplitude and phase. Consequently, separating (2.11a) into the amplitude and phase components gives

$$\frac{\Gamma \chi_i(n_0)\Omega_m}{\mu^2} = \mathrm{Re}[\frac{1}{\tau_p^{sl}}] \tag{2.14a}$$

for the threshold gain $g(n_o)$ and

$$\omega_m(n_o) - \Omega_m - \frac{1}{2}\mathrm{Im}[\frac{1}{\tau_p^{sl}}] = 0 \qquad (2.14b)$$

for the phase condition. Clearly, $\mathrm{Re}[\frac{1}{\tau_p^{sl}}]$ is a measure of the waveguide and mirror losses, and $\mathrm{Im}[\frac{1}{\tau_p^{sl}}]$ is related to the phase and lasing frequency of the optical field.

From the discussion given above, the photon lifetime τ_p^{sl} depends on the amplitude reflectivities r_1 and r_2, and, in general, τ_p^{sl} is a complex-number quantity. Similarly, lasers with time-dependent effective reflectivity $r_{eff}(t)$ will have complex effective photon lifetime τ_{eff}, which depends on $r_{eff}(t)$. In conclusion, normally, lasers with effective mirrors have complex, time-dependent effective photon lifetimes $\tau_{eff}(t)$. Finding out the relation between $r_{eff}(t)$ and $\tau_{eff}(t)$ will be the subject of Section 2.3-D.

2.3-C. Spatial Mode Expansions of the Optical Field Inside Cavities Formed by One Facet Mirror and One Effective Mirror

Invoking the concept of the complex, time-dependent effective photon lifetime of Section 2.3-B and the modal expansion method of Section 2.3-A, the zeroth-order optical-field equation for semiconductor lasers with external coupling will be derived in this section. At first, the equation will be derived for the case of a one-dimension resonator. Then, the derivation will be extended to the general case. After that, the justification for the general optical-field equation derived in this section will be given.

Because it is straightforward to find the field outside the composite cavity when the field inside the active region is known, in the following, the space domain will be limited to the cavity of the diode laser. In addition, to simplify

the situation, only the longitudinal field profile of the fundamental transverse mode will be considered.

Thus, for solitary diode lasers with a one-dimensional resonator oriented along the z-axis with boundaries at $z = 0$ and $z = l$, the wave equation for the optical field $\mathcal{E}(z,t)$ is

$$[\frac{\partial^2}{\partial z^2} - \kappa\sigma_{eff}(t)\frac{\partial}{\partial t} - \kappa\epsilon\frac{\partial^2}{\partial t^2}]\mathcal{E}(z,t) = \kappa\frac{\partial^2}{\partial t^2}[\mathcal{P}(z,t) + p(z,t)], \tag{2.15}$$

where $\sigma_{eff}(t)$, the complex, time-dependent effective conductivity, accounts for the effective photon lifetime introduced in Section 2.3-B. The dimensionless mth mode eigenfunction of the unpumped and lossless solitary cavity is

$$e_m^{sl}(z) = \sin k_m z, \tag{2.15a}$$

where the wavenumber k_m satisfies

$$k_m l = m\pi. \tag{2.15b}$$

In arriving at Equations (2.15a) and (2.15b), an infinite conductivity at both $z = 0$ and $z = l$ is assumed.

For the laser with an effective mirror, the detuning of the resonant frequency is

$$\Delta\omega_{mj} = \omega_{mj} - \omega_m,$$

where ω_m is the mth resonant frequency of the unpumped and lossless solitary cavity and ω_{mj} is the resonant frequency of the unpumped and lossless composite laser cavity. As shown in Figure 2.3, the subscript mj denotes the jth resonant frequency of the mth cluster of resonant frequencies, and the mth cluster resonant

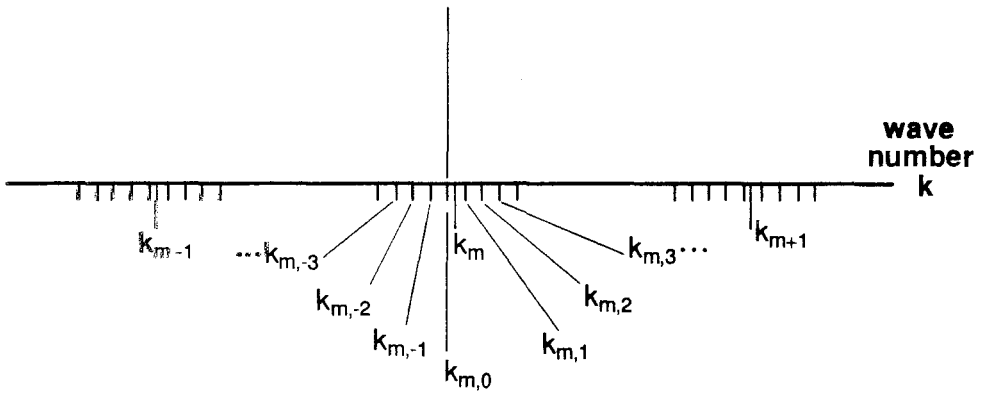

Figure 3.1 (a) Schematic of a single-mode semiconductor laser coupled to an external mirror. (b) A single-mode semiconductor laser coupled to an external mirror is equivalent to a diode laser with an effective mirror.

frequencies are located in the vicinity of ω_m. Similarly, the detuning of the wave number is

$$\Delta k_{mj} = k_{mj} - k_m.$$

The corresponding dimensionless eigenfunction of the unpumped and lossless composite cavity satisfies

$$\frac{d^2}{dz^2} e_{mj}(z) + \kappa\epsilon\omega_{mj}^2 e_{mj}(z) = 0, \tag{2.16}$$

and the eigenfunction of the mjth mode is given by

$$e_{mj}(z) = \sin(k_m + \Delta k_{mj})z. \tag{2.16a}$$

Equation (2.16a) indicates that under the influence of external coupling, the conductivity at $z = l$ is not necessary infinite.

Using the orthonormality of the complete set $\{e_{mj}(z)\}$, in the region $0 \leq z \leq l$, one has the following expansions:

$$\mathcal{E}(z,t) = \sum_m \sum_j \mathcal{E}_{mj}(t) e_{mj}(z) \tag{2.17a}$$

$$\mathcal{P}(z,t) = \sum_m \sum_j \mathcal{P}_{mj}(t) e_{mj}(z) \tag{2.17b}$$

$$p(z,t) = \sum_m \sum_j p_{mj}(t) e_{mj}(z) \tag{2.17c}$$

and

$$\mathcal{P}_{mj}(t) = \epsilon_0 \Gamma \chi(n) \mathcal{E}_{mj}(t). \tag{2.17d}$$

After substituting Equations (2.17a)-(2.17d) into Equation (2.15), multiplying by $e^*_{m'}(z)$, and integrating from $z = 0$ to $z = l$, one gets

$$\sum_m \{\sum_j \mathcal{E}_{mj}(t) \int_0^l [\frac{d^2}{dz^2} e_{mj}(z)] e^*_{m'}(z) dz\}$$

$$-\left[\kappa\sigma_{eff}(t)\frac{\partial}{\partial t}+\kappa\epsilon\frac{\partial^2}{\partial t^2}\right]\sum_m\left[\sum_j \mathcal{E}_{mj}(t)\int_0^l e_{mj}(z)e^*_{m'}(z)dz\right]$$

$$=\kappa\frac{\partial^2}{\partial t^2}\sum_m\left[\sum_j\Big(\epsilon_0\Gamma\chi(n)\mathcal{E}_{mj}(t)+p_{mj}(t)\Big)\int_0^l e_{mj}(z)e^*_{m'}(z)dz\right]. \qquad (2.18)$$

Substituting Equations (2.15a) and (2.16a) into Equation (2.18), one obtains

$$\frac{2}{l}\sum_j \mathcal{E}_{mj}(t)\int_0^l\left[\frac{d^2}{dz^2}e_{mj}(z)\right]e^*_{m'}(z)dz$$

$$=\begin{cases} k^2_{m'}\sum_j \mathcal{E}_{m'j}(t)+\sum_j \mathcal{E}_{m'j}(t)\frac{3\Delta k_{m'j}}{2k_{m'}}+\cdots & m=m' \\ (-1)^{m+m'+1}k^2_m\sum_j \mathcal{E}_{mj}(t)\left[\frac{\Delta k_{mj}}{k_{m'}+k_m}-\frac{\Delta k_{mj}}{k_{m'}-k_m}\right]+\cdots & m\neq m' \end{cases} \qquad (2.19a)$$

and

$$\frac{2}{l}\sum_j \mathcal{E}_{mj}(t)\int_0^l e_{mj}(z)e^*_{m'}(z)dz$$

$$=\begin{cases} \sum_j \mathcal{E}_{m',j}(t)-\sum_j \mathcal{E}_{m'j}(t)\frac{\Delta k_{m'j}}{2k_{m'}}+\cdots & m=m' \\ (-1)^{m+m'+1}\sum_j \mathcal{E}_{mj}(t)\left[\frac{\Delta k_{mj}}{k'_m+k_m}-\frac{\Delta k_{mj}}{k'_m-k_m}\right]+\cdots & m\neq m'. \end{cases} \qquad (2.19b)$$

Since

$$\left|\frac{\Delta k_{m'j}}{2k_{m'}}\right|\ll\left|\frac{\Delta k_{mj}}{k_{m'}-k_m}\right|, \qquad \left|\frac{\Delta k_{mj}}{k_{m'}+k_m}\right|\ll\left|\frac{\Delta k_{mj}}{k_{m'}-k_m}\right|,$$

only the order of magnitude of

$$\sum_j \mathcal{E}_{mj}(t)\frac{\Delta k_{mj}}{k_{m'}-k_m}=\sum_j E_{mj}(t)e^{i\Omega_{mj}t}\frac{\Delta k_{mj}}{k_{m'}-k_m}$$

needs to be estimated.

For a quick estimation, consider the field spectrum of Figure 2.3, where $E_{m0}(t)$ is the largest mode and $\beta_{m,j}(t)=\beta_{m,-j}(t)$. Therefore, one has

$$e^{-i\Omega_{m0}t}\sum_j \beta_{mj}(t)e^{i\Omega_{mj}t}\frac{\Delta k_{mj}}{k_{m'}-k_m}=\beta_{m0}(t)\frac{\Delta k_{m0}}{k_{m'}-k_m}$$
$$+\sum_{j>0}\beta_{mj}(t)\left[\frac{2\Delta k_{m0}}{k_{m'}-k_m}\cos(j\Delta\Omega t)+\frac{2j\Delta k}{k_{m'}-k_m}\sin(j\Delta\Omega t)\right], \qquad (2.20)$$

where $\Delta k = |k_{m,j} - k_{m,j+1}|$ and $\Delta\Omega = |\Omega_{m,j} - \Omega_{m,j+1}|$. For most of the diode lasers of great interest and practical importance,

$$|\frac{\Delta k_{m0}}{k_{m'} - k_m}| < \frac{\Delta k}{|k_{m'} - k_m|} \ll 1$$

Accordingly, in terms of $\frac{\Delta k}{k_{m'} - k_m}$ and in the zeroth-order approximation, Equation (2.18) is reduced to

$$\sum_j \{\frac{d^2}{dt^2}[(1 + \frac{\Gamma\chi(n)}{\mu^2})\mathcal{E}_{mj}(t)] + \frac{1}{\tau_p^{eff}(t)}\frac{d}{dt}\mathcal{E}_{mj}(t) + \omega_m^2\mathcal{E}_{mj}(t) + \frac{1}{\epsilon_0\mu^2}\ddot{p}_{mj}(t)\} = 0, \tag{2.21}$$

where $\tau_p^{eff}(t) = \epsilon/\sigma_{eff}(t)$ is the effective photon lifetime. Therefore, the optical-field equation of the mjth mode $\mathcal{E}_{mj}(t)$ is

$$\frac{d^2}{dt^2}[(1 + \frac{\Gamma\chi(n)}{\mu^2})\mathcal{E}_{mj}(t)] + \frac{1}{\tau_p^{eff}(t)}\frac{d}{dt}\mathcal{E}_{mj}(t) + \omega_m^2\mathcal{E}_{mj}(t) = \Delta(t)e^{i\Omega_{mj}t}. \tag{2.22}$$

Using (2.8a) and (2.8b), Equation (2.22) can be simplified to a first-order differential equation:

$$\frac{d}{dt}E_{mj}(t) - [i(\omega_m - \Omega_{mj} - \frac{\Gamma\chi_r(n)\Omega_{mj}}{2\mu^2}) + \frac{1}{2}(\frac{\Gamma\chi_i(n)\Omega_{mj}}{\mu^2} - \frac{1}{\tau_p^{eff}(t)})]E_{mj}(t) = \frac{\Delta(t)}{2i\Omega_{mj}} \tag{2.23}$$

where $E_{mj}(t)$ is the complex amplitude of the optical field $\mathcal{E}_{mj}(t)$.

Up to this point, the derivation is for a one-dimensional resonator with a special boundary condition. Although everything in this derivation is transparent and straightforward, it is desirable to broaden the theoretical basis of the theory. In the following, the derivation will be performed for a three-dimensional resonator without invoking special boundary conditions. The spatial dependence of the dielectric constant ϵ, which was neglected in the semiclassical laser theory [4] and the derivation given above, will also be included. Along the line,

some subtle points will be spelled out, and one will find that the one-dimensional model is a useful and illustrative example of the theory developed below.

In principle, the optical field $\vec{\mathcal{E}}(\vec{r},t)$ consists of a large number of lateral, transverse, and longitudinal modes lasing at different frequencies. But in practice, lasers designed to support only a fundamental lateral and transverse mode are very important for many practical applications. Very often, this fundamental mode operation is also desired for semiconductor lasers with external coupling. Therefore, only semiconductor lasers of this kind, with or without external coupling, will be considered below and throughout Chapters 3, 4, and 5. In addition, the x-axis and y-axis are designated as the lateral-axis and tranverse-axis, respectively. Each longitudinal mode of solitary semiconductor lasers is a superposition of the forward and backward propagating waves that form a standing wave pattern in the z-axis direction, and the optical field $\vec{\mathcal{E}}(\vec{r},t)$ can be written as

$$\vec{\mathcal{E}}(\vec{r},t) = \vec{e}_t(x,y)\mathcal{E}(z,t), \tag{2.24a}$$

where $\vec{e}_t(x,y)$is the lateral and tranverse profile of the fundamental mode.

Because the external coupling considered in this thesis is coupled longitudinally through one facet mirror of the conventional solitary diode laser, it is expected that the lateral and transverse profile will basically remain undisturbed. Consequently, it is assumed that (2.24a) also holds for diode lasers with external coupling. Inside the diode cavity, the wave equation for the optical field $\vec{\mathcal{E}}(\vec{r},t)$ is

$$[\nabla^2 - \kappa\sigma_{eff}(t)\frac{\partial}{\partial t} - \kappa\epsilon(x,y)\frac{\partial^2}{\partial t^2}]\vec{\mathcal{E}}(\vec{r},t) = \kappa\frac{\partial^2}{\partial t^2}[\vec{P}(\vec{r},t) + \vec{p}(\vec{r},t)], \tag{2.24b}$$

where the spatially varying dielectric constant $\epsilon(x,y)$ is dependent on the laser waveguide structure which supports only the fundamental modes. Notice that

the optical field of main concern is confined inside the diode cavity; therefore, it is assumed that the dielectric constant $\epsilon(x,y)$ is not a function of the longitudinal coordinate z.

For the unpumped and lossless composite cavity, there is a complete orthonormal set $\{\vec{e}_t(x,y)e_{mj}(z)\}$ of dimensionless eigenfunctions $\vec{e}_t(x,y)e_{mj}(z)$, which obey

$$\nabla^2\vec{e}_t(x,y)e_{mj}(z)+\kappa\epsilon(x,y)\omega_{mj}^2\vec{e}_t(x,y)e_{mj}(z)=0 \tag{2.25}$$

with the appropriate boundary conditions. The choice of having dimensionless eigenfunctions $e_t(x,y)e_{mj}(z)$ is purely a matter of convenience. For the optical field $\vec{\mathcal{E}}(\vec{r},t)$ inside the diode cavity, one has the following expansions:

$$\vec{\mathcal{E}}(\vec{r},t)=\vec{e}_t(x,y)\sum_m\sum_j\mathcal{E}_{mj}(t)e_{mj}(z) \tag{2.26a}$$

$$\vec{\mathcal{P}}(\vec{r},t)=\vec{e}_t(x,y)\sum_m\sum_j\mathcal{P}_{mj}(t)e_{mj}(z) \tag{2.26b}$$

$$\vec{p}(\vec{r},t)=\vec{e}_t(x,y)\sum_m\sum_j p_{mj}(t)e_{mj}(z) \tag{2.26c}$$

and

$$\mathcal{P}_{mj}(t)=\epsilon_0\Gamma\chi(n)\mathcal{E}_{mj}(t). \tag{2.26d}$$

To understand why the expansions (2.26a)-(2.26c) are limited to the region inside the solitary diode cavity, one has first to grasp the physical meaning behind these expansions. For a composite laser lasing in its mjth mode, according to (2.26a), its optical field inside the diode cavity is

$$\vec{\mathcal{E}}(\vec{r},t)=\mathcal{E}_{mj}(t)\vec{e}_t(x,y)e_{mj}(z).$$

Therefore, the field intensity ratio between points $\vec{r}_1$ and $\vec{r}_2$ is given by

$$\left|\frac{\vec{\mathcal{E}}(\vec{r}_1,t)}{\vec{\mathcal{E}}(\vec{r}_2,t)}\right|^2 = \left|\frac{\vec{e}_t(x_1,y_1)e_{mj}(z_1)}{\vec{e}_t(x_2,y_2)e_{mj}(z_2)}\right|^2,$$

and is time-independent. For a solitary diode resonator, this is expected and agrees with the spirit of the semiclassical laser theory [4]. Similarly, let us suppose that the expansions (2.26a)-(2.26c) are for the whole composite cavity. Then, for instance, in the case of a single-mode two-section laser, the field intensity ratio between points of different cavity is time-independent. But according to the results that will be presented in Chapter 5, each cavity of a two-section laser has its own average optical field, and the ratio between these two fields generally is not time-independent. Therefore, the expansions (2.26a)-(2.26c) are valid only for the region inside the diode cavity.

Substituting Equations (2.26a)-(2.26d) into Equation (2.24b), multiplying by $\vec{e}_t^{\,*}(x,y)e_{m'}^*(z)$, and integrating over the whole volume of diode cavity, one obtains

$$-\kappa < \epsilon > \omega_{mj}^2 \sum_m \{\sum_j \mathcal{E}_{mj}(t) \int_0^l e_{mj}(z)e_{m'}^*(z)dz\}$$

$$-\left[\kappa\sigma_{eff}(t)\frac{\partial}{\partial t} + \kappa < \epsilon > \frac{\partial^2}{\partial t^2}\right] \sum_m [\sum_j \mathcal{E}_{mj}(t) \int_0^l e_{mj}(z)e_{m'}^*(z)dz]$$

$$= \kappa\frac{\partial^2}{\partial t^2} \sum_m \Big[\sum_j \Big(\epsilon_0\Gamma\chi(n)\mathcal{E}_{mj}(t) + p_{mj}(t)\Big) \int_0^l e_{mj}(z)e_{m'}^*(z)dz\Big] \qquad (2.27)$$

with

$$< \epsilon >= \frac{\int_{-\infty}^{\infty}\int_{-\infty}^{\infty} \epsilon(x,y)\vec{e}_t(x,y)\vec{e}_t^{\,*}(x,y)\,dx\,dy}{\int_{-\infty}^{\infty}\int_{-\infty}^{\infty} \vec{e}_t(x,y)\vec{e}_t^{\,*}(x,y)\,dx\,dy}, \qquad (2.27a)$$

where $e_{m'}(z)$ is the m'th longitudinal mode of the unpumped and lossless diode cavity. The $< \epsilon >$ defined in (2.27a) can be interpreted as the spatially averaged

dielectric constant. In arriving at Equation (2.27), Equation (2.25) has been used.

Using the expansion in the region $0 \leq z \leq l$,

$$e_{mj}(z) = \sum_k c_{kj} e_k(z),$$

one obtains

$$\int_0^l e_{mj}(z) e^*_{m'}(z) dz = c_{m'j} \int_0^l e_{m'}(z) e^*_{m'}(z) dz. \tag{2.28a}$$

For most diode lasers of great interest and practical importance, the detuning Δk_{mj} is very small and can be characterized by

$$\left| \frac{\Delta k_{mj}}{k_m - k_{m+1}} \right| \ll 1. \tag{2.28b}$$

Therefore, for lasers falling in this category, it is assumed that $c_{m'j}$ of Equation (2.28a) is in the form of a power series expansion in $\bar{\varepsilon}$:

$$c_{m'j} = \begin{cases} O(\bar{\varepsilon}) + \cdots & m \neq m' \\ 1 + O(\bar{\varepsilon}) + \cdots & m = m', \end{cases} \tag{2.28c}$$

where $\bar{\varepsilon}$ is a real dimensionless parameter much less than 1, and $O(\bar{\varepsilon})$ denotes that $O(\bar{\varepsilon})$ is on the order of magnitude $\bar{\varepsilon}$. Accordingly, Equation (2.28a) becomes

$$\int_0^l e_{mj}(z) e^*_{m'}(z) dz = \begin{cases} (O(\bar{\varepsilon}) + \cdots) \int_0^l e_{m'}(z) e^*_{m'}(z) dz & m \neq m' \\ (1 + O(\bar{\varepsilon}) + \cdots) \int_0^l e_{m'}(z) e^*_{m'}(z) dz & m = m'. \end{cases} \tag{2.28d}$$

Similarly, in terms of $\bar{\varepsilon}$, $\mathcal{E}_{mj}(t)$ can be expanded as

$$\mathcal{E}_{mj}(t) = \mathcal{E}^0_{mj}(t) + \bar{\varepsilon} \mathcal{E}^1_{mj}(t) + \cdots. \tag{2.28e}$$

After substituting (2.28d) and (2.28e) into (2.27) and equating the coefficients of successive powers of $\bar{\varepsilon}$ on both sides of that equation, the solution arising from

the zeroth-order term in $\bar{\epsilon}$ yields

$$\sum_j \{ \frac{d^2}{dt^2}[(1+\frac{\Gamma\chi(n)}{\bar{\mu}^2})\mathcal{E}^0_{mj}(t)] + \frac{1}{\tau_p^{eff}(t)}\frac{d}{dt}\mathcal{E}^0_{mj}(t) + \omega_m^2\mathcal{E}^0_{mj}) + \frac{1}{\epsilon_0\bar{\mu}^2}\ddot{p}^0_{mj}(t)\} = 0. \tag{2.29}$$

where

$$\tau_p^{eff}(t) = \frac{<\epsilon>}{\sigma_{eff}(t)} \tag{2.29a}$$

is the effective photon lifetime. Because the superscript 0 on $E^0_{mj}(t)$ and $\ddot{p}^0_{mj}(t)$ is omitted in Equation (2.22), this equation is exactly the same as Equation (2.22), except that the spatially averaged refractive index $\bar{\mu}$ given by

$$\bar{\mu} = \sqrt{\frac{<\epsilon>}{\epsilon_0}} \tag{2.29b}$$

is used in Equation (2.29). Thus, the optical-field equation of semiconductor lasers with external coupling is

$$\frac{d}{dt}E_{mj}(t) - [i(\omega_m - \Omega_{mj} - \frac{\Gamma\chi_r(n)\Omega_{mj}}{2\bar{\mu}^2}) + \frac{1}{2}(\frac{\Gamma\chi_i(n)\Omega_{mj}}{\bar{\mu}^2} - \frac{1}{\tau_p^{eff}(t)})]E_{mj}(t) = \frac{\Delta(t)}{2i\Omega_{mj}}. \tag{2.30}$$

From the simple model presented in the first part of this section, it has been shown that (2.28d) follows directly from the condition (2.28b). Therefore, although (2.28d) is an assumption in the discussion given in the second part of this section in general, it is expected that the condition (2.28b) will lead to the other condition (2.28d). Despite the fact that most lasers of great interest and practical importance obey the conditions imposed by (2.28b), (2.28d), or by (2.28b) and (2.28d), one can not rule out possible cases that violate these conditions. In any case, the inequality (2.28b) can be checked experimentally from the frequency detuning data. On the other hand, the condition (2.28d) can be examined only from calculations on a specific case basis.

The major points of this section are reviewed in the following. The optical-field equation (2.30) is derived directly from Maxwell's wave equation. At first, the derivation is based on a model of a one-dimensional resonator. Then, the same equation is rederived in the general case. The simple model offers the advantage that calculations can be carried out with relative ease in great detail , whereas the second approach is more accurate and realistic than the first one because of the inclusion of the spatial dependence of the dielectric constant $\epsilon(x, y)$. In addition, both approaches complement one another.

2.3-D. Relation Between $1/\tau_p^{eff}(t)$ and $r_{eff}(t)$

As shown in Section 2.3-B, in the semiclassical laser theory [4], the photon lifetime of a solitary semiconductor laser is directly related to the amplitude reflectivities of its facet mirrors. For semiconductor lasers with external coupling, it is expected that a similar relation between the effective photon lifetime $\tau_{eff}(t)$ and effective reflectivity $r_{eff}(t)$ exists. Therefore, establishing this relation will be the first concern of this section. Then, the physical meaning of this relation will be described.

Recall that the Langevin force $\Delta(t)$ accounts for the spontaneous-emission driven quantum noise. Therefore, $\Delta(t)$ of Equation (2.30) is neglected in the following derivation. Integrating Equation (2.30) yields

$$E_{mj}(t+\tau_l) = E_{mj}(t)\exp[i(\omega_m\tau_l - \Omega_{mj}\tau_l - 1/2\int_t^{t+\tau_l}\frac{\Gamma\chi_r(n)}{\bar{\mu}^2}\Omega_{mj}dt)]$$

$$\times\exp[1/2\int_t^{t+\tau_l}(\frac{\Gamma\chi_i(n)}{\bar{\mu}^2}\Omega_{mj} - \frac{1}{\tau_p^{eff}(t)})dt], \qquad (2.31)$$

where $\tau_l = 2\bar{n}l/c$ is the round-trip time of the optical field inside the crystal cavity. Since, in the period of $\tau_l \simeq 6 \times 10^{-12}s$, all the terms in the integrands of Equation (2.31) remain almost unchanged, thus Equation (2.31) can be simplified to

$$E_{mj}(t+\tau_l)e^{i\Omega_{mj}\tau_l} = E_{mj}(t)\exp[i(\omega_m\tau_l - 1/2\frac{\chi_r(n)}{\bar{\mu}^2}\Omega_{mj}\tau_l)]$$
$$\times\exp[1/2(\frac{\Gamma\chi_i(n)}{\bar{\mu}^2}\Omega_{mj}\tau_l - \frac{\tau_l}{\tau_p^{eff}(t)})]. \qquad (2.32)$$

On the other hand, after following the optical field through a round trip inside the diode cavity, one has

$$E_{mj}(t+\tau_l) = E_{mj}(t) \times r_1 \times r_{eff}(t) \times \exp[(\frac{\Gamma\chi_i(n)}{\bar{\mu}^2}\Omega_{mj}\tau_l - \alpha_o\tau_l)/2]. \qquad (2.33)$$

Since

$$\exp\left[i(\omega_m\tau_l - \frac{\Gamma\chi_r(n)}{2\bar{\mu}^2}\Omega_{mj}\tau_l - \Omega_{mj}\tau_l)\right] = 1+\delta$$

with $|\delta| \ll 1$, relating Equations (2.32) and (2.33) gives

$$\frac{1}{\tau_p^{eff}(t)} = \alpha_0 - \frac{c}{\bar{n}l}\ln r_1 r_{eff}(t) = \frac{1}{\tau_p^{sl}} - \frac{c}{\bar{n}l}\ln\frac{r_{eff}(t)}{r_2}, \qquad (2.34)$$

where r_2 is the amplitude reflectivity of the right facet of the solitary diode laser (Figure 2.1a). Notice that the condition $|\delta| \ll 1$ follows directly from condition (2.28b) of the last section. The similarity between Equations (2.13) and (2.34) confirms the argument that a diode laser with external coupling indeed behaves like a solitary diode laser with an effective mirror. Equation (2.34) shows that the time-dependent amplitude reflectivity of the effective mirror gives rise to the time-dependent effective photon lifetime.

Substituting Equation (2.34) into Equation (2.30) yields the optical-field equation of semiconductor lasers with external coupling:

$$\frac{d}{dt}E_{mj}(t) - [i(\omega_m - \Omega_{mj} - \frac{\Gamma\chi_r(n)\Omega_{mj}}{2\bar{\mu}^2})$$

$$+\frac{1}{2}\left(\frac{\Gamma\chi_i(n)\Omega_{mj}}{\bar{\mu}^2}-\frac{1}{\tau_p^{sl}}+\frac{c}{\bar{n}l}\ln\frac{r_{eff}(t)}{r_2}\right)\Big]E_{mj}(t)=\frac{\Delta(t)}{2i\Omega_{mj}}. \quad (2.35)$$

Clearly, the effect on the laser dynamics contributed by the external coupling is contained in the term

$$-\frac{c}{\bar{n}l}\ln\frac{r_{eff}(t)}{r_2}$$

of Equation (2.35). The real part of this term is the change in loss caused by the external coupling, and its imaginary part is related to the change in the phase of the optical field. With no external coupling,

$$r_{eff}(t)=r_2,$$

so that

$$\frac{c}{\bar{n}l}\ln\frac{r_{eff}(t)}{r_2}=0,$$

and Equation (2.35) gives the well-known optical-field equation of the solitary semiconductor lasers.

Equation (2.35) is the key result of this chapter and will be the basis for analyzing the dynamics and steady-state characteristics of the diode laser with external coupling.

2.3-E. Steady State Characteristics

After uncovering the role played in laser dynamics by the effective reflectivity $r_{eff}(t)$ and showing that Equation (2.35) is consistent with the well-known optical-field equation of solitary diode lasers, the next concern would be the consistency between Equation (2.35) and the oscillation condition of Reference 5. It will be the purpose of this section to answer this question.

Suppose the steady-state effective reflectivity is r^0_{eff} and

$$r^0_{eff} = |r^0_{eff}|e^{i\theta};$$

then the oscillation condition [5] is

$$r_1|r^0_{eff}|e^{i\theta}e^{(g-\alpha_0)\bar{n}l/c}e^{-2i\Omega_m\bar{n}l/c} = 1. \tag{2.36}$$

In the meantime, the optical-field equation (2.35) gives

$$\omega_m - \Omega_{mj} - \frac{\Gamma\chi_r(n_0)}{2\bar{\mu}^2}\Omega_{mj} + \frac{c}{2\bar{n}l}\mathrm{Im}(\ln(r_1 r^0_{eff})) = 0 \tag{2.37a}$$

and

$$\frac{\Gamma\chi_i(n)\Omega_{mj}}{\bar{\mu}^2} - \alpha_0 + \frac{c}{\bar{n}l}\ln(r_1|r^0_{eff}|) = 0, \tag{2.37b}$$

which govern the steady state of the composite lasers. Following the procedure of Section 2.3-B, it can be shown that the combining of Equations (2.37a) and (2.37b) is equivalent to Equation (2.36).

Clearly, the secular equation for the lasing frequency Ω_{mj} is given by Equation (2.30a). The phase of r^0_{eff} determines the detuning of the lasing frequency, and the amplitude of r^0_{eff} dictates the amount of threshold gain reduction. In conclusion, the optical-field equation (2.35) gives the same steady-state oscillation condition as that predicted by Reference 5, and in the steady-state domain, a diode laser with an external coupling is, in fact, equivalent to a solitary diode laser with an effective mirror.

2.4 Application of the Theory

To demonstrate the usefulness of the theory presented above, the general optical-field Equation (2.28) will be applied to obtain optical-field equations for

three different types of composite cavities in this section. Lasers under consideration are (1) a diode laser coupled to an external mirror, (2) an injection-locked diode laser, and (3) an axially coupled two-section laser. With these examples, one will have a firm grasp of the abstract concept of the time-dependent effective reflectivity. The optical-field equations will be given, and accompanying discussions will be based solely on inspecting the newly obtained optical-field equations. The dynamics of each type of composite cavities deserve detailed study and will be treated separately in Chapters 3, 4, and 5.

2.4-A. A Diode Laser Coupled to An External Mirror

For a single-mode diode laser coupled to an external mirror, the optical-field equation is

$$\frac{d}{dt}E(t)-\Big[i\Big(\omega_m-\Omega-\frac{\Gamma\chi_r(n)\Omega}{2\bar{\mu}^2}\Big) + \frac{1}{2}\Big(\frac{\Gamma\chi_i(n)\Omega}{\bar{\mu}^2}-\frac{1}{\tau_p^{sl}}+\frac{c}{\bar{n}l}\ln\frac{r_{eff}(t)}{r_2}\Big)\Big]E(t)=\frac{\Delta(t)}{2i\Omega}, \qquad (2.38)$$

where ω_m is the mth resonant frequency of the unpumped solitary laser-cavity, Ω is the lasing frequency, and $r_{eff}(t)$ is given in Equation (2.3c).

In the limit $|r_3| \ll |r_2|$, Equation (2.3c) gives

$$\ln\frac{r_{eff}(t)}{r_2} \simeq (1-r_2^2)\frac{r_3}{r_2}e^{-i\Omega\tau}\frac{E(t-\tau)}{E(t)},$$

and Equation (2.38) becomes

$$\frac{d}{dt}E(t)-\Big[i\Big(\omega_m-\Omega-\frac{\Gamma\chi_r(n)\Omega}{2\bar{\mu}^2}\Big)+\frac{1}{2}\Big(\frac{\Gamma\chi_i(n)\Omega}{\bar{\mu}^2}-\frac{1}{\tau_p^{sl}}\Big)\Big]E(t) - \frac{c}{2\bar{n}l}\frac{r_3}{r_2}(1-r_2^2)e^{-i\Omega\tau}E(t-\tau)=\frac{\Delta(t)}{2i\Omega}. \qquad (2.39)$$

Dropping the Langevin noise term, Equation (2.39) becomes the equation introduced by Lang and Kobayashi [1]. Clearly, the equation introduced by Lang and Kobayashi is a special case of Equation (2.38), and unlike their equation, Equation (2.38) takes into account the optical field trapped for many round trips inside the external cavity. Therefore, Equation (2.38) will make feasible the analysis for lasers with strong external feedback. A thorough investigation of this type of lasers based on this equation will be presented in Chapter 3 [7].

2.4-B. An Injection-Locked Diode Laser

For a single-mode injection-locked laser shown in Figure 2.4a, at any instance there are two counterpropagating waves at the point inside the diode cavity just to the left of the right air-crystal boundary. Suppose the incident wave from the left at plane R is

$$E_i(t)e^{i\Omega t} = aE(t)e^{i\Omega t}, \tag{2.40a}$$

and the wave travelling to the left at plane R is

$$E_r(t)e^{i\Omega t} = r_2 aE(t)e^{i\Omega t} + t_2 E_{in}(t)e^{i\Omega t}, \tag{2.40b}$$

where $E_{in}(t)$ is the complex amplitude of the field before being injected into the cavity, $E(t)$ is the complex amplitude of the field inside the injected diode cavity, t_2 is the transmission coefficient from the air to the cavity, Ω is the lasing frequency, and a is already defined in Equation (2.3a). Thus, this injected laser has an effective mirror with effective reflectivity $r_{eff}(t)$ at plane R defined by Equation (2.1).

Substituting (2.40a) and (2.40b) into (2.1) gives

$$r_{eff}(t) = r_2 + \frac{t_2 E_{in}(t)}{aE(t)}. \tag{2.40c}$$

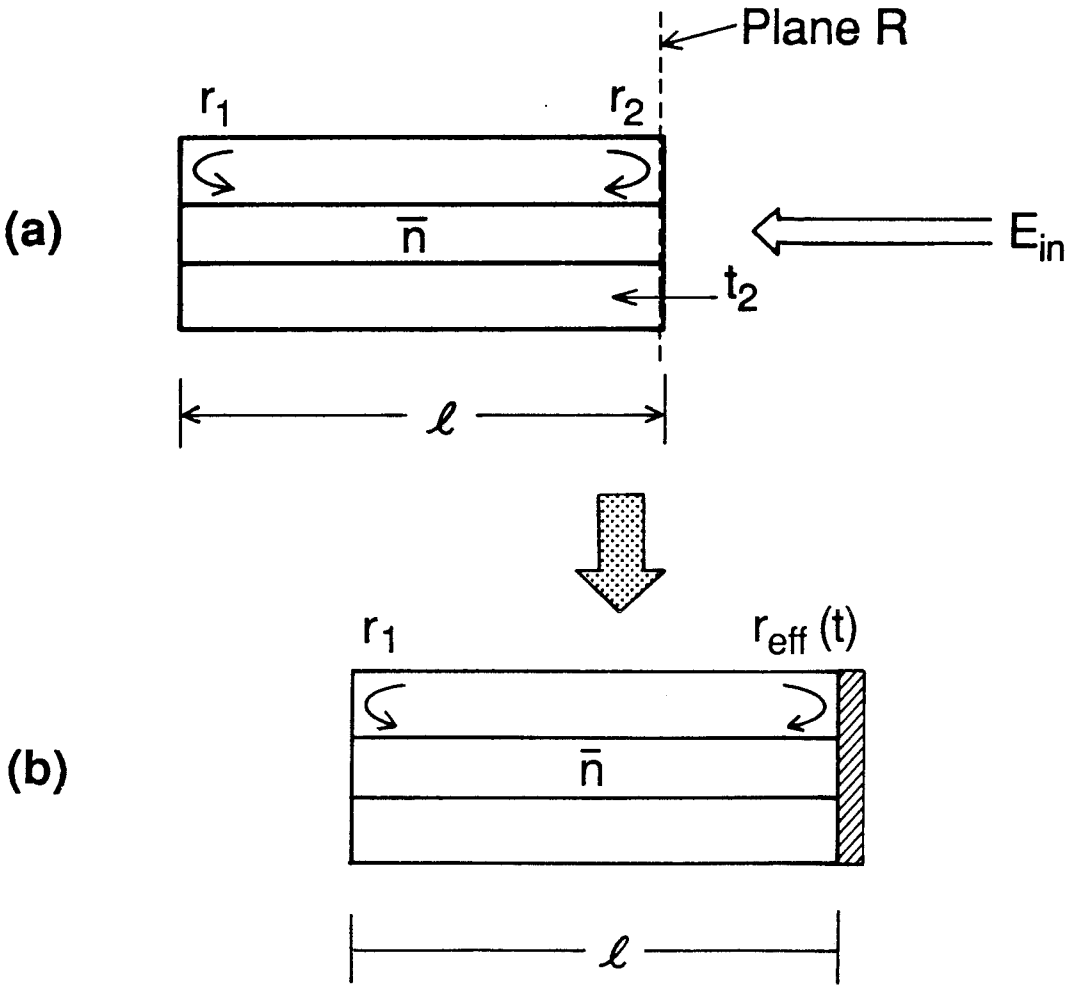

Figure 2.4 (a) Schematic of an injection-locked semiconductor laser. (b) An injection-locked semiconductor laser is equivalent to a diode laser with an effective mirror.

Equation (2.40c) indicates that as the injected field $E_{in}(t)$ varies, the effective reflectivity $r_{eff}(t)$ changes as well. This confirms that as illustrated in Figure 2.4b, there is an instantaneous effective reflectivity $r_{eff}(t)$ for injection-locked lasers. Following the same argument given in Section 2.2, one has $a \simeq 1/(1+|r_2|^2)$. For uncoated or AR-coated diode lasers, $a \simeq 1$. Therefore, substituting (2.40c) into (2.35) yields

$$\frac{d}{dt}E(t) - \Big[i\Big(\omega_m - \Omega - \frac{\Gamma\chi_r(n)\Omega}{2\bar{\mu}^2}\Big) + \frac{1}{2}\Big(\frac{\Gamma\chi_i(n)\Omega}{\bar{\mu}^2} - \frac{1}{\tau_p^{sl}} + \frac{c}{\bar{n}l}\ln\Big(1+\frac{t_2}{r_2}\frac{E_{in}(t)}{E(t)}\Big)\Big)\Big]E(t) = \frac{\Delta(t)}{2i\Omega}. \quad (2.41)$$

In general,

$$\Big|\frac{t_2 E_{in}(t)}{r_2 E(t)}\Big| \ll 1,$$

and Equation (2.41) becomes

$$\frac{d}{dt}E(t) - \Big[i\Big(\omega_m - \Omega - \frac{\Gamma\chi_r(n)\Omega}{2\bar{\mu}^2}\Big) + \frac{1}{2}\Big(\frac{\Gamma\chi_i(n)\Omega}{\bar{\mu}^2} - \frac{1}{\tau_p^{sl}}\Big)\Big]E(t) - \frac{c}{2\bar{n}l}\Big(\frac{t_2}{r_2}\Big)E_{in}(t) = \frac{\Delta(t)}{2i\Omega}. \quad (2.42)$$

Except for the factor $1/r_2$ in the term $-\frac{c}{2\bar{n}l}(\frac{t_2}{r_2})E_{in}(t)$ and the Langevin force term, Equation (2.42) is the same as the equation introduced by Lang [2]. One immediate implication of this factor is that decreasing r_2/t_2 will reduce the injected field intensity necessary for locking. This is consistent with the analysis given by Hadley [8], which was carried out in the spatial domain. Apparently, as shown in Equation (2.42), r_2 is an important parameter that is missing in the equation introduced by Lang, and it should be included in the optical-field equation. Chapter 4 will present an in-depth study of this laser [9].

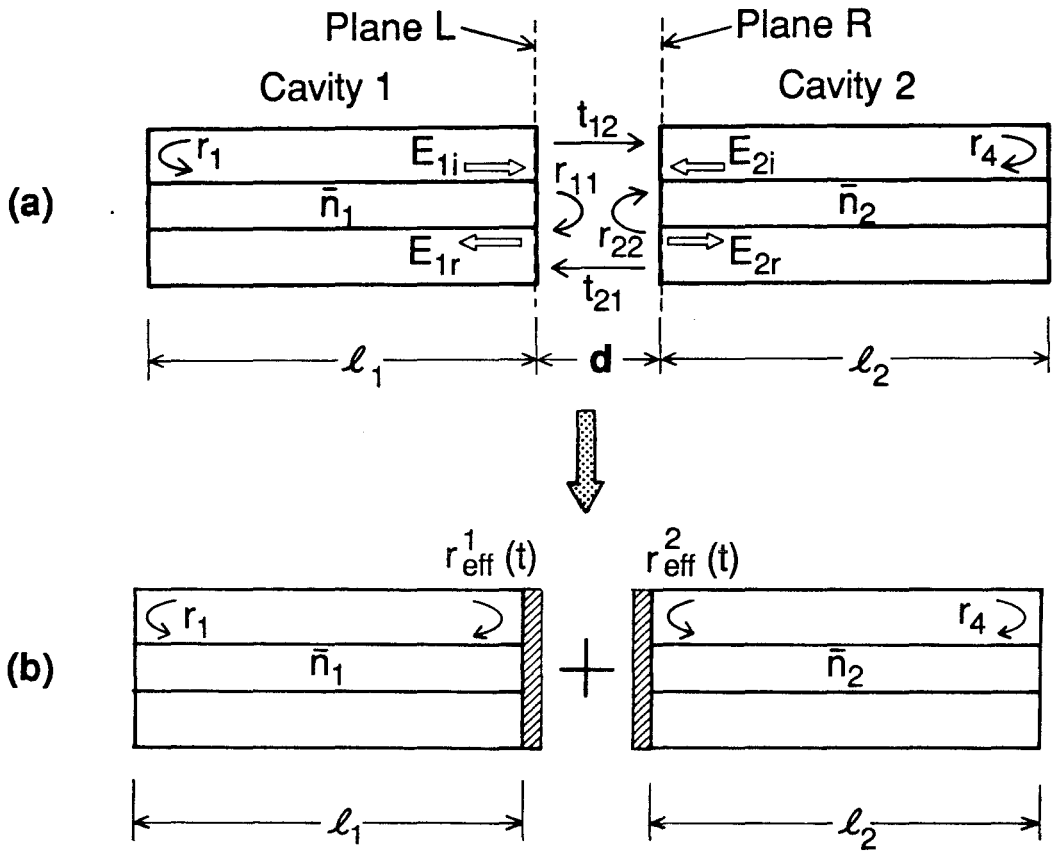

Figure 2.5 (a) Schematic of an axially coupled two-section semiconductor laser. (b) Each cavity of the two-section semiconductor laser is equivalent to a diode laser with an effective mirror.

2.4-C. An Axially Coupled Two-Section Diode Laser

An axially coupled two-section diode laser is illustrated in Figure 2.5a. It consists of two cavities of lengths l_1 and l_2 with facet reflectivity r_1 on one end and r_4 on the other end of the composite cavity. The coupling between the two cavities is characterized by the transmission and reflection coefficients t_{12}, t_{21}, r_{11}, and r_{22}, as shown in Figure 2.5a. Each cavity is equivalent to a solitary laser with an effective mirror. A single-mode laser with lasing frequency Ω is assumed in this section and in Chapter 5.

Following the discussion of Section 2.2, for the left effective mirror of Figure 2.5b, the incident wave from the left at plane L is

$$E_{1i}(t)e^{i\Omega t} = a_1 E_1(t)e^{i\Omega t}, \tag{2.43a}$$

and the wave travelling to the right at plane L is

$$E_{1r}(t)e^{i\Omega t} = r_{11}a_1 E_1(t)e^{i\Omega t} + t_{21}a_2 E_2(t)e^{i\Omega t}, \tag{2.43b}$$

where $E_j(t)$ is the complex amplitude of the optical field inside the jth cavity. The a_1 (a_2) is defined for points inside Cavity 1 (2), right next to the crystal-air boundary. The a_1 is the fraction of field $E_1(t)e^{i\Omega t}$ travelling from the left toward the right crystal-air boundary of Cavity 1, and a_2 is the fraction of field $E_2(t)e^{i\Omega t}$ travelling from the right toward the left crystal-air boundary of Cavity 2. Similarly, for the right effective mirror of that same figure, the incident wave from the right at plane R is

$$E_{2i}(t)e^{i\Omega t} = a_2 E_2(t)e^{i\Omega t}, \tag{2.43c}$$

and the wave travelling to the left at plane R is

$$E_{2r}(t)e^{i\Omega t} = r_{22}a_2 E_2(t)e^{i\Omega t} + t_{12}a_1 E_1(t)e^{i\Omega t}. \tag{2.43d}$$

For lasers with $a_1 = a_2$, these two factors will disappear in the effective reflectivities $r_{eff}^{(1)}(t)$ and $r_{eff}^{(2)}(t)$. For lasers with $a_1 \neq a_2$, these two factors can be incorporated into the transmission coefficients; i.e., $t'_{12} = (a_1/a_2)t_{12}$ and $t'_{21} = (a_2/a_1)t_{21}$. To simplify the situation, $a_1 = a_2$ will be assumed in this section and throughout Chapter 5.

Following the discussion given in Section 2.2, the two effective reflectivities $r_{eff}^{(1)}(t)$ and $r_{eff}^{(2)}(t)$ shown in Figure 2.5b are defined as

$$r_{eff}^{(1)}(t) = \frac{E_{1r}(t)}{E_{1i}(t)} \tag{2.44a}$$

for Cavity 1 and

$$r_{eff}^{(2)}(t) = \frac{E_{2i}(t)}{E_{2r}(t)} \tag{2.44b}$$

for Cavity 2, respectively. Substituting (2.43a)-(2.43d) into (2.44a) and (2.44b) yields

$$r_{eff}^{(1)}(t) = r_{11} + t_{21}\frac{E_2(t)}{E_1(t)} \tag{2.45a}$$

and

$$r_{eff}^{(2)}(t) = r_{22} + t_{12}\frac{E_1(t)}{E_2(t)}. \tag{2.45b}$$

Consider a two-section laser with two separate and isolated current sources. By adjusting its two pumping currents independently, one should be able to observe the time dependence in $E_2(t)/E_1(t)$. This means that the two effective reflectivities shown in (2.45a) and (2.45b) are truly functions of time. Therefore, the time-dependent effective photon lifetime is much more than a concept; it is a well-defined physical quantity.

For a single-mode axially coupled two-section diode laser, after invoking Equations (2.35), (2.45a) and (2.45b), one obtains the following set of nonlinear

optical-field equations:

$$\frac{d}{dt}E_1(t) - \Big[i\Big(\omega_1 - \Omega - \frac{\Gamma_1\chi_{1r}(n_1)\Omega}{2\bar{\mu}_1^2}\Big) + \frac{1}{2}\Big(\frac{\Gamma_1\chi_{1i}(n_1)\Omega}{\bar{\mu}_1^2} - \alpha_{1o} + \frac{c}{\bar{n}_1 l_1}\ln(r_1 r_{eff}^{(1)}(t))\Big)\Big]E_1(t) = \frac{\Delta_1(t)}{2i\Omega} \quad (2.46a)$$

$$\frac{d}{dt}E_2(t) - \Big[i\Big(\omega_2 - \Omega - \frac{\Gamma_2\chi_{2r}(n_2)\Omega}{2\bar{\mu}_2^2}\Big) + \frac{1}{2}\Big(\frac{\Gamma_2\chi_{2i}(n_2)\Omega}{\bar{\mu}_2^2} - \alpha_{2o} + \frac{c}{\bar{n}_2 l_2}\ln(r_4 r_{eff}^{(2)}(t))\Big)\Big]E_2(t) = \frac{\Delta_2(t)}{2i\Omega}, \quad (2.46b)$$

where for the jth cavity, Γ_j is the filling factor, ω_j is the m_jth resonant frequency of the unpumped cavity, $\chi_j(n) = \chi_{jr}(n) + i\chi_{ji}(n)$ is the susceptibility when the carrier density is n_j, $\bar{\mu}_j$ is the spatially averaged nonresonant contribution to refractive index, $\alpha_{jo}$is the waveguide loss, $\Delta_j(t)$ is the Langevin force term, $\bar{n}_j$ is the real refractive index in the active region, and l_j is the cavity length.

In the steady state, Equations (2.46a) and (2.46b) give

$$2i(\omega_1(n_{1o}) - \Omega)\frac{\bar{n}_1 l_1}{c} + \Big(\frac{\Gamma_1\chi_{1i}(n_{1o})\Omega}{\bar{\mu}_1^2} - \alpha_{1o}\Big)\frac{\bar{n}_1 l_1}{c} + \ln\Big(r_1\Big(r_{11} + t_{21}\frac{E_{2o}}{E_{1o}}\Big)\Big) = 0, \quad (2.47a)$$

$$2i(\omega_2(n_{2o}) - \Omega)\frac{\bar{n}_2 l_2}{c} + \Big(\frac{\Gamma_2\chi_{2i}(n_{2o})\Omega}{\bar{\mu}_2^2} - \alpha_{2o}\Big)\frac{\bar{n}_2 l_2}{c} + \ln\Big(r_4\Big(r_{22} + t_{12}\frac{E_{1o}}{E_{2o}}\Big)\Big) = 0, \quad (2.47b)$$

where n_{jo} is the steady-state carrier density and E_{jo} is the steady-state amplitude of the optical field inside the jth cavity. Since

$$\exp[2i\omega_1(n_{1o})\bar{n}_1 l_1/c] = \exp[2i\omega_2(n_{2o})\bar{n}_2 l_2/c] = 1,$$

Equations (2.47a) and (2.47b) can be rewritten as

$$\frac{1}{r_1 r_{11}}\exp\Big[i\Omega\frac{2\bar{n}_1 l_1}{c} - \frac{1}{2}\Big(\frac{\Gamma_1\chi_{1i}(n_{1o})\Omega}{\bar{\mu}_1^2} - \alpha_{1o}\Big)\frac{\bar{n}_1 l_1}{c}\Big] - 1 = \frac{t_{21}}{r_{11}}\frac{E_{2o}}{E_{1o}} \quad (2.48a)$$

$$\frac{1}{r_4 r_{22}}\exp[i\Omega\frac{2\bar{n}_2 l_2}{c}-\frac{1}{2}(\frac{\Gamma_2\chi_{2i}(n_{2o})\Omega}{\bar{\mu}_2^2}-\alpha_{2o})\frac{\bar{n}_2 l_2}{c}]-1=\frac{t_{12}}{r_{22}}\frac{E_{1o}}{E_{2o}}. \qquad (2.48b)$$

Putting Equations (2.48a) and (2.48b) together gives the eigenvalue equation derived by Henry and Kazarinov [10].

Consider the cases with the following conditions:

$$|\frac{t_{21}}{r_{11}}\frac{E_2(t)}{E_1(t)}|\ll 1, \qquad |\frac{t_{12}}{r_{22}}\frac{E_1(t)}{E_2(t)}|\ll 1. \qquad (2.49)$$

Equations (2.46a) and (2.46b) are reduced to a set of first-order differential equations:

$$\frac{d}{dt}E_1(t)-[i(\omega_1-\Omega-\frac{\Gamma_1\chi_{1r}(n_1)\Omega}{2\bar{\mu}_1^2})$$
$$+\frac{1}{2}(\frac{\Gamma_1\chi_{1i}(n_1)\Omega}{\bar{\mu}_1^2}-\alpha_{1o}+\frac{c}{\bar{n}_1 l_1}\ln(r_1 r_{11}))]E_1(t)+\frac{c}{2\bar{n}_1 l_1}\frac{t_{21}}{r_{11}}E_2(t)=\frac{\Delta_1(t)}{2i\Omega} \qquad (2.50a)$$

$$\frac{d}{dt}E_2(t)-[i(\omega_2-\Omega-\frac{\Gamma_2\chi_{2r}(n_2)\Omega}{2\bar{\mu}_2^2})$$
$$+\frac{1}{2}(\frac{\Gamma_2\chi_{2i}(n_2)\Omega}{\bar{\mu}_2^2}-\alpha_{2o}+\frac{c}{\bar{n}_2 l_2}\ln(r_4 r_{22}))]E_2(t)+\frac{c}{2\bar{n}_2 l_2}\frac{t_{12}}{r_{22}}E_1(t)=\frac{\Delta_2(t)}{2i\Omega}. \qquad (2.50b)$$

Apparently, the two optical fields $E_1(t)$ and $E_2(t)$ are coupled linearly only under the condition of (2.49). In most cases, as indicated in Equation (2.46a) and (2.46b), $E_1(t)$ and $E_2(t)$ are coupled together nonlinearly.

Comparing with Marcuse's coupled mode theory [3], the coupled Equations (2.46a) and (2.46b) do not have terms of cross-coupling and self-coupling among eigenfunctions of the composite cavity as well as individual cavities. In Marcuse's theory, the dynamics are oversimplified by considering one average photon density. Normally, as will be shown in Chapter 5, the two cavities have different average photon densities as indicated by Equations (2.46a) and (2.46b).

When there is no coupling, i.e., $t_{12}=t_{21}=0$, Equations (2.46a) and (2.46b) become, as expected, the equations of two uncoupled solitary lasers. Although

the optical-field equations (2.46a) and (2.46b) are much more complicated than Equations (2.38) or (2.42), a substantial amount of information regarding the characteristics of this laser can still be obtained [11]. Important results arising from these two equations will be given in Chapter 5.

2.5 Conclusion

By viewing a laser with an external coupling as a solitary laser with an effective mirror, the concepts of time-dependent effective reflectivity and complex, time-dependent effective photon lifetime have been introduced. A general formalism has been developed directly from Maxwell's wave equation. This formalism provides intuitive understanding of the physics involved in the external coupling. Its importance and significance will be fully realized in the following chapters. The optical-field equation derived from this formalism gives steady-state characteristics that agree with the resonant oscillation condition. With no external coupling, this equation becomes the optical-field equation for the solitary laser.

This formalism has been applied to obtain the optical-field equations for three different types of lasers. For the diode laser coupled to an external mirror, the derived equation takes into account multiple reflections that were neglected in Lang and Kobayashi's equation [1]. For the injection-locked diode laser, the equation obtained includes the amplitude reflectivity of the diode facet, which was overlooked by Lang [2]. For an axially coupled two-section diode laser, its optical-field equations give the steady-state condition, which agrees with those obtained by applying a resonant oscillation condition [6]. Compared with Marcuse's coupled mode theory [3], these equations were more general. The usefulness of these two equations will be demonstrated in Chapter 5.

References

[1] R. Lang and K. Kobayashi, *IEEE J. Quantum Electron.*, **QE-16**, 347, 1982.

[2] R. Lang, *IEEE J. Quantum Electron.*, **QE-18**, 976, 1980.

[3] D. Marcuse, *IEEE J. Quantum Electron.*, **QE-21**, 1819, 1985.

[4] K. Vahala and A. Yariv, *IEEE J. Quantum Electron.*, **QE-19**, 1102, 1983.

[5] A. Yariv, *Introduction to Optical Electronics* , 2nd ed., Holt, New York, 1976, p. 114.

[6] T. L. Koch and L. A. Coldren, *J. Appl. Phys.* **57**, 740, 1985.

[7] L.-T. Lu and A.Yariv, "Small signal analysis of a single-mode semiconductor laser coupled to an external mirror," unpublished.

[8] G. R. Hadley, *IEEE J. Quantum Electron.*, **QE-22**, 419, 1986.

[9] L.-T. Lu and A. Yariv, "Semiclassical theory of an injection-locked semiconductor laser," unpublished.

[10] C. H. Henry and R. F. Kazarinov, *IEEE J. Quantum Electron.*, **QE-20**, 733, 1984.

[11] L.-T. Lu and A. Yariv, "Dynamics and linewidth of an axially coupled two-section semiconductor laser," unpublished.

Chapter 3

Dynamics, Noise Properties, and Linewidth of Single-Mode Semiconductor Lasers Coupled to an External Mirror

3.1 Introduction

The characteristics of semiconductor lasers can be significantly improved by external feedback under appropriate conditions. For example, by coupling to an external grating, the laser linewidth can be reduced from on the order of 10 MHz to on the order of 10 KHz [1]. This linewidth reduction makes the semiconductor laser suitable for a number of applications requiring greater spectral purity such as coherent communications [2]. Furthermore, using a semiconductor laser coupled to an external cavity, a narrow-band signal transmitter in the Ku band frequency range (12-20 GHz) was demonstrated [3]. All these indicate that semiconductor lasers coupled to an external cavity are practical and important devices.

On the other hand, because of the non-ideal isolation provided by the optical isolator, a weak external feedback is unavoidable in practical applications of semiconductor lasers. In optical communication systems, for instance, this kind of unwanted reflection may come from the near end or the far end of the fiber link. Very often, such weak external feedback can drastically affect the performance of the semiconductor laser as well as the entire system.

In the past several years, because of these different and important aspects, the steady-state characteristics and noise properties of semiconductor lasers with

external feedback have been the subject of intensive study. The most widely employed approach to study this kind of laser is based on the optical-field equation introduced by Lang and Kobayashi [4]. However, as pointed out in Chapter 1, since it accounts only for the weak external feedback case, this equation is not appropriate for cases where light trapped for many round trips cannot be neglected. Recently, two papers [5] [6] considered the high Q passive external cavity. Although these papers gave the linewidth formula, many important experimental observations remain unexplained: the intensity noise data reported by Temkin et al. [8], the observations made by Cronin-Golomb et al. [21], that mode locking can be achieved only when biasing the laser near threshold, and the modulation response in the Ku-band frequency range obtained by Lau and Yariv [3]. Furthermore, as demonstrated in References [1], [3], and [7], these kinds of lasers have great potential in practical applications. Therefore, under these circumstances, a detailed study on the effect of strong optical feedback is necessary.

In this chapter, the coupling of an active Fabry-Perot semiconductor laser to a distant reflector will be considered. The coupling provides an arbitrary amount of feedback to the laser. This analysis will be based on the optical-field equation derived earlier in Chapter 2, which takes light trapped for many round trips into consideration. The major purpose of this chapter is twofold. One is to study lasers with strong external feedback, and the other is to show the usefulness of the general theory established in Chapter 2 through the accomplishments of this study.

In Section 3.2, the small-signal equations for the optical field and the carrier density will be derived. Based on these equations, the rest of this chapter will

be devoted to the subjects of noise, laser linewidth narrowing, and small-signal current modulation response. By including the carrier dependence of the refractive index and multiple reflections from the external mirror, the relative-intensity and frequency fluctuation spectra will be derived in Section 3.3. The experimental intensity noise data of Temkin et al. [8] will be explained. From this close examination, the major factor that prevents mode locking at higher DC current bias levels [21] will be identified. In the limit $r_3 \ll r_2$, it will be shown that these relative-intensity and frequency fluctuation spectra are equivalent to those of Spano et al. [9].

By ignoring the high-frequency structure in the field spectrum, a general method for obtaining the Lorentzian laser linewidth will be developed in Section 3.4. This method will be used to derive an analytical expression for laser linewidth which agrees with that reported by Kazarinov and Henry [5] and Hjelme and Mickelson [6]. It will also be shown that when $r_3 \ll r_2$, this linewidth formula gives the result derived by Agrawal [10] who applied Lang and Kobayashi's optical-field equation.

In Section 3.5, the small-signal equations of Section 3.2 will be used to obtain an analytical expression for the small-signal current modulation response. The results of this analysis will then be compared with experimental results reported by Lau and Yariv [3].

3.2 Small-Signal Equations for the Optical Field and Carrier Density

The optical field and carrier density are the two dynamic variables in describing the physics of semiconductor lasers. The equations of these variables are the starting point for studying the dynamics, spectral properties and noise char-

acteristics. Consequently, the optical-field equation derived in Chapter 2 and the equation of the carrier density will be briefly reviewed. Since these two equations are nonlinearly coupled and the small-signal analysis is a very fruitful technique in analyzing nonlinear and coupled equations, the small-signal equations for the optical field and the carrier density are indispensable and will be derived. These linearized equations will pave the way for the studies of the following sections.

A single-mode diode laser coupled to an external mirror is schematically depicted in Figure 3.1a. According to the theory presented in Chapter 2, this laser can be viewed as a solitary diode laser with one of its two facet mirrors replaced by an effective mirror (Figure 3.1b). The time-dependent effective reflectivity $r_{eff}(t)$ is given by Equation (2.3c) and, for convenience, is given below:

$$\begin{aligned} r_{eff}(t) = r_2 &+ r_3(1-r_2^2)e^{-i\Omega\tau}\frac{E(t-\tau)}{E(t)} \\ &- r_3(1-r_2^2)(r_2r_3)e^{-2i\Omega\tau}\frac{E(t-2\tau)}{E(t)} \\ &+ r_3(1-r_2^2)(r_2r_3)^2e^{-3i\Omega\tau}\frac{E(t-3\tau)}{E(t)} + \cdots, \end{aligned} \tag{3.1}$$

where $\tau = 2L/c$ is the external-cavity round-trip time of the optical field, $E(t)$ is the complex amplitude of the optical field, and Ω is the laser (average) frequency. r_1, r_2, and r_3 denote the amplitude reflectivities of the diode laser facets and the external mirror, respectively. The amplitude reflectivity r_3 of the external mirror includes all coupling, absorption, and diffraction losses during each round trip in the external cavity. In the steady state, Equation (3.1) gives the steady-state effective reflectivity

$$r_{eff}^{\circ}(\Omega) = \frac{r_2 + r_3e^{-i\Omega\tau}}{1 + r_2r_3e^{-i\Omega\tau}} \equiv r_2\tilde{r}e^{-i\theta}, \tag{3.2}$$

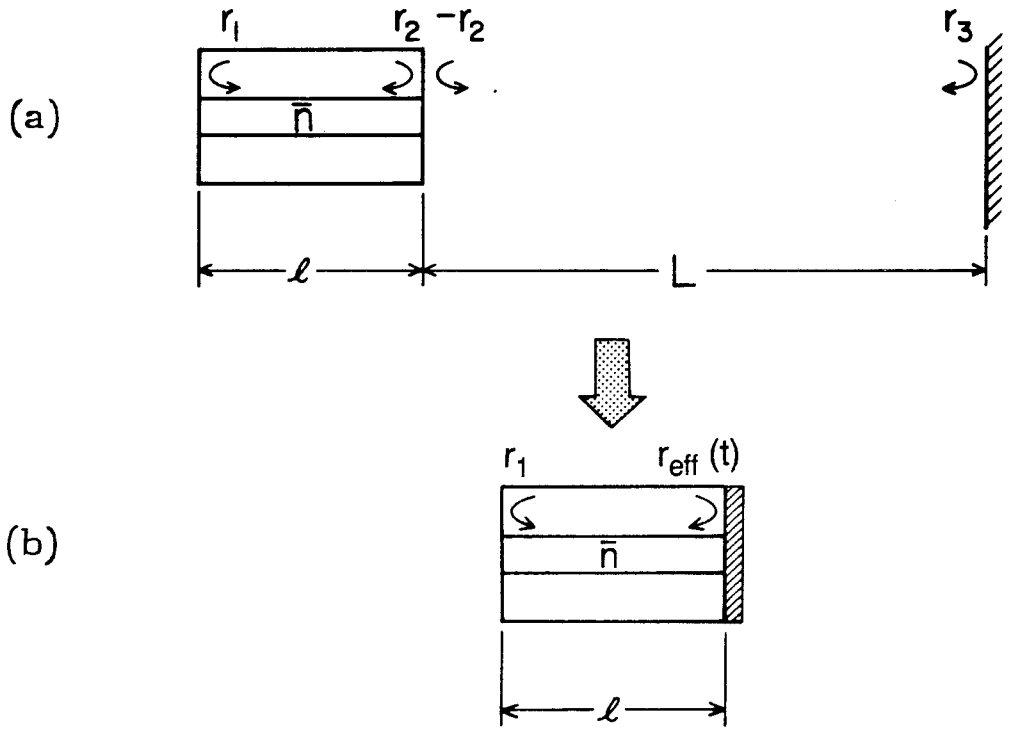

Figure 3.1 (a) Schematic of a single-mode semiconductor laser coupled to an external mirror. (b) A single-mode semiconductor laser coupled to an external mirror is equivalent to a diode laser with an effective mirror.

where $\tilde{r}$ and θ are real numbers. Clearly, this reflectivity depends strongly on the laser frequency Ω.

With the effective reflectivity $r_{eff}(t)$ given in Equation (3.1), the optical-field equation derived in Chapter 2 is

$$\frac{d}{dt}E(t)-\Big[i\Big(\omega_m-\Omega-\frac{\Gamma\chi_r(n)\Omega}{2\bar{\mu}^2}\Big) + \frac{1}{2}\Big(\frac{\Gamma\chi_i(n)\Omega}{\bar{\mu}^2}-\frac{1}{\tau_p^{sl}}+\frac{c}{\bar{n}l}\ln\frac{r_{eff}(t)}{r_2}\Big)\Big]E(t)=\frac{\Delta(t)}{2i\Omega}, \tag{3.3}$$

where ω_m is the mth resonant frequency of the unpumped and lossless diode cavity, Γ is the confinement factor resulting from the spreading of the optical field beyond the active region, $\bar{\mu}$ is the spatially averaged nonresonant index given by Equation (2.27a), $\bar{n}$ is the real refractive index of the active region, and l is the cavity length of the solitary diode laser. $\Delta(t)$ is the slowly varying complex amplitude of the Langevin force, which originates from spontaneous emission. $\chi_r(n)$ and $\chi_i(n)$ are the real and imaginary parts of the susceptibility $\chi(n)$, respectively, and n is the carrier density in the active region. τ_p^{sl} is the photon lifetime of the solitary semiconductor laser. In the limit $r_3 \ll r_2$, Equation (3.1) is reduced to

$$\ln\frac{r_{eff}(t)}{r_2}=(1-r_2^2)\frac{r_3}{r_2}e^{-i\Omega\tau}\frac{E(t-\tau)}{E(t)} \tag{3.4}$$

and Equation (3.3) becomes

$$\frac{d}{dt}E(t)-\Big[i\Big(\omega_m-\Omega-\frac{\Gamma\chi_r(n)\Omega}{2\bar{\mu}^2}\Big)+\frac{1}{2}\Big(\frac{\Gamma\chi_i(n)\Omega}{\bar{\mu}^2}-\frac{1}{\tau_p^{sl}}\Big)\Big]E(t) - \frac{c}{2\bar{n}l}\frac{r_3}{r_2}(1-r_2^2)e^{-i\Omega\tau}E(t-\tau)=\frac{\Delta(t)}{2i\Omega}. \tag{3.5}$$

As expected, dropping the Langevin noise term, Equation (3.5) becomes the equation introduced by Lang and Kobayashi [4].

The equation for the carrier density n is

$$\frac{dn}{dt} = -g(n)p - \frac{n}{\tau_s} + J(t) + \eta(t), \tag{3.6}$$

with $g(n) = \frac{\Gamma\Omega\chi_i(n)}{\bar{\mu}^2}$ and $p = \frac{\varepsilon_0\bar{\mu}^2}{2\hbar\Omega}|E|^2$, where g(n) is the gain, p is the photon density, τ_s is the spontaneous lifetime, J(t) is the pumping rate of carriers per unit volume, and $\eta(t)$ is the Langevin noise force associated with the discrete nature of the carrier generation and recombination process.

In Equations (3.3) and (3.6), the deviations caused by the Langevin forces are small when compared to their steady-state values. However, depending on the pumping source $J(t)$, the current-driven deviations can be in the large-signal regime or in the small-signal regime. Since the interest is in the small-signal regime, the laser considered is biased with a DC source J_o and a small time varying component $J_1(t)$ such that

$$|J_1(t)| \ll J_o.$$

Under this condition, the small-signal equations for the optical field and the carrier density are sufficient for studying all the subjects outlined in Section 3.1 and will be derived below. These equations will then be used throughout this chapter to derive analytical expressions for the frequency and the relative-intensity fluctuation spectra, the laser linewidth, and the small-signal current modulation response.

For the small-signal analysis, let

$$E(t) = (E_0 + E_1(t))e^{i\phi(t)} \tag{3.7a}$$

$$n(t) = n_0 + n_1(t), \qquad J(t) = J_0 + J_1(t) \tag{3.7b}$$

$$\chi(n) = \chi(n_0) + \xi n_1(t), \qquad E_0^2 + 2E_0E_1(t) = I_0 + I_1(t), \tag{3.7c}$$

where $E_1(t)$, $\phi(t)$, $n_1(t)$, $J_1(t)$, and $I_1(t)$ are real and time-dependent quantities, and their magnitude are small as compared to E_o, 1, n_o, J_o, and I_o, respectively. The $\xi = \xi_r + i\xi_i$ is the first-order Taylor coefficient in the expansion of

$$\chi(n) = \chi_r(n) + i\chi_i(n)$$

about the steady-state carrier density n_0. The small terms $E_1(t)$, $\phi(t)$, $n_1(t)$, $J_1(t)$, $I_1(t)$, and the Langevin forces ($\Delta(t)$ and $\eta(t)$) are assumed to have zero mean value. It is also assumed that the time variations of $E_1(t)$, $\phi(t)$, $n_1(t)$, $J_1(t)$, $I_1(t)$, $\Delta(t)$, and $\eta(t)$ are slow compared to the optical term $\exp(i\Omega t)$.

Neglecting products of small quantities and assuming $|\phi(t) - \phi(t - N\tau)| \ll \pi/2$ yields

$$\frac{1}{\tau_p^{eff}} = \frac{1}{\tau_p^{eff}} - \frac{c}{\bar{n}l}\ln\frac{r_{eff}(t)}{r_2} = \frac{1}{\tau_p^{sl}} - \frac{c}{\bar{n}l}\ln(\tilde{r}e^{-i\theta}) + H_R(t) + iH_I(t) \tag{3.8a}$$

with

$$\begin{aligned} H_R(t) =& \frac{c}{\bar{n}l}\frac{(1-r_2^2)}{\tilde{r}}\frac{r_3}{r_2}\{K_R\frac{E_1(t)}{E_0} - K_I\phi(t) \\ & - [\frac{E_1(t-\tau)}{E_0}\cos(\Omega\tau - \theta) + \phi(t-\tau)\sin(\Omega\tau - \theta)] \\ & + r_2r_3[\frac{E_1(t-2\tau)}{E_0}\cos(2\Omega\tau - \theta) + \phi(t-2\tau)\sin(2\Omega\tau - \theta)] \\ & -(r_2r_3)^2[\frac{E_1(t-3\tau)}{E_0}\cos(3\Omega\tau - \theta) + \phi(t-3\tau)\sin(3\Omega\tau - \theta)] + \cdots\} \end{aligned} \tag{3.8b}$$

and

$$\begin{aligned} H_I(t) =& \frac{c}{\bar{n}l}\frac{(1-r_2^2)}{\tilde{r}}\frac{r_3}{r_2}\{K_I\frac{E_1(t)}{E_0} + K_R\phi(t) \\ & - [\phi(t-\tau)\cos(\Omega\tau - \theta) + \frac{E_1(t-\tau)}{E_0}\sin(\Omega\tau - \theta)] \\ & + r_2r_3[\phi(t-2\tau)cos(2\Omega\tau - \theta) + \frac{E_1(t-2\tau)}{E_0}\sin(2\Omega\tau - \theta)] \\ & -(r_2r_3)^2[\phi(t-3\tau)cos(3\Omega\tau - \theta) + \frac{E_1(t-3\tau)}{E_0}\sin(3\Omega\tau - \theta)] + \cdots\}, \end{aligned} \tag{3.8c}$$

where

$$K_R \equiv \mathrm{Re}\Big[\frac{e^{-i(\Omega\tau-\theta)}}{1+r_2r_3e^{-i\Omega\tau}}\Big], \qquad K_I \equiv \mathrm{Im}\Big[\frac{e^{-i(\Omega\tau-\theta)}}{1+r_2r_3e^{-i\Omega\tau}}\Big]. \tag{3.8d}$$

Similarly, after using Equations (3.7a)-(3.8a) and neglecting products of small quantities, Equations (3.3) and (3.6) are linearized. The small-signal equations are

$$\dot{\phi}(t) + \frac{1}{2}\alpha g' n_1(t) + \frac{1}{2}H_I(t) = \frac{-\Delta_r(t)}{2\Omega I_0^{1/2}} \tag{3.9a}$$

$$\dot{I}_1(t) - g' I_o n_1(t) + I_0 H_R(t) = \frac{\Delta_i(t)}{\Omega} I_0^{1/2} \tag{3.9b}$$

$$\dot{n}_1(t) = -\frac{\Gamma\varepsilon_0}{2\hbar}\chi_i(n_0)I_1(t) - \frac{1}{\tau_R}n_1(t) + J_1(t) + \eta(t), \tag{3.9c}$$

where

$$\alpha \equiv \frac{\xi_r}{\xi_i}, \qquad g' \equiv \frac{\Gamma\xi_i\Omega}{\bar{\mu}^2}, \tag{3.10a}$$

and

$$\frac{1}{\tau_R} \equiv \Gamma\frac{\varepsilon}{2\hbar}\xi_i I_o + \frac{1}{\tau_s} = g' p_o + \frac{1}{\tau_s}. \tag{3.10b}$$

The α is the ratio of the real to the imaginary parts of refractive index and is referred commonly as the linewidth enhancement factor [11] [12] [13]. The g' is the differential optical gain constant, and the τ_R is the damping time constant in the relaxation oscillation of solitary semiconductor lasers.

The gain, the laser frequency, I_0, and n_0 for the steady state are determined by the following equations:

$$\frac{1}{\tau_p^{sl}} - \frac{c}{\bar{n}l}\ln\tilde{r} - g(n_o) = 0 \tag{3.11a}$$

$$\omega_m(n_o) - \Omega + \frac{c}{2\bar{n}l}\mathrm{Im}(\ln e^{-i\theta}) = 0 \tag{3.11b}$$

$$-\frac{\varepsilon_0}{2\hbar}\chi_i(n_0)I_0 - \frac{n_0}{\tau_s} + J_0 = 0, \tag{3.11c}$$

where the real quantities $\tilde{r}$ and θ are defined in Equation (3.5), $\omega_m(n_o)$ is the mth resonant frequency of the pumped and lossless cavity. The $\Delta_r(t)$ and $\Delta_i(t)$ are the real and imaginary parts of $\Delta(t)$, respectively. As pointed out in Chapter 2, Equations (3.11a) and (3.11b) are equivalent to the resonant oscillation condition [14],

$$r_1 r_{eff}^{o} \exp[(\frac{\Gamma \chi_i(n_o)\Omega}{\bar{\mu}^2} - \alpha_o)\bar{n}l/c - 2i\Omega\bar{n}l/c] = 1. \tag{3.12}$$

This means that the optical-field equations predict the resonant oscillation condition (3.12), which was obtained by viewing the laser as a Fabry-Perot resonator.

With the small current source $J_1(t)$ and the Langevin forces ($\Delta(t)$ and $\eta(t)$), Equations (3.9a)-(3.9c) are the small-signal equations of the single-mode semiconductor laser coupled to an external mirror. From Equations (3.9a) and (3.9b), in the small-signal regime with the multiple reflections included, $H_R(t)$ and $H_I(t)$ are the measures of the external feedback effect on the amplitude and the phase of the optical field, respectively. In addition, Equations (3.11a) and (3.11b) show how the external feedback, with the multiple reflections included, influences the average optical-field amplitude and the average laser frequency of the steady state.

3.3 Relative-Intensity and Frequency Fluctuation Spectra

Over the past twenty years, there have been intense theoretical and experimental investigations of semiconductor laser noise properties. In the following, the semiclassical theory of laser noise [15] will be applied to derive the relative-intensity and frequency fluctuation spectra. The unexplained intensity noise data of Temkin et al. [8] will be examined. Following this investigation, the unknown fundamental mechanism restricting the mode-locking phenomena will be studied.

Let $\delta_\phi(t)$, $\delta_I(t)$ and $\delta_n(t)$ be the noise-driven deviations of phase and intensity of the optical field and carrier density from the steady-state values, respectively. Setting $J_1(t) = 0$ in Equation (3.9c), Equations (3.9a)-(3.9c) become the noise-driven equations for $\delta_\phi(t)$, $\delta_I(t)$ and $\delta_n(t)$:

$$\dot{\delta}_\phi(t) + \frac{1}{2}\alpha g' \delta_n(t) + \frac{1}{2} H_I(t) = \frac{-\Delta_r(t)}{2\Omega I_0^{1/2}} \tag{3.13a}$$

$$\dot{\delta}_I(t) - g' I_o \delta_n(t) + I_0 H_R(t) = \frac{\Delta_i(t)}{\Omega} I_0^{1/2} \tag{3.13b}$$

$$\dot{\delta}_n(t) = -\frac{\varepsilon_0}{2\hbar}\chi_i(n_0)\delta_I(t) - \frac{1}{\tau_R}\delta_n(t) + \eta(t). \tag{3.13c}$$

The correlations of the Langevin forces of Equations (3.13a)-(3.13c) are given as follows [15] [16]:

$$< \Delta_i(t)\Delta_i(t') >=< \Delta_r(t)\Delta_r(t') >= W\delta(t-t') \tag{3.14a}$$

$$< \eta(t)\eta(t') >= W_2\delta(t-t'), \qquad < \eta(t)\Delta_i(t') >= W_1\delta(t-t') \tag{3.14b}$$

$$< \eta(t)\Delta_r(t') >= 0, \qquad < \Delta_i(t)\Delta_r(t') >= 0, \tag{3.14c}$$

with

$$\frac{W}{\Omega^2 I_o} = 2n_{sp}\frac{g}{p_o V}, \qquad \frac{W_1}{\Omega I_o^{1/2}} = -(2n_{sp}-1)\frac{g}{V_c}, \tag{3.15a}$$

and

$$W_2 = \frac{(2n_{sp}-1)gp_oV}{V_c^2} + \frac{n_o}{V_c\tau_s}, \tag{3.15b}$$

where n_{sp} is the ratio of the spontaneous emission rate into the lasing mode to the gain of that same mode [17] [18] [19], p_o is the steady-state photon number density, V_c is the volume occupied by the carriers, <> denotes ensemble average, and V is the average mode volume such that p_oV is the total photon number inside the diode cavity.

Since only the spectral density function will be considered, it is helpful to start with its definition. The spectral density for stationary random functions f(t) and g(t) is defined by the Wiener-Khintchine relation as

$$W_{fg}(\omega) = \int_{-\infty}^{+\infty} ds < f^*(t)g(t+s) > e^{-i\omega s}. \tag{3.16}$$

According to the Wiener-Khintchine relation, the relative-intensity noise spectrum $W_{\Delta I}(\omega)$ is defined by

$$W_{\Delta I}(\omega) = \frac{1}{I_o^2} \int_{-\infty}^{+\infty} ds < \delta_I^*(t)\delta_I(t+s) > e^{-i\omega s}, \tag{3.17a}$$

and the frequency fluctuation spectrum $W_{\Delta\omega}(\omega)$ is defined by

$$W_{\Delta\omega}(\omega) = \int_{-\infty}^{+\infty} ds < \dot{\delta}_\phi^*(t)\dot{\delta}_\phi(t+s) > e^{-i\omega s}. \tag{3.17b}$$

Because of the complexity of Equations (3.13a) and (3.13b), the Laplace transform method is not practical in deriving the noise spectra (3.17a) and (3.17b). Instead, as will be seen in the following, the Fourier transform method is a very powerful technique. For a square integrable function f(t), the Fourier transforms are defined by

$$\tilde{f}(\omega) = \int_{-\infty}^{+\infty} dt f(t) e^{-i\omega t}, \qquad f(t) = \frac{1}{2\pi} \int_{-\infty}^{+\infty} d\omega \tilde{f}(\omega) e^{i\omega t}.$$

Next, the major step will be to write the Wiener-Khintchine relation entirely in the frequency domain. Invoking the Fourier transform technique and taking the ensemble average of Equation (3.16), the Wiener-Khintchine relation can be written as

$$W_{fg}(\omega) = \frac{\delta\omega}{2\pi} < \tilde{f}^*(\omega)\tilde{g}(\omega) >, \tag{3.18}$$

where $\delta\omega/2\pi$ is the bandwidth resolution of the instrument used in the ensemble average. Therefore, the relative-intensity fluctuation spectrum is given by

$$W_{\Delta I}(\omega) = \frac{\delta\omega}{2\pi}\frac{1}{I_0^2} < \tilde{\delta}_I^*(\omega)\tilde{\delta}_I(\omega) >, \tag{3.19}$$

and the frequency fluctuation spectrum is given by

$$W_{\Delta\omega}(\omega) = \frac{\delta\omega}{2\pi}\omega^2 < \tilde{\delta}_\phi^*(\omega)\tilde{\delta}_\phi(\omega) > . \tag{3.20}$$

It will be seen in the following that Equations (3.19) and (3.20) are indispensable in deriving the relative-intensity fluctuation spectrum $W_{\Delta I}(\omega)$ and the frequency fluctuation spectrum $W_{\Delta\omega}(\omega)$.

Similarly, using Equation (3.18), the correlations given in (3.14a)-(3.14c) can also be expressed as

$$< \tilde{\Delta}_i^*(\omega)\tilde{\Delta}_i(\omega) >=< \tilde{\Delta}_r^*(\omega)\tilde{\Delta}_r(\omega) >= \frac{2\pi}{\delta\omega}W, \tag{3.21a}$$

$$< \tilde{\eta}^*(\omega)\tilde{\eta}(\omega) >= \frac{2\pi}{\delta\omega}W_2, \qquad < \tilde{\eta}^*(\omega)\tilde{\Delta}_i(\omega) >= \frac{2\pi}{\delta\omega}W_1, \tag{3.21b}$$

$$< \tilde{\eta}^*(\omega)\tilde{\Delta}_r(\omega) >= 0, \qquad < \tilde{\Delta}_i^*(\omega)\tilde{\Delta}_r(\omega) >= 0. \tag{3.21c}$$

With all these key ingredients obtained above, the relative-intensity noise and frequency fluctuation spectra will be derived in the following.

Taking the Fourier transforms of Equations (3.13a)-(3.13c) yields

$$[\frac{Q}{4} - \frac{\alpha\omega_R^2}{2(i\omega + 1/\tau_R)}]\frac{\tilde{\delta}_I(\omega)}{I_0} + (i\omega + P)\tilde{\delta}_\phi(\omega) = \frac{-\tilde{\Delta}_r(\omega)}{2\Omega I_0^{1/2}} - \frac{\alpha g'\tilde{\eta}(\omega)}{2(i\omega + 1/\tau_R)} \tag{3.22a}$$

$$[i\omega + P + \frac{\omega_R^2}{i\omega + 1/\tau_R}]\tilde{\delta}_I(\omega) - QI_0\tilde{\delta}_\phi(\omega) = \frac{\tilde{\Delta}_i(\omega)I_0^{1/2}}{\Omega} + \frac{g'\eta(\omega)I_0}{i\omega + 1/\tau_R} \tag{3.22b}$$

$$\tilde{\delta}_n(\omega) = \frac{1}{i\omega + 1/\tau_R}[-\frac{\varepsilon_0}{2\hbar}\chi_i(n_0)\tilde{\delta}_I(\omega) + \tilde{\eta}(\omega)], \tag{3.22c}$$

where

$$P(\omega) \equiv \kappa(R_2 - \frac{(1-r_2^2)r_3 C(\omega)}{2\tilde{r}r_2}) \tag{3.23a}$$

$$Q(\omega) \equiv \kappa(2I_2 + \frac{(1-r_2^2)r_3 D(\omega)}{i\tilde{r}r_2}) \tag{3.23b}$$

$$\omega_R^2 \equiv \frac{\Gamma^2 \xi_i \Omega I_0 \epsilon_0 \chi_i(n_0)}{2\hbar\bar{\mu}^2} = gg'p_o, \tag{3.23c}$$

with

$$C(\omega) \equiv e^{-i\omega\tau}[\frac{e^{i(\Omega\tau-\theta)}}{1+r_2r_3e^{-i\omega\tau}e^{i\Omega\tau}} + \frac{e^{-i(\Omega\tau-\theta)}}{1+r_2r_3e^{-i\omega\tau}e^{-i\Omega\tau}}] \tag{3.23d}$$

$$D(\omega) \equiv e^{-i\omega\tau}[\frac{e^{i(\Omega\tau-\theta)}}{1+r_2r_3e^{-i\omega\tau}e^{i\Omega\tau}} - \frac{e^{-i(\Omega\tau-\theta)}}{1+r_2r_3e^{-i\omega\tau}e^{-i\Omega\tau}}] \tag{3.23e}$$

$$R_2 \equiv (1-r_2^2)(\frac{r_3}{r_2})\mathrm{Re}[\frac{e^{-i\Omega\tau}}{1+\frac{r_3}{r_2}e^{-i\Omega\tau}}] \tag{3.23f}$$

$$I_2 \equiv (1-r_2^2)(\frac{r_3}{r_2})\mathrm{Im}[\frac{e^{-i\Omega\tau}}{1+\frac{r_3}{r_2}e^{-i\Omega\tau}}] \tag{3.23g}$$

and $\kappa = c/2\bar{n}l$. The $\omega_R/2\pi$ is commonly referred to as the relaxation oscillation frequency of the solitary semiconductor lasers. From Equations (3.22a) and (3.22b), solutions for $\tilde{\delta}_\phi(\omega)$ and $\tilde{\delta}_I(\omega)$ are

$$\tilde{\delta}_I(\omega) = \frac{\frac{QI_0^{1/2}}{2\Omega}\tilde{\Delta}_r(\omega) + g'I_0(\frac{\alpha Q}{2} - i\omega - P)\frac{\tilde{\eta}(\omega)}{i\omega+1/\tau_R} - (i\omega+P)I_0^{1/2}\frac{\tilde{\Delta}_i(\omega)}{\Omega}}{[\frac{\alpha\omega_R^2}{2(i\omega+1/\tau_R)} - \frac{Q}{4}]Q - (i\omega+P)[i\omega+P+\frac{\omega_R^2}{i\omega+1/\tau_R}]} \tag{3.24a}$$

$$\begin{aligned}\tilde{\delta}_\phi(\omega) =& \frac{[\frac{Q}{4} - \frac{\alpha\omega_R^2}{2(i\omega+1/\tau_R)}]\frac{\tilde{\Delta}_i(\omega)}{I_0^{1/2}\Omega} + g'(\frac{Q}{4} + \frac{\alpha}{2}(i\omega+P))\frac{\tilde{\eta}(\omega)}{i\omega+1/\tau_R}}{[\frac{\alpha\omega_R^2}{(2i\omega+1/\tau_R)} - \frac{Q}{4}]Q - (i\omega+P)[i\omega+P+\frac{\omega_R^2}{i\omega+1/\tau_R}]} \\ &+ \frac{(i\omega+P+\frac{\omega_R^2}{i\omega+1/\tau_R})\frac{\tilde{\Delta}_r(\omega)}{2\Omega I_0^{1/2}}}{[\frac{\alpha\omega_R^2}{(2i\omega+1/\tau_R)} - \frac{Q}{4}]Q - (i\omega+P)[i\omega+P+\frac{\omega_R^2}{i\omega+1/\tau_R}]}.\end{aligned} \tag{3.24b}$$

After substituting (3.24a) into (3.19) and using the correlations (3.21a)-(3.21c), the relative-intensity noise spectrum is

$$W_{\Delta I}(\omega) = \frac{(4|i\omega+P|^2+|Q|^2)\frac{W}{4\Omega^2 I_0}+(g')^2|\frac{\alpha}{2}Q-i\omega-P|^2\frac{W_2}{\omega^2+1/\tau_R^2}}{|[\frac{\alpha\omega_R^2}{2(i\omega+1/\tau_R)}-\frac{Q}{4}]Q-(i\omega+P)[i\omega+P+\frac{\omega_R^2}{i\omega+1/\tau_R}]|^2} - \frac{2\mathrm{Re}[g'\frac{(\frac{\alpha}{2}Q-i\omega-P)(-i\omega+P^*)W_1}{(i\omega+1/\tau_R)\Omega I_0^{1/2}}]}{|[\frac{\alpha\omega_R^2}{2(i\omega+1/\tau_R)}-\frac{Q}{4}]Q-(i\omega+P)[i\omega+P+\frac{\omega_R^2}{i\omega+1/\tau_R}]|^2}. \quad (3.25)$$

Following the same procedure, the frequency fluctuation spectrum is

$$W_{\Delta\omega}(\omega) = \frac{|\frac{\alpha\omega_R^2}{2(i\omega+1/\tau_R)}-\frac{Q}{4}|^2\frac{\omega^2 W}{\Omega^2 I_0}+|i\omega+P+\frac{\omega_R^2}{i\omega+1/\tau_R}|^2\frac{\omega^2 W}{4\Omega^2 I_0}}{|[\frac{\alpha\omega_R^2}{2(i\omega+1/\tau_R)}-\frac{Q}{4}]Q-(i\omega+P)[i\omega+P+\frac{\omega_R^2}{i\omega+1/\tau_R}]|^2} + \frac{2\mathrm{Re}\{(\frac{Q}{4}+\frac{\alpha}{2}(i\omega+P))[\frac{Q^*}{4}-\frac{\alpha\omega_R^2}{2(-i\omega+1/\tau_R)}]\frac{g'W_1\omega^2}{(i\omega+1/\tau_R)\Omega I_0^{1/2}}\}}{|[\frac{\alpha\omega_R^2}{2(i\omega+1/\tau_R)}-\frac{Q}{4}]Q-(i\omega+P)[i\omega+P+\frac{\omega_R^2}{i\omega+1/\tau_R}]|^2} + \frac{|\frac{Q}{4}+\frac{\alpha}{2}(i\omega+P)|^2(g')^2\frac{\omega^2 W_2}{\omega^2+1/\tau_R^2}}{|[\frac{\alpha\omega_R^2}{2(i\omega+1/\tau_R)}-\frac{Q}{4}]Q-(i\omega+P)[i\omega+P+\frac{\omega_R^2}{i\omega+1/\tau_R}]|^2}. \quad (3.26)$$

In the limit $r_3 \ll r_2$, these relative-intensity and frequency fluctuation spectra are equivalent to those of Spano et al. [9]. Clearly, when no feedback is present, the spectral density functions $W_{\Delta I}(\omega)$ and $W_{\Delta\omega}(\omega)$ given by Equations (3.25) and (3.26) are identical to those derived in [15].

In the following, Equation (3.25) will be used to study the unexplained experimental intensity fluctuation data reported by Temkin et al. [8]. Since the purpose of this study is to understand the basic physics involved in the intensity noise, only cases of single-mode operation with $e^{-i\Omega\tau} = 1$ will be considered. Under this condition, the relative-intensity noise spectrum (3.25) is simplified to

$$W_{\Delta I}(\omega) = \frac{\frac{W}{\Omega^2 I_o}+\frac{g'^2 W_2}{\omega^2+1/\tau_R^2}+2\mathrm{Re}[\frac{g'W_1}{(i\omega+1/\tau_R)\Omega I_o^{1/2}}]}{|i\omega+P_o(\omega)+\frac{\omega_R^2}{i\omega+1/\tau_R}|^2}, \quad (3.27)$$

with

$$P_o(\omega) = \frac{c}{2\bar{n}l}(1 - r_2^2)\frac{r_3}{r_2}\frac{1}{(1 + r_3/r_2)}\frac{e^{i\omega\tau} - 1}{e^{i\omega\tau} + r_2 r_3}. \tag{3.28}$$

Equation (3.27) shows that the effect of external feedback on $W_{\Delta I}(\omega)$ is governed by $P_o(\omega)$.

Physical quantities, with their values chosen close to the experimental settings of Temkin et al., used in the calculations, are $\tau = 0.4 \times 10^{-8}$ sec; $r_2 = 0.6$; $n_{sp} = 1.8$; $\bar{n}l = 1$ mm; $g = 0.5 \times 10^{12}\text{s}^{-1}$; $\tau_s = 3 \times 10^{-9}$ sec; $g' = 1 \times 10^{-6}\text{cm}^3\text{s}^{-1}$; $V_c = 3.0 \times 10^{-10}\text{cm}^3$; $V = 2V_c$; $\Gamma = 0.5$; and $n_o = 1 \times 10^{18}\text{cm}^{-3}$.

Figure 3.2a plots the calculated $W_{\Delta I}(\omega)$ versus ω for $r_3 = 0.219$ and $p_o = 1 \times 10^{14}\text{cm}^{-3}$. It shows that the calculated relative-intensity noise spectrum has the same features as that (Figure 3.2b) reported by Temkin et al. [8]. A large number of sharp and intense peaks can be explained with the periodic nature of $P_o(\omega)$. The periodic frequency of $P_o(\omega)$ is the external cavity round trip frequency. Similar to the relaxation oscillation peak of solitary diode lasers' intensity noise spectra [20], the envelope of these sharp and intense peaks has a relaxation oscillation peak, too. All these features are dictated by the denominator of Equation (3.27). Thus, the overall features can be considered as the superposition of features that come from $P_o(\omega)$ and $(i\omega + \frac{\omega_R^2}{i\omega + 1/\tau_R})$. The former contributes to the large number of sharp and intense peaks and the latter gives the relaxation oscillation peak in the envelope of the whole spectrum.

Temkin et al. reported that only when the laser is biased near threshold, the first harmonic of the entire series of sharp peaks occurs at the external round-trip frequency $\sim$ 252 MHz. With an increased bias current, the first harmonic shifts up to 310 MHz at $\sim 3.5 I_{th}$, a frequency offset of nearly 60MHz, and no further frequency offset could be observed at higher currents. Temkin et al. [8] made

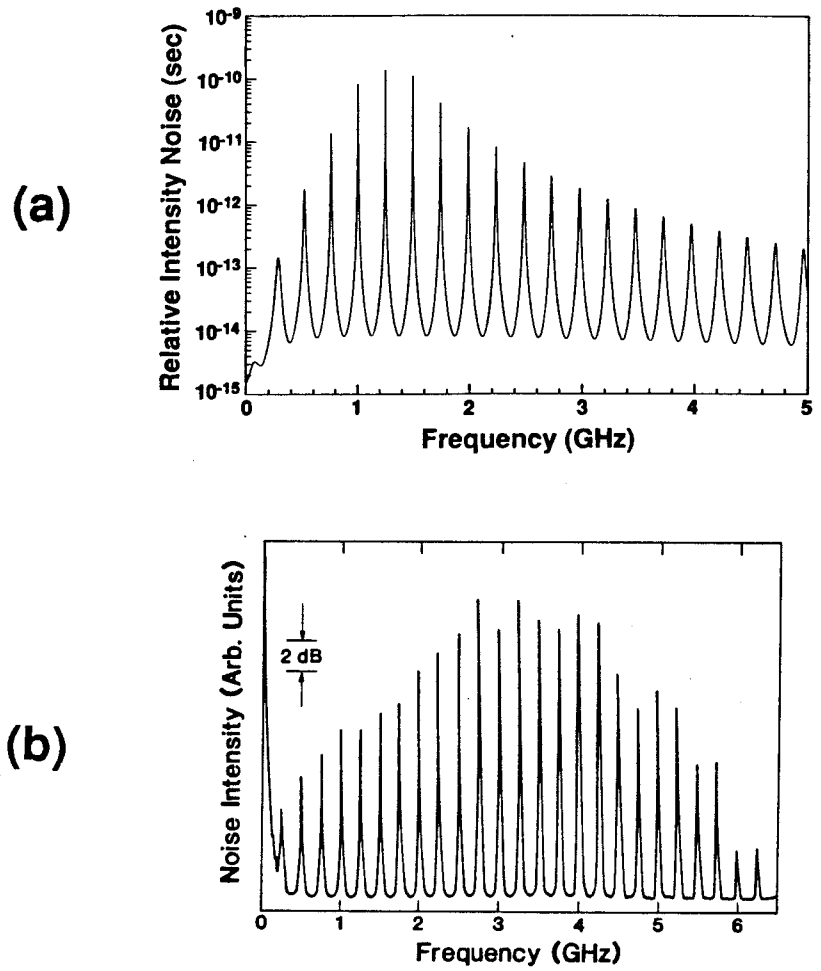

Figure 3.2 (a) The calculated relative-intensity noise spectrum at $p_o = 1 \times 10^{14}\text{cm}^{-3}$; (b) The experimental intensity noise spectrum of Temkin et al. [8].

a detailed measurement on the first-harmonic frequency offset versus the bias current (Figure 3.3a). From Figures 3.3a and 3.3b, there is a very good agreement between the experimental results of Temkin et al. [8] and calculated results (Figure 3.3b). Further discussion regarding this frequency offset will be given in the following.

Other than observing the occurrence of the first-harmonic frequency offset at higher bias current level, Cronin-Golomb et al. [21] also observed that when the noise spikes do not occur at the integral multiple of external cavity frequencies, mode locking can not be accomplished. In other words, mode locking will occur only when the diode laser is biased around the threshold. This interesting, important, and unexplained finding can be interpreted in the following way.

Apparently, it is the frequency offset discussed above that prevents the mode locking. Therefore, the fundamental mechanism that prevent the occurrence of the mode locking lies behind the frequency offset phenomenon. As already pointed out above, the frequency offset is the result of combining both factors $P_o(\omega)$ and $(i\omega+\frac{\omega_R^2}{i\omega+1/\tau_R})$. Around the threshold, the smaller ω_R^2 makes the second factor less important and, consequently, the frequency offset is at its minimum. On the other hand, at the higher bias level, the larger relaxation oscillation frequency ω_R makes the second factor more important, and the net result is a higher frequency offset. Therefore, the main mechanism of the frequency offset and the fundamental mechanism preventing the mode locking at high current level operation is the competition between the external-feedback periodic action to the field inside the diode cavity and the inherent relaxation oscillation response to this periodic external influence. Therefore, the precondition to mode lock diode lasers at the higher bias level is to use lasers with small relaxation

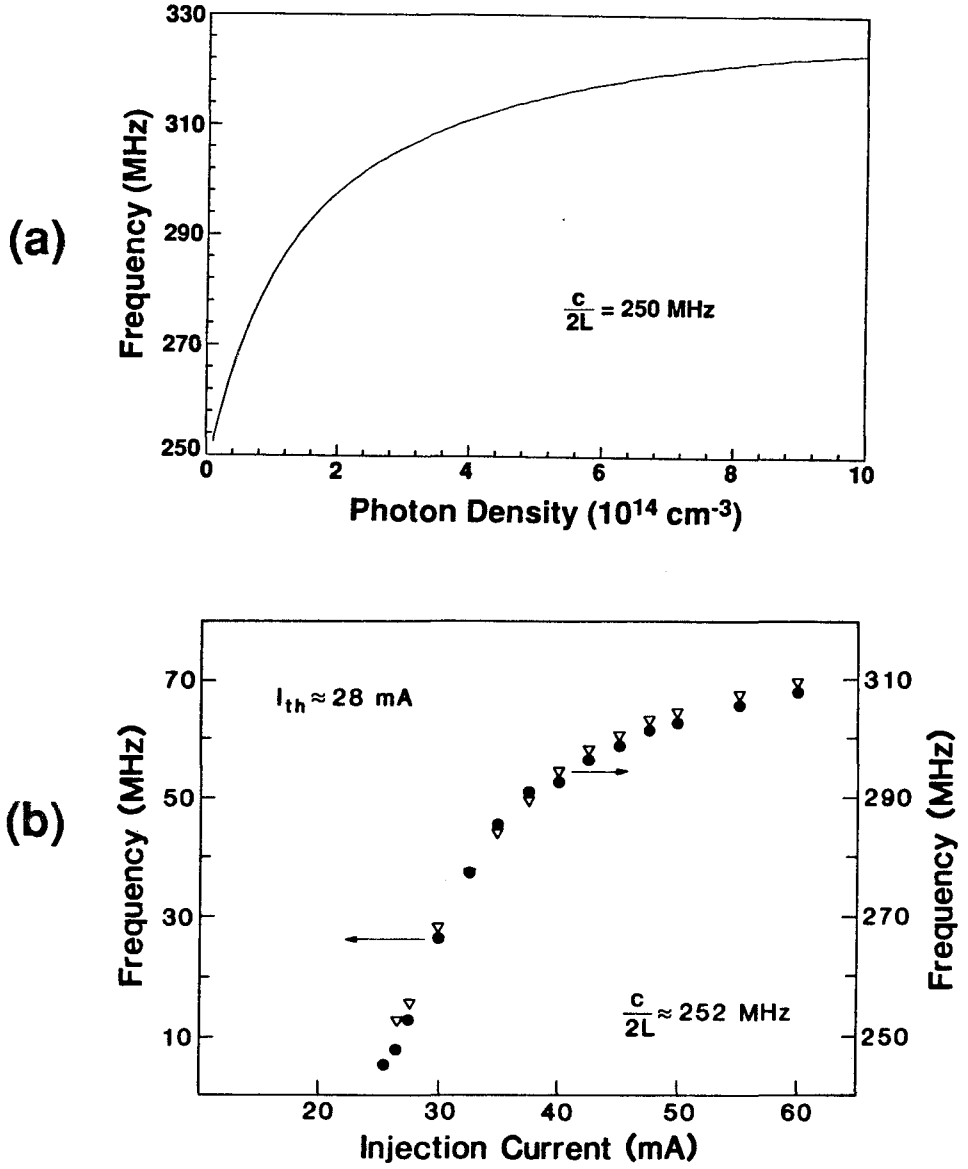

Figure 3.3 (a) The calculated first-harmonic frequency of the relative-intensity noise spectra versus photon density p_o inside the active region; (b) The experimental results on the biased current dependence of the first harmonic of the high- (open triangles) and the low- (solid dots) frequency noise components [8].

oscillation frequency ω_R.

Although Equation (3.27) does not give the low-frequency intensity noise component, subtracting the calculated first-harmonic frequency with the external cavity round trip frequency of 250 MHz gives the frequency of the low frequency noise component. Therefore, the low frequency noise was caused by the beating among different harmonics. This is supported by the simulations with a noise-driven multimode travelling wave mode reported recently [22].

3.4 Laser Linewidth

The linewidth is one of the most important properties of semiconductor lasers. Because of the carrier density dependence of the refractive index and the strong amplitude-phase coupling, the semiconductor laser linewidth is typically on the order of 10 MHz. This excessive large linewidth is inadequate for a number of applications requiring greater spectral purity. However, by using an external grating, the linewidth has been reduced to the order of 10 KHz [1]. This linewidth reduction will make external-cavity semiconductor lasers useful for many applications.

For the laser field $\mathcal{E}(t) = E(t)e^{i\Omega t}$, its spectral density function is

$$W_{EE}(\omega) = \int_{-\infty}^{+\infty} dt' < \mathcal{E}^*(t)\mathcal{E}(t+t') > e^{-i\omega t'}. \tag{3.29}$$

If the correlation between phase and amplitude fluctuations is neglected, one has

$$W_{EE}(\omega) = E_o^2 \int_{-\infty}^{+\infty} dt' \exp[-i(\omega-\Omega)t' - \frac{1}{2} < (\delta_\phi(t+t') - \delta_\phi(t))^2 >], \tag{3.30}$$

with

$$< (\delta_\phi(t+t') - \delta_\phi(t))^2 >= \frac{\delta\omega}{2\pi}\frac{1}{\pi}\left| \int_{-\infty}^{+\infty} d\omega < \tilde{\delta}_\phi^*(\omega)\tilde{\delta}_\phi(\omega) > (1 - e^{i\omega t'}) \right|. \tag{3.31}$$

For the solitary diode laser, Vahala and Yariv [15], using the Laplace transform technique, evaluated the field spectrum directly from (3.30). They found that the lineshape is Lorentzian in the center with high-frequency weak side mode structure on both sides of the spectrum.

As shown in Equation (3.30), the linewidth is intimately connected with the instantaneous phase $\delta_\phi(t)$ of the optical field. From the $\delta_\phi(\omega)$ shown in (3.24b), $\delta_\phi(t)$ is a complicated function of time. This implies that the derivation of the linewidth formula directly from (3.30) is a formidable task. In other words, the Laplace transform technique is not practical. In addition, through the use of (3.31), the contour integration technique [23] will not make the integration of (3.31) surmountable. Therefore, at first it is essential to find a new way for deriving the linewidth formula. Then, using the small-signal equations derived in Section 3.2, an analytical expression for the Lorentizan laser linewidth will be derived. This derivation will include the effects of the multiple reflections. This result will be compared with the results of Kazarinov and Henry [5], Hjelme and Mickelson [6], and Agrawal [10].

As mentioned above, the field spectrum of the solitary laser is predominantly Lorentzian. It is reasonable to assume that this is also true for semiconductor lasers with external coupling. Notice that the Lorentzian lineshape arises from the term in $< (\delta_\phi(t+t') - \delta_\phi(t))^2 >$, which is linearly proportional to $|t'|$. When integrating (3.31) by the contour integration technique, the contribution to this term comes solely from the simple pole $\omega = 0$ of the integrand

$$\frac{\delta\omega}{2\pi} < \tilde{\delta}_\phi^*(\omega)\tilde{\delta}_\phi(\omega) > (1 - e^{i\omega|t'|}). \tag{3.32}$$

Accordingly, after inspecting Equations (3.30) and (3.31), one can see that the

Lorentzian linewidth is given by

$$\Delta\nu_{sl} = \frac{1}{2\pi}\left|\frac{1}{t'}\mathrm{Res}(0)\right|, \tag{3.33}$$

where Res(0) is the residue of (3.32) at the simple pole $\omega = 0$.

Since (3.30) and (3.31) are for semiconductor lasers with or without external coupling, Equation (3.33) is true for lasers considered in this chapter as well as in the following two chapters. For solitary semiconductor lasers, it is easy to show that (3.33) indeed gives the same linewidth as that reported in [11] and [15].

Apparently, Equation (3.33) makes it possible to obtain the linewidth by knowing only the residue at the simple pole $\omega = 0$ of the integrand shown in Equation (3.31). For the external cavity laser diode, as $\omega \to 0$, Equation (3.24b) gives

$$\begin{aligned}\frac{\delta\omega}{2\pi} &< \tilde{\delta}_\phi^*(\omega)\tilde{\delta}_\phi(\omega) > (1 - e^{i\omega t'}) \\ &= \frac{t'[|\frac{i}{2}\omega\kappa\tau F_I - \frac{\alpha\omega_R^2}{2(i\omega+1/\tau_R)}|^2\frac{W}{\Omega^2 I_0} + |i\omega(1+\kappa\tau F_R) + \frac{\omega_R^2}{i\omega+1/\tau_R}|^2\frac{W}{4\omega^2 I_0}]}{i\omega|\alpha\kappa\tau F_I\frac{\omega_R^2}{i\omega+1/\tau_R} - (1+\kappa\tau F_R)[i\omega + i\omega\kappa\tau F_R + \frac{\omega_R^2}{i\omega+1/\tau_R}]|^2} \\ &\quad - \frac{2Re|t'|\{\frac{\alpha\Gamma g'\omega^2 W_1\omega_R^2}{2I_0^{1/2}\Omega(\omega^2+1/\tau_R^2)}[\frac{1}{2}\kappa\tau F_I + \frac{\alpha}{2}(1+\kappa\tau F_R)]\}}{i\omega|\alpha\kappa\tau F_I\frac{\omega_R^2}{i\omega+1/\tau_R} - (1+\kappa\tau F_R)[i\omega + i\omega\kappa\tau F_R + \frac{\omega_R^2}{i\omega+1/\tau_R}]|^2} \\ &\quad + \frac{|t'|(\Gamma g'\omega)^2|\frac{1}{2}\kappa\tau F_I + \frac{\alpha}{2}(1+\kappa\tau F_R)|^2\frac{W_2}{\omega^2+1/\tau_R^2}}{i\omega|\alpha\kappa\tau F_I\frac{\omega_R^2}{i\omega+1/\tau_R} - (1+\kappa\tau F_R)[i\omega + i\omega\kappa\tau F_R + \frac{\omega_R^2}{i\omega+1/\tau_R}]|^2}\end{aligned} \tag{3.34a}$$

where

$$F_I = (1-r_2^2)(\frac{r_3}{r_2})\mathrm{Im}[\frac{e^{-i\Omega\tau}}{(1+\frac{r_3}{r_2}e^{-i\Omega\tau})(1+r_2r_3e^{-i\Omega\tau})}] \tag{3.34b}$$

$$F_R = (1-r_2^2)(\frac{r_3}{r_2})\mathrm{Re}[\frac{e^{-i\Omega\tau}}{(1+\frac{r_3}{r_2}e^{-i\Omega\tau})(1+r_2r_3e^{-i\Omega\tau})}]. \tag{3.34c}$$

Clearly, the integrand (3.32) has a pole of order 1 at $\omega = 0$. Following the argument given above, assuming that other poles of the integrand make negligible

contributions to the field spectrum, and using (3.33), the linewidth $\Delta\nu$ is given by

$$\Delta\nu = \frac{\Delta\nu_{sl}}{(1+\frac{L}{\bar{n}l}(F_R - \alpha F_I))^2}\frac{(I_0)_{r_3=0}}{I_0}, \tag{3.35}$$

where $\Delta\nu_{sl}$ and $(I_o)_{r_3=0}$ are the linewidth and field intensity of the solitary semiconductor lasers, respectively.

From the linewidth formula given above, the effects of strong external feedback on the linewidth are determined by factors $L/\bar{n}l$, $(I_o)_{r_3=0}/I_o$, and $(F_R - \alpha F_I)$. Since the linewidth is inversely proportional to the energy stored in the cavity, for lasers with strong external feedback, the factor $L/\bar{n}l$ accounts for the increase in the Q factor or the energy stored in the composite cavity. The factor $(I_o)_{r_3=0}/I_o$ accounts for the change of field intensity created by the external feedback. The factor $(F_R - \alpha F_I)$ comes from the strong amplitude-phase coupling and the interference between the field inside the diode cavity and the field reflected back by the external reflector.

Equation (3.35) agrees with that derived by Kazarinov and Henry [5] and Hjelme and Mickelson [6]. In the absence of optical feedback, $F_I = 0$ and $F_R = 0$, the linewidth given in Equation (3.35) becomes that of the solitary laser. When $r_3 \ll r_2$, Equation (3.35) is reduced to

$$\Delta\nu = \frac{\Delta\nu_{sl}}{[1+\frac{L}{\bar{n}l}(1-r_2^2)(\frac{r_3}{r_2})(\cos\Omega\tau + \alpha\sin\Omega\tau)]^2}. \tag{3.36}$$

As expected, the linewidth given by Equation (3.36) is equivalent to the result derived by Agrawal [10], who applied the optical-field equation of Lang and Kobayashi [4].

To summarize, in this section, a method has been developed for obtaining the Lorentzian linewidth. The method has been applied to derive the linewidth formula for lasers with strong optical feedback.

3.5 Small-Signal Current Modulation Response

The modulation bandwidth of the solitary laser is widely accepted to be equal to the relaxation oscillation frequency $\omega_R/2\pi$. From Equation (3.23c), the relaxation oscillation frequency is

$$\frac{\omega_R}{2\pi} = \frac{1}{2\pi}\sqrt{\frac{g'p_0}{\tau_p^{sl}}}, \tag{3.48}$$

where $p_0 = \frac{\varepsilon_0\bar{\mu}^2}{2\hbar\Omega}I_0$ is the photon density and $g' = \frac{\Gamma\Omega\xi_i}{\bar{\mu}^2}$ is the differential optical gain constant. From Equation (3.48), the modulation bandwidth is dictated by the photon lifetime, the photon density and the differential optical gain constant. This basic understanding has led to the development of advanced laser structures, which can be modulated directly by modulating the pumping current at frequencies beyond 10 GHz [25]. On the other hand, Lau and Yariv [3] reported that the semiconductor laser can be directly modulated up to 18 GHz by using an external cavity. However, their results were not studied. In order to utilize all the advantages that the external cavity may offer, a basic understanding of how the external feedback affects the modulation characteristics is necessary. In this section, the small-signal current modulation response of a semiconductor laser coupled to an external mirror will be derived analytically. The experimental demonstration of Lau and Yariv will be examined.

From Equations (3.9a)-(3.9c), the small-signal equations for the deterministic components $I_1(t)$, $n_1(t)$ and $\phi_1(t)$, That are due to the modulation source $J_1(t)$, are

$$\dot{\phi}_1(t) + \frac{1}{2}\alpha g' n_1(t) + \frac{1}{2}H_I(t) = 0 \tag{3.49a}$$

$$\dot{I}_1(t) - g' I_o n_1(t) + I_0 H_R(t) = 0 \tag{3.49b}$$

$$\dot{n}_1(t) = -\frac{\varepsilon_0}{2\hbar}\chi_i(n_0)I_1(t) - \frac{1}{\tau_R}n_1(t) + J_1(t). \tag{3.49c}$$

Let

$$J_1(t) = \tilde{J}_1(\Omega_m)e^{i\Omega_m t}, \qquad I_1(t) = \tilde{I}_1(\Omega_m)e^{i\Omega_m t} \tag{3.50a}$$

$$n_1(t) = \tilde{n}_1(\Omega_m)e^{i\Omega_m t}, \qquad \phi_1(t) = \tilde{\phi}_1(\Omega_m)e^{i\Omega_m t}, \tag{3.50b}$$

where Ω_m is the frequency of the modulation current. Taking the Fourier transforms of Equations (3.49a)-(3.49c) yields

$$[\frac{Q}{4} - \frac{\alpha\omega_R^2}{2(i\omega + 1/\tau_R)}]\frac{\tilde{I}_1(\omega)}{I_0} + (i\omega + P)\tilde{\phi}_1(\omega) = -\frac{\alpha g' \tilde{J}_1(\omega)}{2(i\omega + 1/\tau_R)} \tag{3.51a}$$

$$[i\omega + P + \frac{\omega_R^2}{i\omega + 1/\tau_R}]\tilde{I}_1(\omega) - QI_0\tilde{\phi}_1(\omega) = \frac{g'\tilde{J}_1(\omega)}{i\omega + 1/\tau_R} \tag{3.51b}$$

$$\tilde{n}_1(\omega) = \frac{-1}{i\omega + 1/\tau_R}[\frac{\varepsilon_0}{2\hbar}]\chi_i(n_0)\tilde{I}_1(\omega) + \tilde{J}_1(\omega). \tag{3.51c}$$

From Equations (3.51a)-(3.51c), $\tilde{I}_1(\Omega_m)$ is given by

$$\tilde{I}_1(\Omega_m) = \frac{\Gamma g' I_0(\frac{\alpha Q}{2} - i\Omega_m - P)\frac{\tilde{J}(\Omega_m)}{i\Omega_m + 1/\tau_R}}{[\frac{\alpha\omega_R^2}{2(i\Omega_m + 1/\tau_R)} - \frac{Q}{4}]Q - (i\Omega_m + P)[i\Omega_m + P + \frac{\omega_R^2}{i\Omega_m + 1/\tau_R}]}. \tag{3.52}$$

Defining the normalized laser response as

$$A_{mod} = |\frac{\tilde{I}_1(\Omega_m)/\tilde{I}_1(0)}{\tilde{J}_1(\Omega_m)/\tilde{J}_1(0)}| \tag{3.53}$$

and using Equations (3.52) and (3.53), one obtains

$$A_{mod} = |\frac{(\frac{\alpha Q}{2} - i\Omega_m - P)\frac{\omega_R^2}{i\Omega_m + 1/\tau_R}}{[\frac{\alpha\omega_R^2}{2(i\Omega_m + 1/\tau_R)} - \frac{Q}{4}]Q - (i\Omega_m + P)[i\Omega_m + P + \frac{\omega_R^2}{i\Omega_m + 1/\tau_R}]}|. \tag{3.54}$$

As expected, when $r_3 = 0$, Equation (3.54) yields the normalized laser response

$$A_{mod} = \frac{\omega_R^2}{|-\Omega_m^2 + \omega_R^2 + i\frac{\Omega_m}{\tau_R}|} \tag{3.55}$$

for the solitary laser.

Assuming a semiconductor laser with $\omega_R = 6.28 \times 10^{10}$ radians/sec, $\bar{n}l = 800\bar{\mu}m$, $\alpha = -5$, $r_2 = 0.5477$, and $\tau_R^{-1} = 1.1 \times 10^{10} sec^{-1}$, the calculated A_{mod} is plotted in Figure 3.4b as a function of the modulation frequency Ω_m for different r_3. From Figure 3.4b , as the feedback coupling increases, the 3 dB modulation bandwidth is reduced, while the frequency of the resonance peak increases. These characteristics agree qualitatively with the experimental results shown in Figure 3.4a reported by Lau and Yariv [3].

3.6 Conclusion

Using the optical-field equation derived in the last chapter, which takes into account the effect of multiple reflections from the external mirror, the dynamics in the small-signal regime, the noise properties, and the laser linewidth of the semiconductor laser with external feedback have been studied. The small-signal equations for the optical field and the carrier density have been derived. Based on these small-signal equations, the analytical expressions for the frequency and the relative-intensity fluctuation spectra, the laser linewidth, and the small-signal current modulation response have also been derived. When there is no feedback, these derivations give the results for the solitary laser. Under the weak feedback condition, these derivations agree with the results derived by using Lang and Kobayashi's optical-field equation.

The analysis on the intensity fluctuation spectra have explained Temkin et al.'s [8] experimental results very well. The main mechanism of the first-harmonic frequency offset in the intensity noise spectrum is the interaction between the periodic beating from the external cavity and the inherent relaxation oscillation

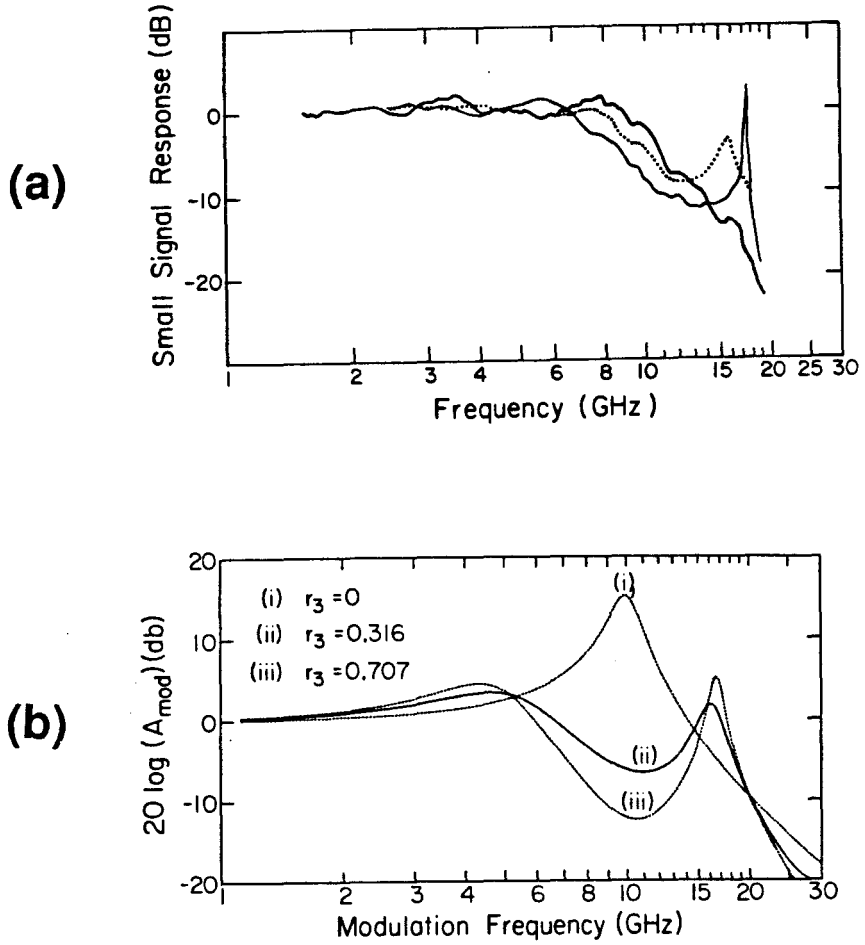

Figure 3.4 (a) Small-signal modulation response of a window BH on SI laser: (1) intrinsic laser response (dark solid curve), (2) weakly coupled to an external fiber cavity (dottet curve), and (3) with increased coupling (light solid curve) [3]; (b) The simulated small-signal modulation response A_{mod} for different r_3 with L = 0.577 cm and $\omega_m \tau = 10° + N \times 360°$, where N is an integer.

of the diode lasers. It has been found that the inherent relaxation oscillation prevents the mode locking of the diode lasers at higher bias current level.

A method has been developed for obtaining the Lorentzian linewidth. This method has been applied to obtain the linewidth formula for lasers with an arbitrary amount of optical feedback. Our linewidth formula agrees with that obtained by Kazarinov and Henry [5] and Hjelme and Mickelson [6]. It has been shown that the small-signal current modulation response of semiconductor lasers is drastically affected by external feedback. This analysis agrees qualitatively with the reported modulation response results of Lau and Yariv.

In summary, based on the optical-field equation derived in Chapter 2, a small-signal analysis of a single-mode semiconductor laser coupled to an external mirror has been presented. The analysis is useful, not only for understanding how the external feedback affects the laser properties, but also for giving guides on how to tailor the external parameters in practical applications. The optical-field equation derived in Chapter 2 has been successfully applied in the small-signal regime.

References

[1] R. Wyatt and W. J. Devlin, *Electron. Lett.*, **19**, 110, 1983.

[2] T. Kimura and Y. Yamamoto, *Opt. and Quantum Electron.*, **15**, 1, 1983.

[3] K. Y. Lau and A. Yariv, *Appl. Phys. Lett.*, **46**, 326, 1985.

[4] R. Lang and Kobayashi, *IEEE J. Quantum Electron.*, **QE-16**, 347, 1980.

[5] R. F. Kazarinov and C. H. Henry, *lEEE J. Quantum Electron.*, **QE-23**, 1401, 1987.

[6] D. R. Hjelme and A. R. Mickelson, *IEEE J. Quantum Electron.*, **QE-23**, 1401, 1987.

[7] R. Wyatt, *Electron. Lett.*, **21**, 658, 1985.

[8] H. Temkin, N. A. Olsson, J. H. Abeles, R. A. Logan, and M. B. Panish, *IEEE J. Quantum Electron.*, **QE-22**, 286, 1986.

[9] P. Spano, S. Piazzolla, and M. Tamburrini, *IEEE J. Quantum Electron.*, **QE-20**, 350, 1984.

[10] G. P. Agrawal, *IEEE J. Quantum Electron.*, **QE-20**, 468, 1984.

[11] C. H. Henry, *IEEE J. Quantum Electron.*, **QE-18**, 259, 1982.

[12] C. Harder, K. Vahala, and A. Yariv, *Appl. Phys. Lett.*, **42**, 328, 1983.

[13] K. Vahala, L. C. Chiu, S. Margalit, and A. Yariv, *Appl. Phys. Lett.*, **42**, 631, 1983.

[14] A. Yariv, *Introduction to Optical Electronics*, 2nd ed., Holt, New York, 1976, p. 114.

[15] K. Vahala and A. Yariv, *IEEE J. Quantum Electron.*, **QE-19**, 1102, 1983.

[16] C. Harder, J. Katz, S. Margalit, J. Shacham, and A. Yariv, *IEEE J. Quantum Electron.*, **QE-18**, 333, 1982.

[17] C. H. Henry, R. A. Logan, and F. R. Merritt, *J. Appl. Phys.*, **51**, 3042, 1980.

[18] D. Welford and A. Mooradian, *Appl. Phys. Lett.*, **40**, 865, 1982.

[19] C. H. Henry, R. A. Logan, H. Temkin, and F. R. Merritt, *IEEE J. Quantum Electron.*, **19**, 941, 1983.

[20] H. Jäckel and G. Guekos, *Opt. Quantum Electron*, **9**, 233, 1977.

[21] M. Cronin-Golomb, K. Y. Lau, and A. Yariv, *Appl. Phys. Lett.*, **47**, 567, 1985.

[22] J. Mork, B. Tromborg, and P. L. Christiansen, *IEEE J. Quantum Electron.*, **QE-24**, 123, 1988.

[23] F. B. Hildbrand, *Advanced Calculus for Applications* , Prentice Hall, New York, 1962.

[24] C. H. Henry, *J. Lightwave Technol.* **LT-4**, 288, 1986.

[25] For a review, see K. Y. Lau and A. Yariv, *IEEE J. Quantum Electron.*, **QE-21**, 121, 1985.

Chapter 4

Instability, Locking Bandwidth, Noise Properties, and Linewidth of Injection-Locked Semiconductor Lasers

4.1 Introduction

Injection locking has been demonstrated in electric oscillators, microwave oscillators, gas lasers, and semiconductor lasers. For semiconductor lasers, injection locking can be used to reduce the laser linewidth [1], suppress the relaxation-oscillation [2], and reduce the partition noise [3]. In coherent communication systems [4] [5] [6], the injection-locked diode laser may find practical applications. There have been many experimental and theoretical investigations on the injection locking of semiconductor lasers.

In Chapter 2, using the general formalism established in that chapter, the optical field equation for an injection-locked semiconductor laser was derived. The diode's facet reflectivity is an important parameter in this equation. This optical field equation will be the basis for the work presented in this chapter. The first purpose of this chapter is to shed light on the dynamics, noise properties and spectral characteristics of an injection-locked semiconductor laser. Another is to demonstrate the usefulness of the theory presented in Chapter 2.

In Section 4.2, the small-signal equations for the optical field as well as the carrier density and the steady-state condition will be derived. In Section 4.3-A, based on a simple physical picture, the origin of the facet reflectivity in the optical field equation will be explained. In Section 4.3-B, the steady-state

conditions will not only show the importance of the facet reflectivity but also provide an inside view of the locking mechanism.

Because of its importance, the subject of the locking bandwidth and the instability had drawn considerable attention despite the mathematical complexity involved [7] [8] [9] [10]. However, this subject was never fully examined. Only approximate analyses were given in the past, and the analytical expressions for the instability condition and the locking bandwidth remained unclear. In Section 4.3-C, the exact instability condition and locking bandwidth will be derived, and it will be shown that the exact locking bandwidth can be obtained numerically without difficulty. Based on this instability condition, the locking bandwidth data reported by Goldberg et al. [12] will be examined. Furthermore, the instability occurring only on the high-frequency side of the locking range [8] [11] will be explored, and the major physical parameter behind this asymmetry will be identified. Finally, a physical picture will be given to explain the connection between the instability and pulsating behavior.

The rest of this chapter will be devoted to the important subjects of noise and laser linewidth. Using the small-signal equations of Section 4.2, the frequency and relative-intensity noise spectra will be derived in Section 4.4. These results will be compared to those derived by Spano et al. [13]. The relative-intensity noise spectrum of diode lasers locked by a noiseless injected field will be examined. After that, the method established in Chapter 3 will be applied to evaluate the linewidth of the locked laser. It will be shown in general that the linewidth of the locked field is equal to that of the injected field.

4.2 Small-Signal Equations for the Optical Field and Carrier Density

In this section, the governing equations for the optical field and carrier density will first be briefly reviewed. Then, the small-signal equations for the optical field and carrier density will be derived. These small-signal equations will be the starting point for the results presented in Sections 4.3-C, 4.4, and 4.5. In addition, the steady-state condition obtained will be used in Section 4.3-B to determine the maximum locking range.

As shown in Chapter 2, using the concepts of time-dependent effective reflectivity and time-dependent effective photon lifetime, an injection-locked semiconductor laser can be veiwed as a solitary laser with one of its two facet mirrors replaced by an effective mirror. This is depicted schematically in Figures 4.1a and 4.1b. According to the theory presented in that chapter, the optical field equation of a single-mode injection-locked semiconductor laser is

$$\frac{d}{dt}E(t)-\Big[i\Big(\omega_m-\Omega-\frac{\Gamma\chi_r(n)\Omega}{2\bar{\mu}^2}\Big) + \frac{1}{2}\Big(\frac{\Gamma\chi_i(n)\Omega}{\bar{\mu}^2}-\frac{1}{\tau_p^{sl}}\Big)\Big]E(t)-\frac{c}{2\bar{n}l}\Big(\frac{t_2}{r_2}\Big)E_{in}(t)=\frac{\Delta(t)}{2i\Omega}, \qquad (4.1)$$

where $E_{in}(t)$ is the complex amplitude of the injected field just outside the cavity; E(t) is the complex amplitude of the field inside the injected diode cavity; ω_m is the mth resonant frequency of the unpumped and lossless solitary laser cavity; Ω is the laser (average) frequency; Γ is the confinement factor resulting from the spreading of the optical field beyond the active region; $\bar{\mu}$ is defined by Equation (2.27a) and is the spatially averaged nonresonant index; $\bar{n}$ is the real refractive index of the active region; l is the cavity length of the solitary diode laser; and $\Delta(t)$ is the slowly varying complex amplitude of the Langevin force that originates from the spontaneous emission. $\chi_r(n)$ and $\chi_i(n)$ are the real and imaginary parts

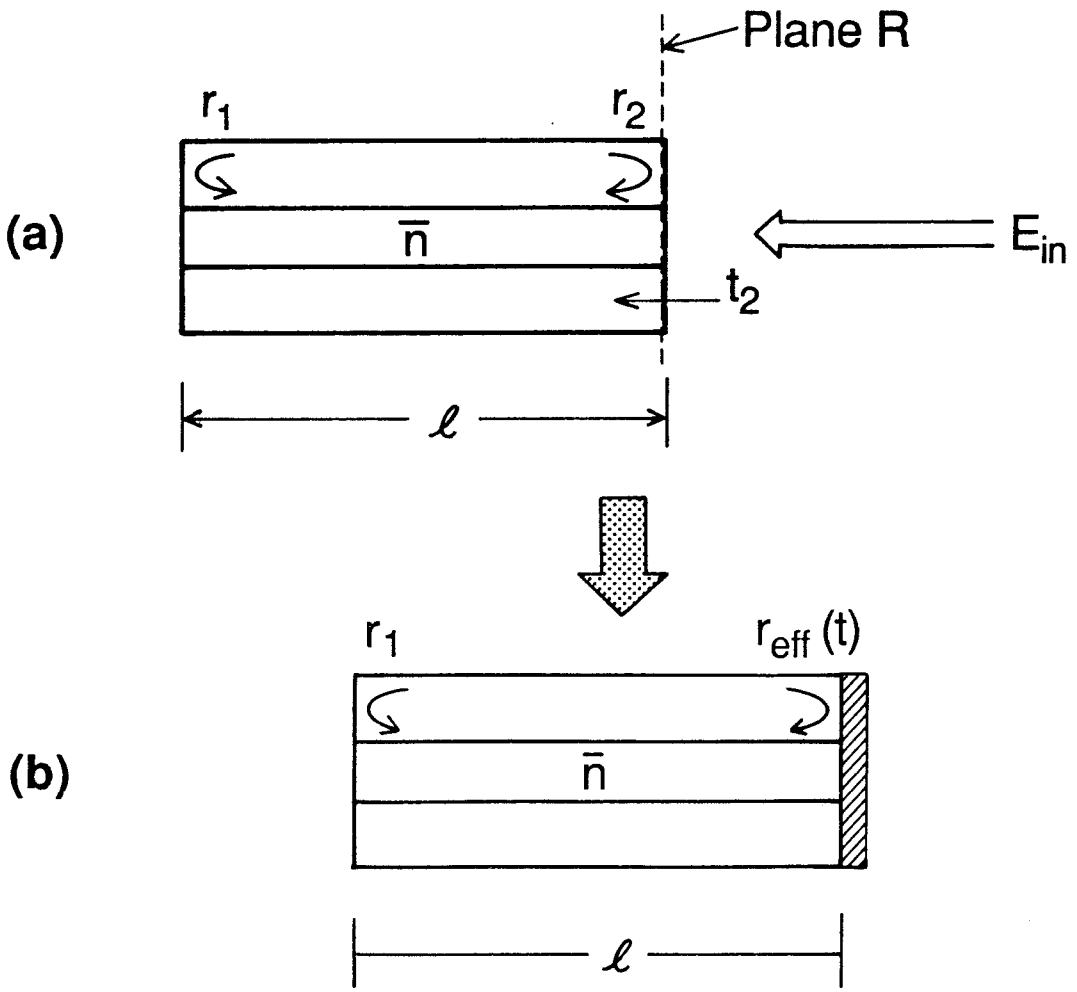

Figure 4.1 (a) Schematic of an injection-locked semiconductor laser. (b) The injection-locked semiconductor laser is equivalent to a solitary laser with one of its two facet mirrors replaced by an effective mirror which has a time-dependent effective reflectivity $r_{eff}(t)$.

of the susceptibility $\chi(n)$, respectively, and n is the carrier density in the active region. r_1 and r_2 denote the amplitude reflectivities of the diode laser's left and right facets, respectively. As shown in Figure 4.1a, the t_2 is the amplitude transmission coefficient from the air to the crystal cavity. τ_p^{sl} is the photon lifetime of the free-running semiconductor laser. Except the factor $1/r_2$ in the term

$$\frac{c}{2\bar{n}l}\frac{t_2}{r_2}E_{in}(t), \tag{4.2}$$

Equation (4.1) is the same as the equation introduced by Lang [8]. The origin of $1/r_2$ will be explained in Section 4.3-A.

The equation for the carrier density n is

$$\frac{dn}{dt} = -g(n)p - \frac{n}{\tau_s} + J(t) + \eta(t), \tag{4.3}$$

with $g(n) = \frac{\Gamma\Omega\chi_i(n)}{\bar{\mu}^2}$ and $p = \frac{\varepsilon_0\bar{\mu}^2}{2\hbar\Omega}|E|^2$, where g(n) is the gain, p is the photon density, τ_s is the spontaneous lifetime, J(t) is the pumping rate of carriers per unit volume, and $\eta(t)$ is the Langevin noise force associated with the discrete nature of the carrier generation and recombination process.

Since the lasers considered are biased with a DC pumping source J_o and a small time varying pumping source $J_1(t)$, the other driving forces to the optical field and carrier density are Langevin forces $\Delta(t)$ of Equation (4.1), $\eta(t)$ of Equation (4.3), and the random fluctuation of the injected field $E_{in}(t)$; i.e.,

$$E_{in}(t) = (E_{in,o} + E_{in,1}(t))e^{i\phi_{in}(t)}, \tag{4.4a}$$

where the subscript *in* denotes that that quantity is for the injected field. $E_{in,1}(t)$ is the real amplitude fluctuation, which is much smaller than $E_{in,o}$, and $\phi_{in}(t)$ is the random phase of the injected field. In writing (4.4a), it is assumed that the

injected field is emitted by a DC biased master laser. From (4.4a), the average intensity $I_{in,o}$ and intensity fluctuation $I_{in,1}(t)$ are given by

$$I_{in,o} = E_{in,o}^2, \qquad I_{in,1}(t) = 2E_{in,o}E_{in,1}(t). \tag{4.4b}$$

Similarly, for the optical field and the carrier density inside the diode cavity, one has

$$E(t) = (E_0 + E_1(t))e^{i\phi(t)}, \qquad \phi(t) = \phi_o + \phi_1(t) \tag{4.4c}$$

$$n = n_0 + n_1(t), \qquad J(t) = J_o + J_1(t), \qquad \chi(n) = \chi(n_0) + \xi n_1(t) \tag{4.4d}$$

$$E_0^2 + 2E_0E_1(t) = I_0 + I_1(t), \tag{4.4e}$$

where $E_1(t)$, $\phi(t)$, $n_1(t)$, $J_1(t)$ and $I_1(t)$ are real and time-dependent quantities and their magnitudes are small when compared to E_o, 1, n_o, J_o, and I_o, respectively. $\xi = \xi_r + i\xi_i$ is the first-order Taylor coefficient in the expansion of $\chi(n) = \chi_r(n) + i\chi_i(n)$ about the operating-point carrier density n_0. ξ_r and ξ_i are the real and imaginary parts of ξ, respectively. The small terms $E_1(t)$, $E_{in,1}(t)$, $\phi_1(t)$, $\phi_{in}(t)$, $n_1(t)$, $J_1(t)$, $I_1(t)$, and the Langevin forces ($\Delta(t)$ and $\eta(t)$) are assumed to have zero mean value. It is also assumed that the time variations of $E_1(t)$, $E_{in,1}(t)$, $\phi_1(t)$, $\phi_{in}(t)$, $n_1(t)$, $J_1(t)$, $I_1(t)$, $\Delta(t)$, and $\eta(t)$ are slow compared to the optical term $\exp(i\Omega t)$. The ϕ_o denotes the phase difference between the locked field E(t) and the injected field $E_{in}(t)$. It will be seen in the following sections that ϕ_o is a very important parameter.

By assuming $|\phi_1(t)| \ll \pi/2$ and $|\phi_{in}(t)| \ll \pi/2$, and neglecting products of small quantities, Equations (4.1) and (4.3) are linearized. The small-signal equations are

$$\dot{\phi}_1(t) + \omega_o \cos\phi_o\phi_1(t) - \frac{1}{2}\omega_o \sin\phi_o \frac{I_1(t)}{I_o} + \frac{1}{2}\alpha g' n_1(t)$$
$$= \omega_o \cos\phi_o\phi_{in}(t) - \frac{1}{2}\omega_o \sin\phi_o \frac{I_{in}(t)}{I_{in,o}} - \frac{\Delta_r(t)}{2\Omega I_0^{1/2}} \tag{4.5a}$$

$$\frac{\dot{I}_1(t)}{I_o} + \omega_o \cos\phi_o \frac{I_1(t)}{I_o} + 2\omega_o \sin\phi_o \phi_1(t) - g' n_1(t)$$
$$= \omega_o \cos\phi_o \frac{I_{in,1}(t)}{I_{in,o}} + 2\omega_o \sin\phi_o \phi_{in}(t) + \frac{\Delta_i(t)}{\Omega I_0^{1/2}} \quad (4.5b)$$

$$\dot{n}_1(t) = -\frac{\varepsilon_0}{2\hbar}\chi_i(n_0) I_1(t) - \frac{1}{\tau_R} n_1(t) + J_1(t) + \eta(t), \quad (4.5c)$$

where

$$\alpha \equiv \frac{\xi_r}{\xi_i}, \qquad g' \equiv \frac{\Gamma \xi_i \Omega}{\bar{\mu}^2}, \qquad \omega_o \equiv \frac{c}{2\bar{n}l}\frac{t_2}{r_2}\left(\frac{I_{in,o}}{I_o}\right)^{1/2}, \quad (4.6a)$$

and

$$\frac{1}{\tau_R} \equiv \Gamma \frac{\varepsilon}{2\hbar}\xi_i I_o + \frac{1}{\tau_s} = g' p_o + \frac{1}{\tau_s}. \quad (4.6b)$$

$\Delta_r(t)$ and $\Delta_i(t)$ are the real and imaginary parts of $\Delta(t)$, respectively. α is the ratio of the real to the imaginary parts of refractive index and is referred to commonly as the linewidth enhancement factor [14] [15]. g' is the differential optical gain constant, and τ_R is the damping time constant in the relaxation oscillation of solitary semiconductor lasers. ω_o defined in (4.6a) is an important quantity, a measure for the power ratio of the injected field to the field inside the diode cavity.

At the same time, the gain, the locked phase difference ϕ_o, I_o, and n_o for the steady state are determined by the following equations:

$$\frac{1}{\tau_p^{sl}} - 2\omega_o \cos\phi_o - g(n_o) = 0 \quad (4.7a)$$

$$\omega_m(n_o) - \Omega + \omega_o \sin\phi_o = 0 \quad (4.7b)$$

$$-g(n_o)p_o - \frac{n_0}{\tau_s} + J_0 = 0, \quad (4.7c)$$

where $\omega_m(n_o)$ is the mth resonant frequency of the pumped and lossless cavity. As pointed out in Chapter 2, Equations (4.7a) and (4.7b) are equivalent to the

resonant oscillation condition [16]

$$r_1 r_{eff}^{\circ} \exp[(\frac{\Gamma \chi_i(n_\circ)\Omega}{\bar{\mu}^2} - \alpha_\circ)\bar{n}l/c - 2i\Omega\bar{n}l/c] = 1$$

where $\alpha_\circ$ is the distributed wave-guide loss and

$$r_{eff}^{\circ} = r_2 + (t_2 I_{in,\circ}/I_\circ)^{1/2} \exp(i\phi_\circ)$$

is the steady-state effective reflectivity. Equations (4.5a)-(4.5c) will be used to analyze the stability in Section 4.3-c and to derive analytical expressions for the frequency and the relative-intensity fluctuation spectra in Section 4.4.

4.3 $1/r_2$, Locking Bandwidth, and Instability

4.3-A. Origin of the Factor $1/r_2$

As shown in Equation (4.1), the coupling between the injected field $E_{in}(t)$ and the locked field E(t) is given by the term shown in (4.2). Recall that the factor $1/r_2$ in the coupling term makes this optical field equation different from Lang's optical field equation. It is important to understand why the diode's facet reflectivity is a factor in the optical field equation. In the following, a simple physical picture will be given to explain that. Since the optical field equation (4.1) has been derived directly from the general formalism developed in Chapter 2, this will not be a substitution for the derivation shown before.

Recall that, as explained in Chapter 2, inside the diode cavity, there are always two components of the optical field propagating in opposite directions. At the points inside the cavity just to the left of the right crystal-air boundary, one component, $aE(t)e^{i\Omega t}$, is propagating from the left, and another component, $r_2 aE(t)e^{i\Omega t} + t_2 E_{in}(t)e^{i\Omega t}$, is propagating in the opposite direction. In the period of the round-trip time $2\bar{n}l/c$, the reflected field $r_2 aE(t)e^{i\Omega t}$ at the points

just to the left of right crystal-air boundary will be joined by the injected field $t_2 E_{in}(t)e^{i\Omega t}$. In other words, the injection-induced change of the field amplitude $r_2 aE(t)$ in the time interval $\delta t = 2\bar{n}l/c$ is $t_2 E_{in}(t)$; i.e.,

$$\frac{\delta(r_2 aE(t))}{\delta t} = \frac{c}{2\bar{n}l} t_2 E_{in}(t). \tag{4.8a}$$

In this chapter, uncoated or AR-coated lasers will be considered. Thus, from Chapter 2, one has $a \simeq 1$. Consequently, after moving r_2 to the right-hand side of Equation (4.8a), one has

$$\frac{\delta E(t)}{\delta t} = \frac{c}{2\bar{n}l} \frac{t_2}{r_2} E_{in}(t). \tag{4.8b}$$

This is just the coupling term given by (4.2).

Clearly, in this simple-minded physical picture, the factor $1/r_2$ is just a reminder that the injected field $t_2 E_{in}(t)$ is coupled with the field $r_2 E(t)$, which is propagating in the direction of the injected field. Therefore, decreasing r_2/t_2 will have the same effect as decreasing $E_{in}(t)$. This is consistent with Hadley's conclusion [18] that the power necessary to injection-lock an oscillator is proportional to $|r_1 r_2/t_2^2|$.

4.3-B. The Maximum Locking Range and $1/r_2$

In this section, based on Equations (4.7a)-(4.7c), a physical picture will be given to describe the locking mechanism. Then, the maximum locking range will be determined and its relation to $1/r_2$ will be pointed out. Before pursuing the subject, it is necessary to clarify the sign of the linewidth enhancement factor α, which plays a key role in many aspects of injection-locked semiconductor lasers. In the appendix of this chapter, a unique view of the fundamental and

yet overlooked aspect of this subject will be presented. The major finding of that appendix will be incorporated into the discussion given in the following.

The α defined in Equation (4.6a) can be rewritten as

$$\alpha = \frac{\Delta\mu_r}{\Delta\mu_i},$$

where μ_r and μ_i are the real and imaginary parts of the complex refractive index in the active region, respectively. However, the sign of α is dictated by the sign convention used in the exponential notation representation of the optical field. Throughout this thesis, the optical field is represented as $E(t)e^{i\Omega t}$, where $E(t)$ is the complex amplitude and Ω is the laser (average) frequency. The Fourier transforms defined in this thesis are also consistent with this representation. The Kramers-Kronig dispersion relation for the small changes $\Delta\mu_r$ and $\Delta\mu_i$ is

$$\Delta\mu_r(\omega) = -\frac{2}{\pi}\mathrm{P}\int_0^\infty \frac{\omega'\Delta\mu_i(\omega')d\omega'}{\omega'^2 - \omega^2},$$

where P denotes the principal value of the integral. This dispersion relation indicates that depending on the lasing frequency, α can be negative, zero, or positive. In most cases, the decrease in carrier density will cause a significant increase in refractive index and a decrease in gain. Furthermore, the change in gain is proportional to the change in μ_i. Accordingly, α is a negative number. Therefore, only lasers with negative α will be considered. In Section 4.3-C, it will be shown that this is the case, and there has been no report contradicting this assumption. Here, it is important to keep in mind that this assumption is valid only when the optical field is represented by $E(t)e^{i\Omega T}$ and the Fourier transforms are defined by (A.17).

From the schematic representation of the locking mechanism shown in Figure 4.2, a physical picture will be given below to explain the locking phenomenon.

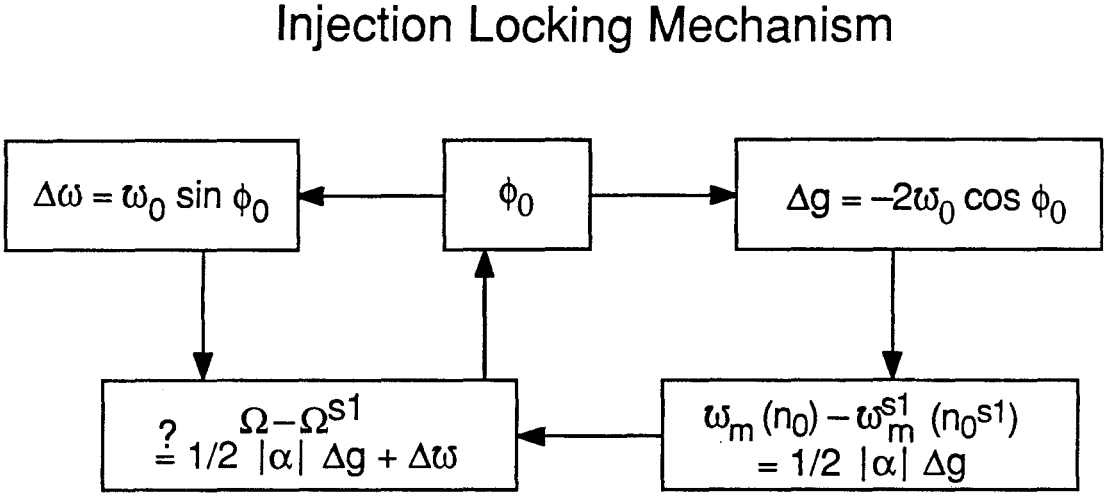

Figure 4.2 Schematic representation of the injection locking mechanism. The detuning is achieved by the threshold gain reduction and the locked phase ϕ_o. When the detuning synchronizes the lasing frequency with the injected field frequency, the diode laser is injection-locked.

This picture will then be used to find the maximum locking range. After encountering the injected field $t_2 E_{in}(t)$, with the same current pumping, the injection-locked laser will try to increase its own output power. This reduction of the threshold gain results in the reduction of the carrier density, which in turn increases the real refractive index of the active region. As a result, the mth pumped and lossless resonant frequency is shifted downward. In the meantime, the phase difference ϕ_o allows the locked laser to adjust its phase relationship with respect to $E_{in}(t)$ in order to synchronize its lasing frequency with that of the injected field.

Without the external injection, the steady state of the solitary diode laser is determined by

$$\frac{1}{\tau_p^{sl}} = g(n_o^{sl}), \qquad \omega_m(n_o^{sl}) = \Omega^{sl} \tag{4.9a}$$

$$-g(n_o^{sl})p_o^{sl} - \frac{n_o^{sl}}{\tau_s} + J_o = 0, \tag{4.9b}$$

where the sl denotes that the quantities that carry them are for the solitary diode laser. With the external injection, the detuning of the injection locking is defined as

$$\Delta\Omega = \Omega - \Omega^{sl}, \tag{4.9c}$$

where Ω is the lasing frequency of the injected field and Ω^{sl} is the original lasing frequency of the solitary laser.

According to Equation (4.7a), for injection-locked lasers, the threshold gain reduction is

$$\Delta g = -2\omega_o \cos\phi_o. \tag{4.9d}$$

As discussed above, this gain reduction leads to the carrier density's decreasing, which, in turn, changes the refractive index in the active region. The accompa-

nying change in the mth resonant frequency of the pumped and lossless solitary cavity is

$$\omega_m(n_o^{sl}) - \omega_m(n_o) = -\frac{|\alpha|}{2}\Delta g. \tag{4.9e}$$

Therefore, from Equations (4.7b), (4.9c), (4.9d), and (4.9e), the detuning is given by

$$\Delta\Omega = -\omega_o(|\alpha|\cos\phi_o - \sin\phi_o). \tag{4.10}$$

Equation (4.10) indicates that there are two contributions to the detuning. The first one is due to the threshold gain reduction and the carrier density dependence of the refractive index. The second term of Equation (4.10) is just the frequency shift introduced by Adler [20] to explain the locking of the radio frequency oscillator.

The optical field equation (4.1) is valid only when the laser is injection-locked and single-mode. However, when the threshold gain reduction is very small, the laser may lase with several longitudinal modes. To simplify the situation, lasers with two longitudinal modes will be considered. These two modes are $E_1(t)e^{i\Omega t}$ and $E_2(t)e^{i\Omega^{sl}t}$. Each mode obeys its own optical field equation. The power distribution between these two modes depends on their gain difference.

When the mode $E_1(t)e^{i\Omega t}$ dominates, the laser is injection-locked. On the other hand, when the mode $E_2(t)e^{i\Omega^{sl}t}$ dominates, the laser is unlocked and becomes a solitary laser. Therefore, the laser is injection-locked only under the condition that the Δg is negative; i.e., $\cos\phi_o$ is larger than zero. The range of the locked phase is from $-\pi/2$ to $\pi/2$. Accordingly, from Equation (4.10), the maximum locking range is from $-\omega_o(\alpha^2+1)^{1/2}$ to ω_o, although, as will be shown in Section 4.3-C, the laser is unstable in part of this locking range. Generally speaking, since ω_o is proportional to the factor t_2/r_2, Equation (4.10) suggests

that one can increase the locking range substantially by decreasing $|r_2/t_2|$.

4.3-C. Locking Bandwidth and Instability

The stability of the injection locking is an important subject and has received considerable attention [7] [8] [9] [10]. The pulsation instability, occurring near the high-frequency side of the maximum locking range, was recognized by Fye [21] and Lang [8]. The locking bandwidth or the range of stability has been studied by Mogensen et al. [9] and Petitbon et al. [10]. However, because of the mathematical complexity involved, they gave only approximate analytical results. The instability condition and the locking bandwidth remain unclear. For the same reason, physical insight about the asymmetric instability mentioned in Section 4.1 and the connection between the instability and pulsation were obscure. In this section, an exact analysis will be performed, and the instability condition will be given. It will be shown that the locking bandwidth obtained from this condition is in excellent agreement with the experimental results of Goldberg et al. [12]. Finally, a physical picture will be described to relate the instability and pulsation behaviour.

For the stability analysis, after a small perturbation, let $\Delta_I(t)$, $\Delta_\phi(t)$, and $\Delta_n(t)$ denote the small deviations from the stationary values of I_o, ϕ_o, and n_o, given by Equations (4.7a)-(4.7c). The driving forces of the small-signal Equations (4.5a)-(4.5c) are not important in this analysis and can be neglected. According to Equations (4.5a)-(4.5c), the equations governing $\Delta_I(t)$, $\Delta_\phi(t)$ and $\Delta_n(t)$ are given as follows:

$$\dot{\Delta}_\phi(t) + \omega_c \Delta_\phi(t) - \frac{1}{2}\omega_s \frac{\Delta_I(t)}{I_o} + \frac{1}{2}\alpha g' \Delta_n(t) = 0 \qquad (4.11a)$$

$$\frac{\dot{\Delta}_I(t)}{I_o} + \omega_c \frac{\Delta_I(t)}{I_o} + 2\omega_s \Delta_\phi(t) - g' \Delta_n(t) = 0 \qquad (4.11b)$$

$$\dot{\Delta}_n(t) = -\frac{\epsilon_o}{2\hbar}\chi_i(n_o)\Delta_I(t) - \frac{1}{\tau_R}\Delta_n(t), \tag{4.11c}$$

where

$$\omega_c = \omega_o \cos\phi_o, \qquad \omega_s = \omega_o \sin\phi_o. \tag{4.11d}$$

Assuming an exponential time-dependence, these deviations can be written as

$$\Delta_\phi(t) = \Delta_\phi e^{i\hat{\omega}t} \tag{4.12a}$$

$$\Delta_I(t) = \Delta_I e^{i\hat{\omega}t} \tag{4.12b}$$

$$\Delta_n(t) = \Delta_n e^{i\hat{\omega}t}, \tag{4.12c}$$

where $\hat{\omega}$ is a complex frequency and is given by

$$\hat{\omega} = \omega_r + i\omega_i. \tag{4.13}$$

ω_r and ω_i are the real and imaginary parts of $\hat{\omega}$, respectively. This complex $\hat{\omega}$ indicates that only when $\omega_i > 0$ will the perturbation decay. Otherwise, the laser is not stable. Substituting Equations (4.12a)-(4.12c) into Equations (4.11a)-(4.11c) yields an equation for $\hat{\omega}$:

$$\hat{\omega}^3 - i(\frac{1}{\tau_R} + 2\omega_c)\hat{\omega}^2 - [2\frac{1}{\tau_R}\omega_c + \omega_o^2 + \omega_R^2]\hat{\omega} + i[\frac{1}{\tau_R}\omega_o^2 + \omega_R^2(\omega_c + \alpha\omega_s)] = 0. \tag{4.14}$$

When

$$a_1 \equiv -(\omega_R^2 + 2\frac{\omega_c}{\tau_R} + \omega_o^2) + \frac{1}{3}(2\omega_c + \frac{1}{\tau_R})^2 < 0,$$

from Reference [22], the three roots $\hat{\omega}_1$, $\hat{\omega}_2$, and $\hat{\omega}_3$ of the cubic Equation (4.14) are

$$\hat{\omega}_1 = \frac{i}{3}(2\omega_c + \frac{1}{\tau_R}) + 2\sqrt{\frac{-a_1}{3}}\cos\theta_1 \tag{4.15a}$$

$$\hat{\omega}_2 = \frac{i}{3}(2\omega_c + \frac{1}{\tau_R}) + 2\sqrt{\frac{-a_1}{3}}\cos(\theta_1 + \frac{2\pi}{3}) \tag{4.15b}$$

$$\hat{\omega}_3 = \frac{i}{3}(2\omega_c + \frac{1}{\tau_R}) + 2\sqrt{\frac{-a_1}{3}}\cos(\theta_1 + \frac{4\pi}{3}), \tag{4.15c}$$

with

$$\theta_1 \equiv \begin{cases} \frac{\pi}{6} - \frac{i}{3}\sinh^{-1}\mathcal{Q} & \text{for} \quad a_2 > 0 \\ \frac{\pi}{6} + \frac{i}{3}\sinh^{-1}\mathcal{Q} & \text{for} \quad a_2 < 0, \end{cases}$$

where

$$a_2 \equiv \frac{1}{27}\{2(2\omega_c + \frac{1}{\tau_R})^3 - 9(2\omega_c + \frac{1}{\tau_R})(\omega_R^2 + 2\frac{\omega_c}{\tau_R} + \omega_o^2) + 27[\omega_o^2/\tau_R + \omega_R^2(\omega_c + \alpha\omega_s)]\}$$

and

$$\mathcal{Q} \equiv \left|\frac{3a_2}{2a_1}\sqrt{\frac{3}{-a_1}}\right|.$$

Since the stability condition is $\omega_i > 0$, from (4.15a)-(4.15c), it is given by

$$\begin{cases} \frac{1}{3}(2\omega_c + \frac{1}{\tau_R}) - 2\sqrt{\frac{-a_1}{3}}\sinh[\frac{1}{3}\sinh^{-1}\mathcal{Q}] > 0 & \text{for} \quad a_2 < 0 \\ \frac{1}{3}(2\omega_c + \frac{1}{\tau_R}) - \sqrt{\frac{-a_1}{3}}\sinh[\frac{1}{3}\sinh^{-1}\mathcal{Q}] > 0 & \text{for} \quad a_2 > 0. \end{cases} \tag{4.16a}$$

Similarly, with $a_1 > 0$, the stability condition is

$$\begin{cases} \frac{1}{3}(2\omega_c + \frac{1}{\tau_R}) - 2\sqrt{\frac{a_1}{3}}\cosh[\frac{1}{3}\cosh^{-1}\mathcal{Q}] > 0 & \text{for} \quad \mathcal{Q} > 1, \quad a_2 < 0 \\ \frac{1}{3}(2\omega_c + \frac{1}{\tau_R}) - \sqrt{\frac{a_1}{3}}\cosh[\frac{1}{3}\cosh^{-1}\mathcal{Q}] > 0 & \text{for} \quad \mathcal{Q} > 1, \quad a_2 > 0 \\ \frac{1}{3}(2\omega_c + \frac{1}{\tau_R}) + 2\sqrt{\frac{a_1}{3}} \times \mathcal{MIN} > 0 & \text{for} \quad \mathcal{Q} \le 1, \end{cases} \tag{4.16b}$$

where $\mathcal{MIN}$ denotes the smallest number of

$$\cos[\frac{1}{3}\cos^{-1}(\frac{3a_2}{2a_1}\sqrt{\frac{3}{a_1}})], \qquad \cos[\frac{1}{3}\cos^{-1}(\frac{3a_2}{2a_1}\sqrt{\frac{3}{a_1}}) + \frac{2\pi}{3}]$$

and

$$\cos[\frac{1}{3}\cos^{-1}(\frac{3a_2}{2a_1}\sqrt{\frac{3}{a_1}}) + \frac{4\pi}{3}].$$

Although the stability condition given above can be applied to yield the maximum locking bandwidth without difficulty, from (4.16a) and (4.16b), there is no clear indication that the pulsation instability occurs on the high-frequency side of the maximum locking range. To fill this gap, a second analysis will be performed below.

Mathematically, the boundary between the stability and instability of the lasers is presumably drawn by the condition that Equation (4.14) have real $\hat{\omega}$. Therefore, to consider $\hat{\omega}$ in the vicinity of this boundary, one may be able to determine the stability condition. Let

$$\hat{\omega} = \omega_r + i\delta_\omega, \tag{4.17}$$

where δ_ω is real and $|\delta_\omega| \ll 1$. Substituting (4.17) into Equation (4.14) yields:

$$\omega_r^3 + 3i\omega_r^2\delta_\omega - i(\frac{1}{\tau_R} + 2\omega_c)(\omega_r^2 + 2i\omega_r\delta_\omega)$$

$$-[\frac{2}{\tau_R}\omega_c + \omega_o^2 + \omega_R^2](\omega_r + i\delta_\omega) + i[\frac{1}{\tau_R}\omega_o^2 + \omega_R^2(\omega_c + \alpha\omega_s)] + O(\delta_\omega^2, \delta_\omega^3) = 0, \tag{4.18}$$

where $O(\delta_\omega^2, \delta_\omega^3)$ denotes terms with order of δ_ω^2 or δ_ω^3. Equating the real and imaginary parts of (4.18) and neglecting $O(\delta_\omega^2, \delta_\omega^3)$, one obtains

$$\omega_r^3 + 2\omega_r\delta_\omega(\frac{1}{\tau_R} + 2\omega_c) - [\frac{2}{\tau_R}\omega_c + \omega_o^2 + \omega_R^2]\omega_r = 0 \tag{4.19a}$$

and

$$3\omega_r^2\delta_\omega - \omega_r^2(\frac{1}{\tau_R} + 2\omega_c) - \delta_\omega[\frac{2}{\tau_R}\omega_c + \omega_o^2 + \omega_R^2]$$

$$+[\frac{1}{\tau_R}\omega_o^2 + \omega_R^2(\omega_c + \alpha\omega_s)] = 0. \tag{4.19b}$$

From Equations (4.19a) and (4.19b), ω_r and δ_ω are given as $\hat{\omega}$:

$$\omega_r = 0, \qquad \delta_\omega \simeq \frac{\omega_o^2/\tau_R + \omega_R^2(\omega_c + \alpha\omega_s)}{2\omega_c/\tau_R + \omega_o^2 + \omega_R^2}$$

or

$$\omega_r^2 \simeq \frac{2}{\tau_R}\omega_c + \omega_o^2 + \omega_R^2,$$

$$2\delta_\omega \simeq \frac{1}{\tau_R} + 2\omega_c - \frac{\omega_o^2/\tau_R + \omega_R^2(\omega_c + \alpha\omega_s)}{2\omega_c/\tau_R + \omega_o^2 + \omega_R^2}.$$

According to the discussion given before and the solutions for δ_ω given above, the instability condition is

$$\frac{1}{\tau_R}\omega_o^2 + \omega_R^2(\omega_c + \alpha\omega_s) < 0 \qquad (4.20a)$$

or

$$(\frac{1}{\tau_R} + 2\omega_c)(\frac{2}{\tau_R}\omega_c + \omega_o^2 + \omega_R^2) < \frac{1}{\tau_R}\omega_o^2 + \omega_R^2(\omega_c + \alpha\omega_s). \qquad (4.20b)$$

Clearly, the instability conditions (4.20a) and (4.20b) are less complicated than the stability conditions given by (4.16a) and (4.16b). Since (4.20a) and (4.20b) are obtained from considering special cases that $\mathrm{Im}(\hat{\omega}) \ll 1$, it is unclear whether (4.20a) and (4.20b) are equivalent to (4.16a) and (4.16b). To find out, numerical calculations are essential.

The numerical values of various parameters used for this analysis are $p_o^{sl} = 3\times10^{14}cm^{-3}$, $\frac{c}{2\bar{n}l} = 1.5\times10^{11}s^{-1}$, $\alpha = -5$, $g_{sl} = 0.5\times10^{12}s^{-1}$, $\tau_s = 3\times10^{-9}sec$, $g' = 1\times10^{-6}cm^3s^{-1}$, and $n_o^{sl} = 1\times10^{18}cm^{-3}$. Notice that the photon density p_o^{sl}, gain g_{sl}, and the carrier density n_o^{sl} are parameters before the injection locking. After injection locking, p_o, g and n_o can be obtained from Equations (4.7a)-(4.7c). The frequency dependence of g_{sl} is neglected.

Figure 4.3 shows the locked phase ϕ_o versus $(\frac{t_2}{\tau_2})^2\frac{I_{in,o}}{I_o}$, and the stable and unstable regions are obtained according to (4.20a) and (4.20b). It is very interesting that (4.16a) and (4.16b) give the same results as those shown in Figure 4.3. Using these results, Figure 4.4 shows the locking bandwidth versus $(\frac{t_2}{\tau_2})^2\frac{I_{in,o}}{I_o}$.

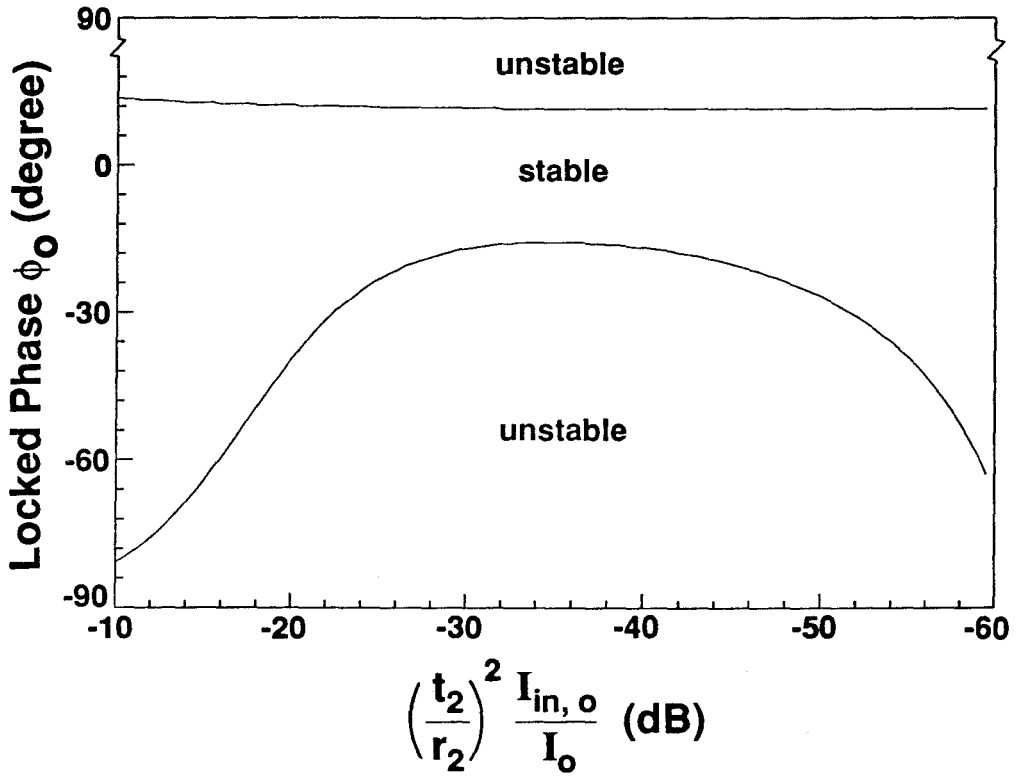

Figure 4.3 The locked phase ϕ_o versus $(\frac{t_2}{r_2})^2 \frac{I_{in,o}}{I_o}$. The stable and unstable regions are obtained according to the unstable conditions given by (4.20a) and (4.20b).

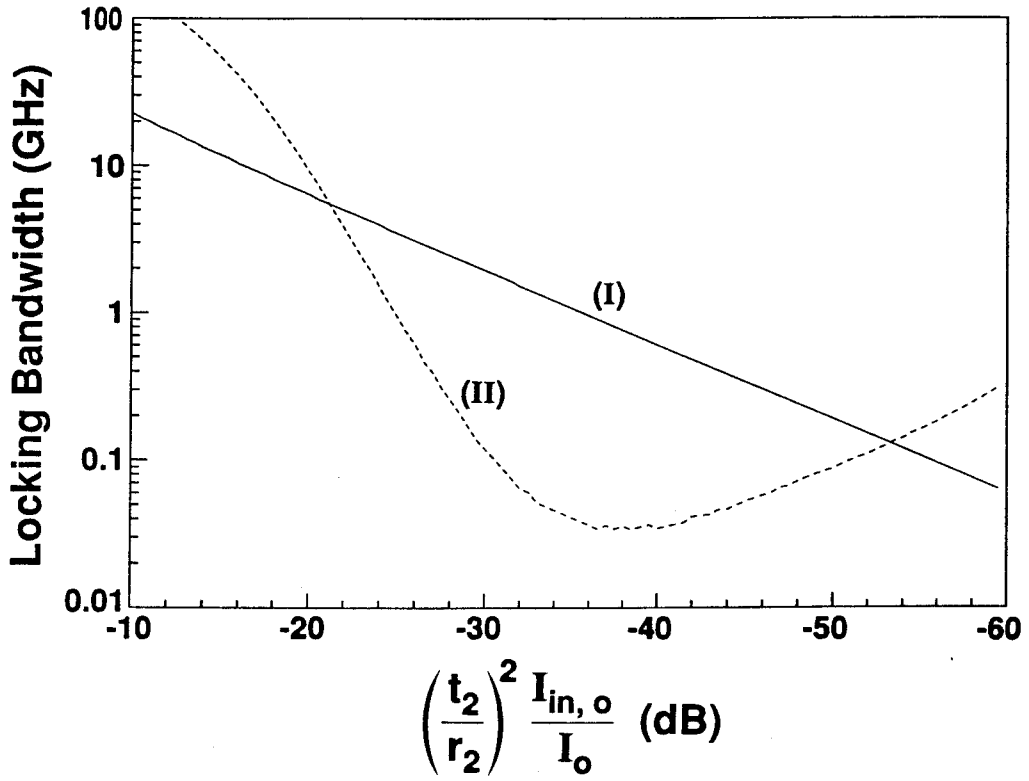

Figure 4.4 The locking bandwidth versus $(\frac{t_2}{r_2})^2 \frac{I_{in,o}}{I_o}$. Curve (I) and Curve (II) are obtained according to the unstable conditions given by (4.20a) and (4.20b), respectively.

The locking bandwidth determined by (4.20a) is not the same as the locking bandwidth determined by (4.20b). At this point, what the real locking bandwidth is, is not clear. To clarify this ambiguity, a discussion based on physical consideration is given as follows.

The detuning given in (4.10) can be rewritten as

$$\Delta\Omega = -\omega_o\sqrt{\alpha^2+1}\cos(\phi_o+\theta_\alpha), \tag{4.21}$$

where

$$\theta_\alpha = \cos^{-1}\frac{|\alpha|}{\sqrt{\alpha^2+1}}.$$

Similarly, the instability condition (4.20a) can be re-expressed as

$$\phi_o > \theta_\alpha + \sin^{-1}\frac{\omega_o}{\tau_R\omega_R^2\sqrt{\alpha^2+1}} \tag{4.22a}$$

and the instability condition (4.20b) is equivalent to

$$\phi_o < -\theta_\alpha - \sin^{-1}\left\{\frac{1}{\omega_o\sqrt{\alpha^2+1}}\left[\frac{2\omega_c}{\tau_R^2\omega_R^2}+\frac{4\omega_c^2}{\omega_R^2\tau_R}+\frac{2\omega_c\omega_o^2}{\omega_R^2}+\frac{1}{\tau_R}\right]\right\}. \tag{4.22b}$$

Equation (4.21) shows that, with a given detuning $\Delta\Omega$ and $(\frac{t_2}{\tau_2})^2\frac{I_{in,o}}{I_o}$, there may be two values of the locked phase difference, ϕ_1 and ϕ_2, both of which satisfy Equations (4.7a)-(4.7c). To be specific, for the first locked phase ϕ_1 falling in the range

$$-\frac{\pi}{2} \le \phi_1 < -\theta_\alpha,$$

the second locked phase ϕ_2 is in the range

$$-\theta_\alpha < \phi_2 \le \frac{\pi}{2} - 2\theta_\alpha.$$

From the discussion given in Section 4.3-B, it is assumed that only the ϕ_o giving a larger magnitude of threshold gain reduction Δg shown in (4.9d) will be the real solution and that another is not physically possible. Since

$$\cos\phi_1 < \cos\phi_2,$$

following this assumption, the locked phase ϕ_o in the range

$$-\frac{\pi}{2} \leq \phi_o < -\theta_\alpha$$

is not possible. Consequently, condition (4.22b) is physically impossible and the instability condition is given solely by (4.20a) or (4.22a). At the same time, the locking bandwidth $\Delta\Omega_{lb}$ is given by

$$\Delta\Omega_{lb} = \omega_o\sqrt{\alpha^2+1}\big[1-\cos(\theta_\alpha+\phi_c)\big], \tag{4.23}$$

with

$$\phi_c = \cos^{-1}\frac{|\alpha|}{\sqrt{\alpha^2+1}} + \sin^{-1}\frac{\omega_o}{\sqrt{\alpha^2+1}\tau_R\omega_R^2}.$$

It is amazing that the solution of the complicated problem posed at the beginning of this section is described by the simple expressions (4.20a) and (4.23).

According to (4.23), the locking bandwidth versus $(\frac{t_2}{r_2})^2\frac{I_{in,o}}{I_o}$ is shown in Figure 4.5a. Figure 4.5b shows the experimental results of Goldberg et al. [12]. In their paper, the data are shown as locking bandwidth versus P_i/P_s, where P_i is the power of the injected field and P_s is the single-facet output power of the locked field, both taken outside the laser cavity. Since, for uncoated lasers, it can be shown that $P_i/P_s \simeq (\frac{t_2}{r_2})^2\frac{I_{in,o}}{I_o}$, their data are shown in Figure 4.5b as locking bandwidth versus $(\frac{t_2}{r_2})^2\frac{I_{in,o}}{I_o}$. Figures 4.5a and 4.5b indicate that there is a good agreement between the theoretical prediction and experimental result. In addition, the detuning given in (4.21) and the instability condition (4.22a) clearly indicate that the instability occurs in the high-frequency side of the maximum locking range, and the appearence of this unique feature is simply because α is negative.

Up to this point, all the results presented above are based on the assumption that α is negative. In order to clarify this assumption, investigation for lasers

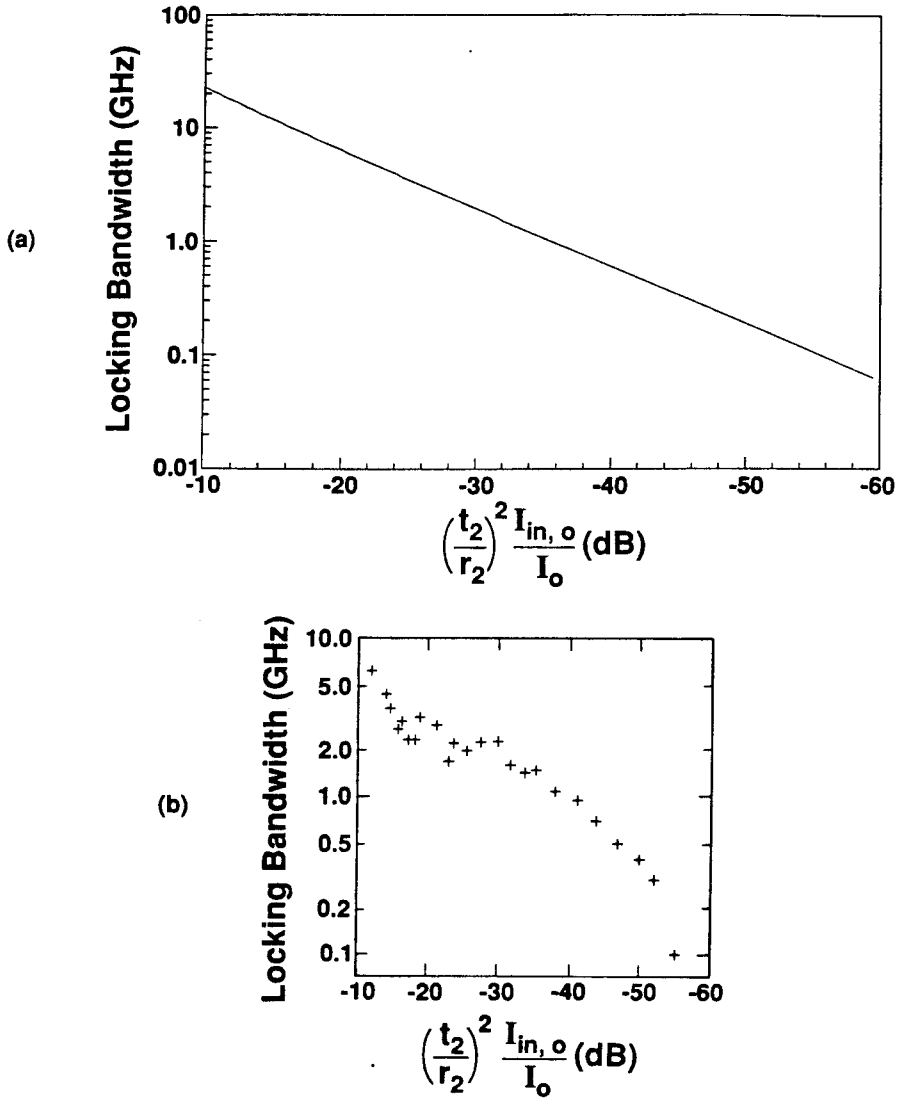

Figure 4.5 (a) The calculated locking bandwidth versus $(\frac{t_2}{r_2})^2 \frac{I_{in,o}}{I_o}$. (b) The experimental results of the locking bandwidth versus $(\frac{t_2}{r_2})^2 \frac{I_{in,o}}{I_o}$ by Goldberg et al. [12].

with positive α is necessary. Following the same procedure used above, one has the following results for lasers with positive α. The detuning $\Delta\Omega$ is given by

$$\Delta\Omega = \omega_o\sqrt{\alpha^2+1}\cos(\phi_o - \theta_\alpha). \tag{4.24}$$

The maximum locking range is from ω_o to $\omega_o\sqrt{\alpha^2+1}$. The instability condition is

$$\phi_o > -\theta_\alpha - \sin^{-1}\frac{\omega_o}{\tau_R\omega_R^2\sqrt{\alpha^2+1}}, \tag{4.25}$$

and the locking bandwidth is given by (4.23). From the detuning given in (4.24) and the instability condition (4.25), the instability occurs in the low-frequency side of the maximum locking range. Except that the locking bandwidth is unaffected by the sign of α, all the other results contradict the experimental findings reported so far [8] [11] [12] [23] [24]. On the other hand, results obtained for negative α agree with the experimental observations of References [8], [11], [12], [23], and [24]. Therefore, the available experimental results and the discussion given above confirm that α is, in fact, negative. Again, it is important to keep in mind that this conclusion is held only when the optical field is represented by $E(t)e^{i\Omega t}$ and the Fourier transforms are defined by (A.17).

To summarize, an exact analysis for the stability has been given, and the reason that the laser is unstable in the high-frequency region of the maximum locking range has been explained. However, the inherent relation between instability and pulsating is still not clear. Therefore, next, a physical picture will be described to shed light on this interesting phenomenon.

At this point, the reader is reminded that the small-signal analysis performed in Section 4.2 can be interpreted in two different ways. For DC biased lasers, the first one is the usual interpretation that, because of the Langevin force

perturbation, the laser is lasing with small variations in carrier density and in the phase and amplitude of the optical field. The other way is to divide a long period of time into many short periods. Although in the long term the optical field and carrier density may vary considerably, in each short period of time the laser can be characterized in the small-signal regime.

The laser is injection-locked and stable only when the steady-state conditions (4.7a)-(4.7c) are satisfied. For example, immediately after the injected field enters the cavity, the laser will assign a phase ϕ_{1o} to its optical field. When the phase ϕ_{1o} does not satisfy the steady-state condition, the laser adjusts ϕ_{1o} to ϕ_{2o} for the second short period of time. This process, shown in Figure 4.2, will continue. The laser may eventually reach a stably locked state, an unlocked state, or an unstable state.

In the unstable region of the maximum locking range, any random perturbation will result in the exponential growth of the optical field intensity. This increase in optical field intensity will deplete the carrier density. This carrier density depletion then changes the refractive index, which in turn shifts the lasing frequency away to a different frequency. The laser is no longer in its original state. But, after several self-adjustments in the phase ϕ, the laser will return to its original state. This whole cycle will trigger the next one, and the whole process repeats itself. Each time, the increase and decrease of the carrier density gives rise to the pulsation in the output power. This explains how the instability leads to the pulsation in the high-frequency region of the maximum locking range. On the contrary, in the low-frequency region of the maximum locking range, since the laser is in its stable state, any perturbation will soon decay to zero. Therefore, there is no pulsation instability in the low-frequency region of

the maximum locking range.

4.4 Frequency and Relative-Intensity Fluctuation Spectra

In many practical applications, such as optical communications, the noise properties of semiconductor lasers will affect the performance of the communication system. There have been intense theoretical and experimental investigations on this subject. In this section, by including the carrier dependence of the refractive index, the semiclassical theory of laser noise [14] will be applied to obtain the frequency and relative-intensity fluctuation spectra. Then, with a noiseless injected field, the relation between the relative-intensity noise spectrum and the detuning $\Delta\Omega$ at fixed injected intensity $I_{in,o}$ will be investigated.

Let $\delta_n(t)$, $\delta_\phi(t)$, and $\delta_I(t)$ be the noise-driven deviations of the carrier density and the phase and intensity of the optical field, respectively. Similarly, $\delta_{\phi_{in}}(t)$ and $\delta_{I_{in}}(t)$ will be the noise-driven deviations of the phase and intensity of the injected field. Letting $J_1(t) = 0$ in Equation (4.5c), Equations (4.5a)-(4.5c) become the noise-driven equations for $\delta_\phi(t)$, $\delta_I(t)$ and $\delta_n(t)$:

$$\dot{\delta}_\phi(t) + \omega_o \cos\phi_o \delta_\phi(t) - \frac{1}{2}\omega_o \sin\phi_o \frac{\delta_I(t)}{I_o} + \frac{1}{2}\alpha g' \delta_n(t)$$
$$= \omega_o \cos\phi_o \delta_{\phi_{in}}(t) - \frac{1}{2}\omega_o \sin\phi_o \frac{\delta_{I_{in}}(t)}{I_{in,o}} - \frac{\Delta_r(t)}{2\Omega I_0^{1/2}} \quad (4.26a)$$

$$\frac{\dot{\delta}_I(t)}{I_o} + \omega_o \cos\phi_o \frac{\delta_I(t)}{I_o} + 2\omega_o \sin\phi_o \delta_\phi(t) - g'\delta_n(t)$$
$$= \omega_o \cos\phi_o \frac{\delta_{I_{in}}(t)}{I_{in,o}} + 2\omega_o \sin\phi_o \delta_{\phi_{in}}(t) + \frac{\Delta_i(t)}{\Omega I_0^{1/2}} \quad (4.26b)$$

$$\dot{\delta}_n(t) = -\frac{\Gamma\varepsilon_0}{2\hbar}\chi_i(n_0)\delta_I(t) - \frac{1}{\tau_R}\delta_n(t) + \eta(t). \quad (4.26c)$$

Equations (4.11a) and (4.11b) strongly indicate that the noise-driven deviations $\delta_{\phi_{in}}(t)$ and $\delta_{I_{in}}(t)$ of the injected field become part of the driving force of the locked laser. The Langevin force correlations are given as follows [14] [25]:

$$< \Delta_i(t)\Delta_i(t') >=< \Delta_r(t)\Delta_r(t') >= W\delta(t-t') \qquad (4.27a)$$

$$< \eta(t)\eta(t') >= W_2\delta(t-t'), \qquad < \eta(t)\Delta_i(t') >= W_1\delta(t-t') \qquad (4.27b)$$

$$< \eta(t)\Delta_r(t') >= 0, \qquad < \Delta_i(t)\Delta_r(t') >= 0, \qquad (4.27c)$$

with

$$\frac{W}{\Omega^2 I_o} = 2n_{sp}\frac{g}{p_o V}, \qquad \frac{W_1}{\Omega I_o^{1/2}} = -(2n_{sp}-1)\frac{g}{V_c},$$

$$W_2 = \frac{(2n_{sp}-1)gp_oV}{V_c^2} + \frac{n_o}{V_c\tau_s},$$

where n_{sp} is the ratio of the spontaneous emission rate into the lasing mode to the gain of that same mode [26] [27] [28], p_o is the steady-state photon number density , V_c is the volume occupied by the carriers, <> denotes ensemble average, and V is the average mode volume such that p_oV is the total photon number inside the diode cavity.

It was shown in Chapter 3 that the Fourier transform is a very powerful technique in deriving the noise spectra and the linewidth formulas. Therefore, the procedure used in the following is similar to that of Section 3.3. For a square integrable function g(t), the Fourier transforms are defined as

$$\tilde{g}(\omega) = \int_{-\infty}^{+\infty} dt g(t)e^{-i\omega t}, \qquad g(t) = \frac{1}{2\pi}\int_{-\infty}^{+\infty} d\omega\tilde{g}(\omega)e^{i\omega t}.$$

By taking the Fourier transforms of Equations (4.11a)-(4.11c), one has

$$\begin{pmatrix} i\omega + \omega_c + \frac{\omega_R^2}{i\omega+1/\tau_R} & 2\omega_s \\ -\frac{1}{2}\omega_s - \frac{\alpha\omega_R^2}{2(i\omega+1/\tau_R)} & i\omega+\omega_c \end{pmatrix} \begin{pmatrix} \frac{\tilde{\delta}_I(\omega)}{I_o} \\ \tilde{\delta}_\phi(\omega) \end{pmatrix}$$

$$= \begin{pmatrix} \frac{\tilde{\Delta}_i(\omega)}{\Omega I_o^{1/2}} + \frac{g'\tilde{\eta}(\omega)}{i\omega+1/\tau_R} + 2\omega_s\tilde{\delta}_{\phi_{in}}(\omega) + \omega_c\frac{\tilde{\delta}_{I_{in}}(\omega)}{I_{in,o}} \\ -\frac{\tilde{\Delta}_r(\omega)}{2\Omega I_o^{1/2}} - \frac{\alpha g'\tilde{\eta}(\omega)}{2(i\omega+1/\tau_R)} - \frac{1}{2}\omega_s\frac{\tilde{\delta}_{I_{in}}(\omega)}{I_{in,o}} + \omega_c\tilde{\delta}_{\phi_{in}}(\omega) \end{pmatrix} \tag{4.28a}$$

$$\tilde{\delta}_n(\omega) = \frac{1}{i\omega + 1/\tau_R}\Big[-\frac{\Gamma\varepsilon_0}{2\hbar}\chi_i(n_0)\tilde{\delta}_I(\omega) + \tilde{\eta}(\omega)\Big], \tag{4.28b}$$

where

$$\omega_c = \omega_o\cos\phi_o, \qquad \omega_s = \omega_o\sin\phi_o, \tag{4.29a}$$

and

$$\omega_R^2 \equiv \frac{\Gamma^2\xi_i\Omega I_0\varepsilon_0\chi_i(n_0)}{2\hbar\bar{\mu}^2} = gg'p_o. \tag{4.29b}$$

The $\omega_R/2\pi$ is commonly referred to as the relaxation oscillation frequency of the free-running semiconductor lasers. From Equation (4.15a), the solutions for $\tilde{\delta}_\phi(\omega)$ and $\tilde{\delta}_I(\omega)$ are

$$\frac{\tilde{\delta}_I(\omega)}{I_o} = \frac{\begin{vmatrix} \frac{\tilde{\Delta}_i(\omega)}{\Omega I_o^{1/2}} + \frac{g'\tilde{\eta}(\omega)}{i\omega+1/\tau_R} + 2\omega_s\tilde{\delta}_{\phi_{in}}(\omega) + \omega_c\frac{\tilde{\delta}_{I_{in}}(\omega)}{I_{in,o}} & 2\omega_s \\ -\frac{\tilde{\Delta}_r(\omega)}{2\Omega I_o^{1/2}} - \frac{\alpha g'\tilde{\eta}(\omega)}{2(i\omega+1/\tau_R)} - \frac{1}{2}\omega_s\frac{\tilde{\delta}_{I_{in}}(\omega)}{I_{in,o}} + \omega_c\tilde{\delta}_{\phi_{in}}(\omega) & i\omega+\omega_c \end{vmatrix}}{\begin{vmatrix} i\omega+\omega_c+\frac{\omega_R^2}{i\omega+1/\tau_R} & 2\omega_s \\ -\frac{1}{2}\omega_s - \frac{\alpha\omega_R^2}{2(i\omega+1/\tau_R)} & i\omega+\omega_c \end{vmatrix}} \tag{4.30a}$$

$$\tilde{\delta}_\phi(\omega) = \frac{\begin{vmatrix} i\omega+\omega_c+\frac{\omega_R^2}{i\omega+1/\tau_R} & \frac{\tilde{\Delta}_i(\omega)}{\Omega I_o^{1/2}} + \frac{g'\tilde{\eta}(\omega)}{i\omega+1/\tau_R} \\ -\frac{1}{2}\omega_s - \frac{\alpha\omega_R^2}{2(i\omega+1/\tau_R)} & -\frac{\tilde{\Delta}_r(\omega)}{2\Omega I_o^{1/2}} - \frac{\alpha g'\tilde{\eta}(\omega)}{2(i\omega+1/\tau_R)} \end{vmatrix}}{\begin{vmatrix} i\omega+\omega_c+\frac{\omega_R^2}{i\omega+1/\tau_R} & 2\omega_s \\ -\frac{1}{2}\omega_s - \frac{\alpha\omega_R^2}{2(i\omega+1/\tau_R)} & i\omega+\omega_c \end{vmatrix}}$$

$$+ \frac{\begin{vmatrix} i\omega+\omega_c+\frac{\omega_R^2}{i\omega+1/\tau_R} & 2\omega_s\tilde{\delta}_{\phi_{in}}(\omega) + \omega_c\frac{\tilde{\delta}_{I_{in}}(\omega)}{I_{in,o}} \\ -\frac{1}{2}\omega_s - \frac{\alpha\omega_R^2}{2(i\omega+1/\tau_R)} & -\frac{1}{2}\omega_s\frac{\tilde{\delta}_{I_{in}}(\omega)}{I_{in,o}} + \omega_c\tilde{\delta}_{\phi_{in}}(\omega) \end{vmatrix}}{\begin{vmatrix} i\omega+\omega_c+\frac{\omega_R^2}{i\omega+1/\tau_R} & 2\omega_s \\ -\frac{1}{2}\omega_s - \frac{\alpha\omega_R^2}{2(i\omega+1/\tau_R)} & i\omega+\omega_c \end{vmatrix}}. \tag{4.30b}$$

As indicated in Chapter 3, the spectral density for stationary random functions f(t) and g(t) is given by

$$W_{fg}(\omega) = \frac{\delta\omega}{2\pi} < \tilde{f}^*(\omega)\tilde{g}(\omega) >, \tag{4.31}$$

where $\delta\omega/2\pi$ is the resolution bandwidth of the instrument used in the ensemble average. Accordingly, the relative-intensity fluctuation spectrum is written as

$$W_{\Delta I}(\omega) = \frac{\delta\omega}{2\pi}\frac{1}{I_0^2} < \tilde{\delta}_I^*(\omega)\tilde{\delta}_I(\omega) >, \tag{4.32}$$

and the frequency fluctuation spectrum is defined as

$$W_{\Delta\omega}(\omega) = \frac{\delta\omega}{2\pi}\omega^2 < \tilde{\delta}_\phi^*(\omega)\tilde{\delta}_\phi(\omega) > . \tag{4.33}$$

These two spectra, (4.32) and (4.33), are the widely studied spectral density functions. Similarly, in the frequency domain, the correlations (4.27a)-(4.27c) are re-expressed as

$$< \tilde{\Delta}_i^*(\omega)\tilde{\Delta}_i(\omega) >=< \tilde{\Delta}_r^*(\omega)\tilde{\Delta}_r(\omega) >= \frac{2\pi}{\delta\omega}W, \tag{4.34a}$$

$$< \tilde{\eta}^*(\omega)\tilde{\eta}(\omega) >= \frac{2\pi}{\delta\omega}W_2, \qquad < \tilde{\eta}^*(\omega)\tilde{\Delta}_i(\omega) >= \frac{2\pi}{\delta\omega}W_1, \tag{4.34b}$$

$$< \tilde{\eta}^*(\omega)\tilde{\Delta}_r(\omega) >= 0, \qquad < \tilde{\Delta}_i^*(\omega)\tilde{\Delta}_r(\omega) >= 0. \tag{4.34c}$$

With all the results given above, it is straightforward to have the spectra $W_{\Delta I}(\omega)$ and $W_{\Delta\omega}(\omega)$. Neglecting the factor $1/r_2$ in ω_c and ω_s, these spectra should be the same spectra as those of Spano et al. [13]. Instead of going through every detail, it will be interesting to take a close look at the relative-intensity noise spectra for the case where the injected field is noiseless. Under this condition, the noise-driven deviations $\frac{\tilde{\delta}_{I_{in}}(\omega)}{I_{in,o}}$ and $\tilde{\delta}_{\phi_{in}}(\omega)$ can be neglected, and the relative-intensity noise spectrum is

$$W_{\Delta I}(\omega) = \frac{\left(\left|i\omega+\omega_c\right|^2+\left|\omega_s\right|^2\right)\frac{W}{\Omega^2 I_o}+\left(\left|i\omega+\omega_c\right|^2+\left|\alpha\omega_s\right|^2\right)\frac{g'^2W_2}{|i\omega+1/\tau_R|^2}}{\left|\left(i\omega+\omega_c+\frac{\omega_R^2}{i\omega+1/\tau_R}\right)(i\omega+\omega_c)+\omega_s\left(\omega_s+\frac{\alpha\omega_R^2}{i\omega+1/\tau_R}\right)\right|^2}$$
$$+\frac{2\mathrm{Re}\left[(-i\omega+\omega_c)\left(\frac{i\omega+\omega_c+\alpha\omega_s}{i\omega+1/\tau_R}\right)\frac{g'W_1}{\Omega I_o^{1/2}}\right]}{\left|\left(i\omega+\omega_c+\frac{\omega_R^2}{i\omega+1/\tau_R}\right)(i\omega+\omega_c)+\omega_s\left(\omega_s+\frac{\alpha\omega_R^2}{i\omega+1/\tau_R}\right)\right|^2}. \tag{4.35}$$

As shown in Equation (4.35), the relative-intensity noise spectrum is explicitly dependent on the locked phase. Since the locked phase can be determined by the detuning and the detuning is a directly measurable quantity, the relationship between the detuning $\Delta\Omega$ and $W_{\Delta I}(\omega)$ will be considered in the following.

The numerical values of various parameters used for this analysis are given as follows: $p_o^{sl} = 3 \times 10^{14} cm^{-3}$; $\frac{c}{2\bar{n}l} = 1.5 \times 10^{11} s^{-1}$; $(\frac{t_2}{\tau_2})^2 \frac{I_{in,o}}{I_o} = 10^{-4}$; $\alpha = -5$; $g_{sl} = 0.5 \times 10^{12} s^{-1}$; $\tau_s = 3 \times 10^{-9} sec$; $g' = 1 \times 10^{-6} cm^3 s^{-1}$; $V_c = 3.0 \times 10^{-10} cm^3$; $V = 2V_c$; $n_{sp} = 1.8$; $\Gamma = 0.5$; and $n_o^{sl} = 1 \times 10^{18} cm^{-3}$. Notice that the power density p_o^{sl}, gain g_{sl}, and carrier density n_o^{sl} are parameters before injection locking. After injection locking, p_o, g and n_o can be obtained from Equations (4.7a)-(4.7c). The frequency dependence of g_{sl} is neglected.

With a noiseless injected field, Figures 4.6 and 4.7 show the relative-intensity noise spectra for different values of detuning $\Delta\Omega$. For the purpose of comparison, the relative-intensity noise spectrum of free-running lasers is also shown in both figures. With the parameters given above, the detuning range of stable operation is from -7.65 GHz to -7.06 GHz. From Figures 4.6 and 4.7, there is a clear trend in the relation between $W_{\Delta\Omega}(\omega)$ and the detuning $\Delta\Omega$. In general, injection-locking shifts the relaxation oscillation frequency to slightly higher frequencies. For frequencies less than 6 MHz, $W_{\Delta\Omega}(\omega)$ increases as the detuning increases, and for -7.06 GHz $< \Delta\Omega <$ -7.5 GHz, $W_{\Delta\Omega}(\omega)$ of the injection-locked lasers is larger than that of the free-running lasers. In other words, the intensity noise increases because of the noiseless injected field. For a frequency larger than 6 MHz, the relative-intensity noise is reduced, and the amount of reduction increases as the detuning is varied from -7.65 GHz to -7.13 GHz. This analysis points out that in designing an injection-locked laser to best suit a particular application, it is

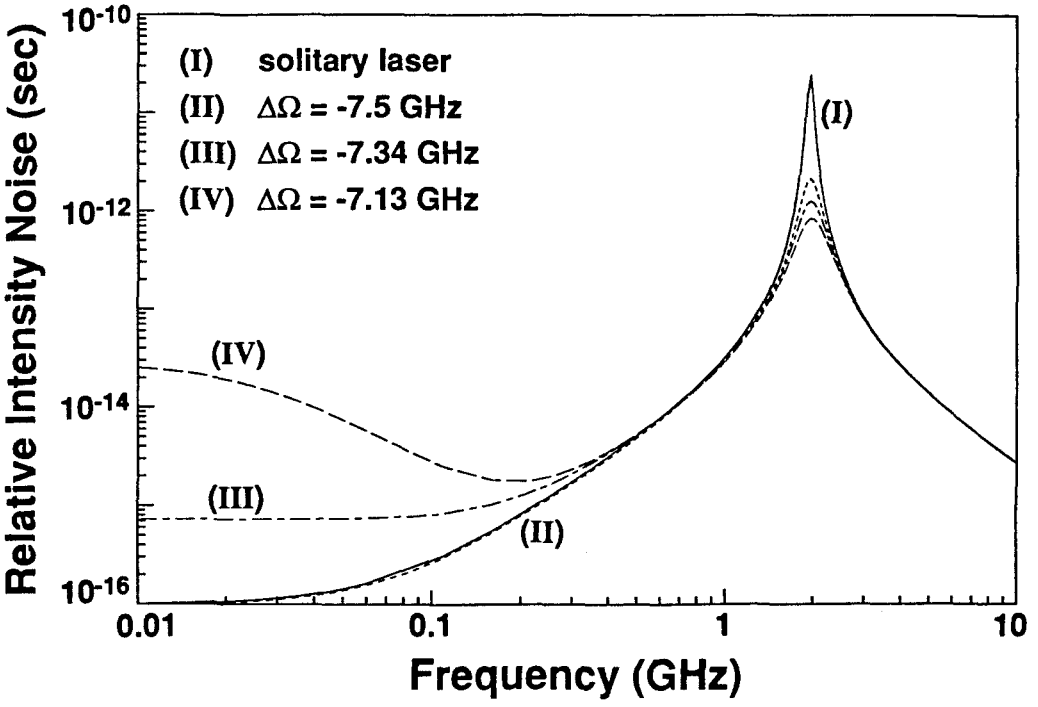

Figure 4.6 Relative-intensity noise spectra for different values of frequency detuning.

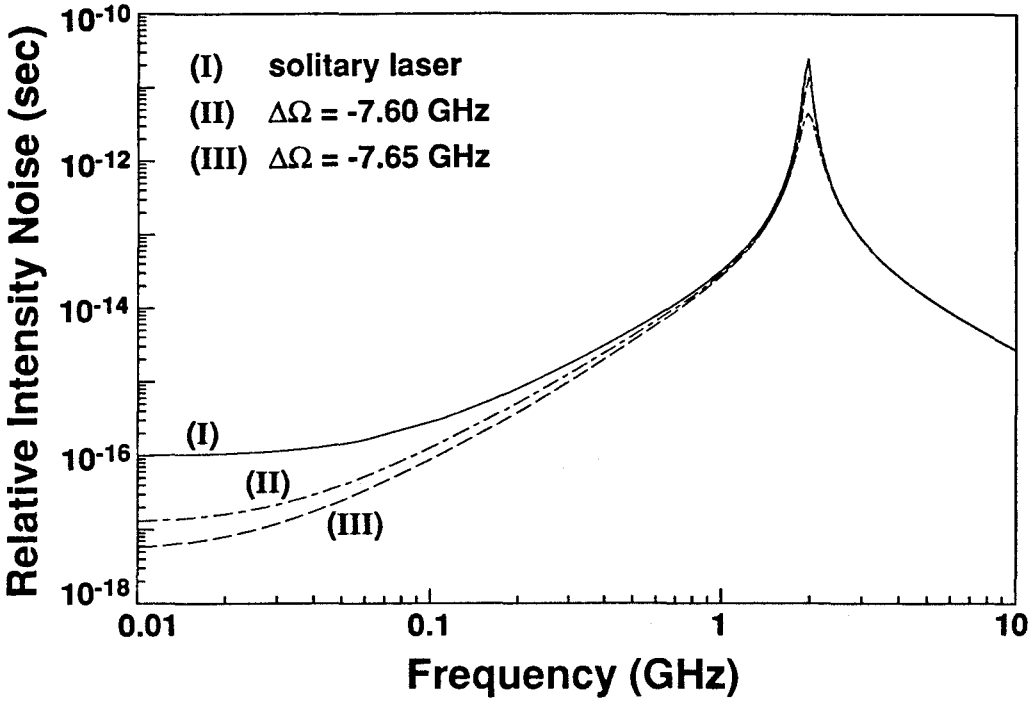

Figure 4.7 Relative-intensity noise spectra for different values of frequency detuning.

important to examine every aspect of the laser performance.

4.5 Linewidth of the Injection-Locked Laser

Because of the carrier dependence of the refractive index and the strong amplitude-phase coupling, the excessively large linewidth of solitary diode lasers precludes its usage in many applications requiring greater spectral purity. With a narrow linewidth injected field, Gallion et al. [1] concluded that the linewidth of the locked laser is equal to that of the injected field. In the following, using the method developed in Chapter 3 and $\delta_\phi(\omega)$ obtained in Section 4.4, it will be shown that on a general basis, the injection-locked diode laser's linewidth is indeed the same as that of the injected field.

For the laser field $\mathcal{E}(t) = E(t)e^{i\Omega t}$, its spectral density function is

$$W_{EE}(\omega) = \int_{-\infty}^{+\infty} dt' < \mathcal{E}^*(t)\mathcal{E}(t+t') > e^{-i\omega t'}. \tag{4.36}$$

If the correlation between phase and amplitude fluctuations is neglected, one has

$$W_{EE}(\omega) = E_o^2 \int_{-\infty}^{+\infty} dt' \exp[-i(\omega-\Omega)t' - \frac{1}{2} < (\delta_\phi(t+t') - \delta_\phi(t))^2 >], \tag{4.37a}$$

with

$$< (\delta_\phi(t+t') - \delta_\phi(t))^2 >= \frac{\delta\omega}{2\pi}\frac{1}{\pi}\Big| \int_{-\infty}^{+\infty} d\omega < \tilde{\delta}_\phi^*(\omega)\tilde{\delta}_\phi(\omega) > (1 - e^{i\omega t'})\Big|. \tag{4.37b}$$

As shown in Chapter 3, neglecting the high-frequency, weak side-mode structure in the field spectrum, the Lorentzian linewidth $\Delta\nu$ is given by

$$\Delta\nu = \frac{1}{2\pi}\Big|\frac{1}{t'}\mathrm{Res}(0)\Big|, \tag{4.38}$$

where Res(0) is the residue of the integrand

$$\frac{\delta\omega}{2\pi} < \tilde{\delta}_{\phi}^{*}(\omega)\tilde{\delta}_{\phi}(\omega) > (1 - e^{i\omega|t'|})$$

at the simple pole $\omega = 0$.

As $\omega \rightarrow 0$, Equation (4.30b) gives

$$\lim_{\omega\to 0}\tilde{\delta}_{\phi}(\omega) = \lim_{\omega\to 0}\tilde{\delta}_{\phi_{in}}(\omega) + \lim_{\omega\to 0}\frac{\begin{vmatrix} \frac{1}{2}\omega_R^2\tau_R(\alpha\omega_c - \omega_s) & \tilde{\delta}_{I_{in}}(\omega) \\ \omega_c + \omega_R^2\tau_R & 2\omega_s \\ -\frac{1}{2}\omega_s - \frac{\alpha}{2}\omega_R^2\tau_R & \omega_c \end{vmatrix}}{I_{in,o}}$$

$$+ \lim_{\omega\to 0}\frac{\begin{vmatrix} \omega_c + \omega_R^2\tau_R & \frac{\tilde{\Delta}_i(\omega)}{\Omega I_o^{1/2}} + g'\tau_R\tilde{\eta}(\omega) \\ -\frac{1}{2}\omega_s\frac{\alpha}{2}\omega_R^2\tau_R & -\frac{\tilde{\Delta}_r(\omega)}{2\Omega I_o^{1/2}} - \frac{\alpha}{2}g'\tau_R\tilde{\eta}(\omega) \end{vmatrix}}{\begin{vmatrix} \omega_c + \omega_R^2\tau_R & 2\omega_s \\ -\frac{1}{2}\omega_s - \frac{\alpha}{2}\omega_R^2\tau_R & \omega_c \end{vmatrix}}. \qquad (4.39)$$

Since the second and the third terms of Equation (4.39) do not contain terms proportional to $\frac{1}{\omega}$, Res(0) becomes the residue of the integrand

$$\frac{\delta\omega}{2\pi} < \tilde{\delta}_{\phi_{in}}^{*}(\omega)\tilde{\delta}_{\phi_{in}}(\omega) > (1 - e^{i\omega|t'|})$$

at the simple pole, $\omega = 0$. Accordingly, the linewidth of the injection-locked semiconductor laser is the same as that of the injected field. This has been experimentally confirmed by Gallion et al. [1]. Figure 4.8 shows their experimental result.

By assuming that $\tilde{\delta}_{\phi}(\omega)$is independent of the frequency components $\tilde{\eta}(\omega)$ and $\tilde{\delta}_{I_{in}}(\omega)$ of the Langevin force $\eta(t)$ and the intensity fluctuation $\delta_{I_{in}}(t)$ of the injected-field, respectively, Gallion et al. have also arrived theoretically at the same conclusion. Contrary to Gallion et al.'s assumption, as shown in Equation (4.26), $\tilde{\delta}_{\phi}(\omega)$ is dependent on $\tilde{\eta}(\omega)$ and $\tilde{\delta}_{I_{in}}(\omega)$. In this section, the same conclusion has been reached without their assumption. To summarize, in this section,

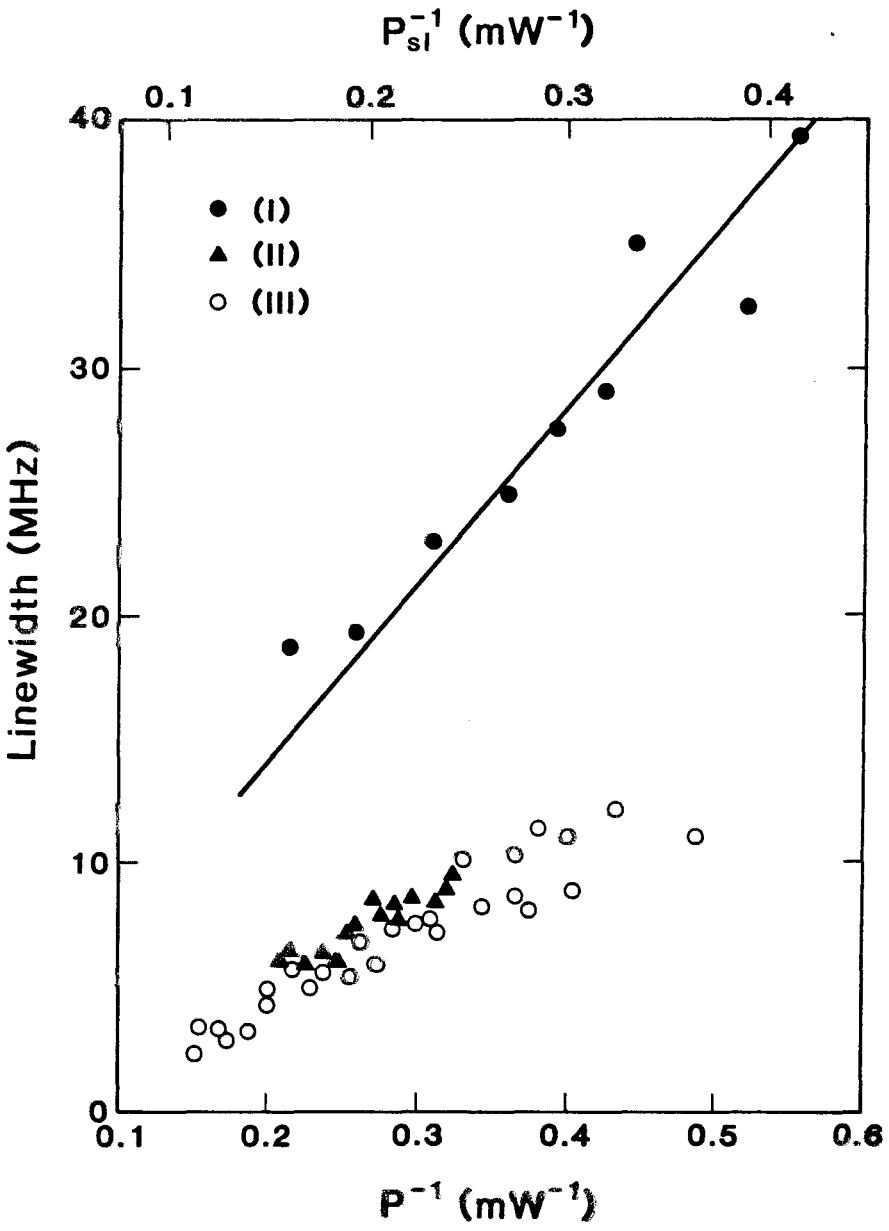

Figure 4.8 Free-running and injection-locked linewidth versus reciprocal output power: (I) linewidth of the solitary laser versus its reciprocal output power P_{sl}^{-1}, (II) linewidth of the injected field versus its reciprocal output power, (III) linewidth of the locked field versus its reciprocal output power.

it has been shown that on a general ground, the linewidth of an injection-locked laser is the same as that of the injected field.

4.6 Conclusion

Based on the optical field equation derived in Chapter 2, new insights into the injection locking phenomena have been realized. It has been shown that reducing the reflectivity will reduce the injected intensity necessary for locking and increase the locking range. The detuning is achieved by the adjustment of the locked phase ϕ_o and the reduction of the threshold gain.

The stability and locking bandwidth have been studied in considerable detail. Analytical expressions for the exact stability condition and locking bandwidth have been given. The calculated locking bandwidth is in excellent agreement with the experimental results of Goldberg et al. [12]. This analysis also explains why the instability occurs on the high-frequency side of the maximum locking range. The fundamental source for this asymmetric instability is the large and negative linewidth enhancement factor α. In addition, a physical picture has been used to illuminate the connection between this instability and the pulsation behavior.

It has been shown in Section 4.5 that on a general basis, the locked laser linewidth is the same as the linewidth of the injected field. Although a narrower linewidth injected field certainly will reduce the linewidth of the locked laser, the possible increase of relative-intensity noise indicated in Section 4.4 implies that in designing an injection-locked semiconductor laser, consideration of every aspect of its performance is necessary.

Appendix: The Sign of the Linewidth Enhancement Factor α

The linewidth enhancement factor α plays an important role in the dynamics, noise properties, and spectral characteristics of semiconductor lasers. Especially, as shown in this thesis, the sign of the linewidth enhancement factor has a fundamental and significant role in the physics of semiconductor lasers. However, there has been little attention given to the sign of this factor α. The purpose of this appendix is to show that the sign of the linewidth enhancement factor α is dependent on the sign convention used in the exponential notation representation of the optical field. It will also be shown that the Kramers-Kronig dispersion relation is dependent on the sign convention used in the Fourier transforms.

Following the sign convention used throughout this thesis, the monochromatic component with frequency Ω of the optical field $\mathcal{E}(t)$ is given by

$$\mathcal{E}_\Omega(t) = E_+(\Omega)e^{i\Omega t} = |E_+(\Omega)|e^{i\phi_{E+}(\Omega)}e^{i\Omega t}, \qquad (A.1)$$

where $E_+(\Omega)$ is the complex amplitude. Similarly, the monochromatic component with frequency Ω of the displacement $\mathcal{D}(t)$ is given by

$$\mathcal{D}_\Omega(t) = D_+(\Omega)e^{i\Omega t} = |D_+(\Omega)|e^{i\phi_{D+}(\Omega)}e^{i\Omega t}. \qquad (A.2)$$

Since all the physical quantities are real, it is understood that Equations (A.1) and (A.2) actually mean

$$\mathcal{E}_\Omega(t) = \mathrm{Re}(E_+(\Omega)e^{i\Omega t}) = |E_+(\Omega)|\cos(\Omega t + \phi_{E+}(\Omega)) \qquad (A.3)$$

and

$$\mathcal{D}_\Omega(t) = \mathrm{Re}(D_+(\Omega)e^{i\Omega t}) = |D_+(\Omega)|\cos(\Omega t + \phi_{D+}(\Omega)). \qquad (A.4)$$

$D_+(\Omega)$ and $E_+(\Omega)$ are connected by

$$D_+(\Omega) = \epsilon_+(\Omega)E_+(\Omega), \tag{A.5}$$

with

$$\epsilon_+(\Omega) = |\epsilon_+|e^{i\phi_{\epsilon+}(\Omega)}.$$

In terms of its amplitude and phase, Equation (A.5) can be separated into two equations:

$$|D_+(\Omega)| = |\epsilon_+(\Omega)E_+(\Omega)| \tag{A.6a}$$

and

$$\phi_{D+}(\Omega) = \phi_{\epsilon+}(\Omega) + \phi_{E+}(\Omega) + 2\pi N_1, \tag{A.6b}$$

where N_1 is an integer.

On the other hand, if the monochromatic component $\mathcal{E}_\Omega(t)$ is written as

$$\begin{aligned}\mathcal{E}_\Omega(t) =& \mathrm{Re}\left[|E_-(\Omega)|e^{i\phi_{E-}(\Omega)}e^{-i\Omega t}\right] \\ =& |E_-(\Omega)|\cos(\Omega t - \phi_{E-}(\Omega))\end{aligned} \tag{A.7}$$

and the monochromatic displacement $\mathcal{D}_\Omega(t)$ is given by

$$\begin{aligned}\mathcal{D}_\Omega(t) =& \mathrm{Re}\left[|D_-(\Omega)|e^{i\phi_{D-}(\Omega)}e^{-i\Omega t}\right] \\ =& |D_-(\Omega)|\cos(\Omega t - \phi_{D-}(\Omega)),\end{aligned} \tag{A.8}$$

then $D_-(\Omega)$ and $E_-(\Omega)$ are connected by

$$D_-(\Omega) = \epsilon_-(\Omega)E_-(\Omega), \tag{A.9}$$

with

$$\epsilon_-(\Omega) = |\epsilon_-|e^{i\phi_{\epsilon-}(\Omega)}.$$

In terms of its amplitude and phase, Equation (A.9) can be separated into two equations:

$$|D_-(\Omega)| = |\epsilon_-(\Omega)E_-(\Omega)| \qquad (A.10a)$$

and

$$\phi_{D-}(\Omega) = \phi_{\epsilon-}(\Omega) + \phi_{E-}(\Omega) + 2\pi N_2, \qquad (A.10b)$$

where N_2 is an integer.

Clearly, comparing Equations (A.3) and (A.4) with Equation (A.7) and (A.8), one has

$$|E_+(\Omega)| = |E_-(\Omega)|, \qquad (A.11a)$$

$$|D_+(\Omega)| = |D_-(\Omega)|, \qquad (A.11b)$$

$$\phi_{E+}(\Omega) = -\phi_{E-}(\Omega) + 2\pi N_3, \qquad (A.11c)$$

$$\phi_{D+}(\Omega) = -\phi_{D-}(\Omega) + 2\pi N_4, \qquad (A.11d)$$

where N_3 and N_4 are integers. From Equations (A.6b), (A.10b), (A.11c) and (A.11d), one obtains

$$|\epsilon_+(\Omega)| = |\epsilon_-(\Omega)|, \qquad (A.12a)$$

$$\phi_{\epsilon+}(\Omega) = -\phi_{\epsilon-}(\Omega) + 2\pi N_5, \qquad (A.12b)$$

where N_5 is an integer.

Next, define α_ϵ as the ratio of the real part to the imaginary part of $\epsilon(\Omega)$:

$$\alpha_\epsilon = \frac{\mathrm{Re}\{\epsilon(\Omega)\}}{\mathrm{Im}\{\epsilon(\Omega)\}}.$$

From Equation (A.12b), it is clear that

$$\alpha_{\epsilon+} = -\alpha_{\epsilon-}. \qquad (A.13)$$

In other words, $\alpha_{\epsilon+}$ and $\alpha_{\epsilon-}$ have the same magnitude with opposite sign. Equation (A.13) shows that the sign of α_ϵ depends on the exponential notation used in representing the optical field and the displacement.

The linewidth enhancement factor α defined in Equation (4.6a) can be rewritten as

$$\alpha = \frac{\Delta\mu_r}{\Delta\mu_i},$$

where μ_r and μ_i are the real and imaginary parts of the complex refractive index in the active region, respectively. Let α_+ and α_- denote the linewidth enhancement factor when the optical term is $e^{i\Omega t}$ and $e^{-i\Omega t}$, respectively. Invoking the relation between the complex refractive index and the complex dielectric constant and following the procedure used above, it can be easily shown that α_+ and α_- have the same magnitude and opposite sign. Apparently, the sign of the linewidth enhancement factor is dependent on the exponential notation representation of the optical field and the displacement.

The discussion given above strongly suggests that the prerequisite in discussing the sign of the factor α is to specify and to know the exponential notation representation of the optical field. Since $\mathrm{Re}\{\epsilon(\omega)\}$ and $\mathrm{Im}\{\epsilon(\omega)\}$ are connected by the Kramers-Kronig dispersion relation, the conclusion obtained above implies that the Kramers-Kronig relation is dependent on the definition of the Fourier transforms. In the following, the focus will be on this implication.

The key point here is to use the exponential notation representation and the Fourier transforms consistently. For example, when the monochromatic components $\mathcal{E}_\Omega(t)$ and $\mathcal{D}_\Omega(t)$ are given by (A.7) and (A.8), respectively, the corresponding Fourier transforms are defined as follows. For a square integrable function

h(t), the Fourier transforms are defined as

$$\tilde{h}(\omega) = \int_{-\infty}^{+\infty} dt h(t) e^{i\omega t}, \qquad h(t) = \frac{1}{2\pi} \int_{-\infty}^{+\infty} d\omega \tilde{h}(\omega) e^{-i\omega t}. \tag{A.14}$$

In terms of $\mathrm{Im}\{\epsilon(\omega)\}$, $\mathrm{Re}\{\epsilon(\omega)\}$ is given by the Kramers-Kronig relation

$$\mathrm{Re}\{\epsilon(\omega)\} = 1 + \frac{2}{\pi} \mathrm{P} \int_0^{\infty} \frac{\omega' \mathrm{Im}\{\epsilon(\omega')\} d\omega'}{\omega'^2 - \omega^2}, \tag{A.15}$$

where P denotes the principal value of the integral. Many advanced textbooks on classical electrodynamics [30] give detailed derivations for Equation (A.15). Similar to Equation (A.15), the small refractive index change $\Delta\mu_r(\omega)$ is expressed in terms of $\Delta\mu_i(\omega)$ by the Kramers-Kronig relation [19]:

$$\Delta\mu_r(\omega) = \frac{2}{\pi} \mathrm{P} \int_0^{\infty} \frac{\omega' \Delta\mu_i(\omega') d\omega'}{\omega'^2 - \omega^2}. \tag{A.16}$$

On the other hand, when the monochromatic components $\mathcal{E}_\Omega(t)$ and $\mathcal{D}_\Omega(t)$ are given by (A.1) and (A.2), respectively, the corresponding Fourier transforms are defined as

$$\tilde{f}(\omega) = \int_{-\infty}^{+\infty} dt f(t) e^{-i\omega t}, \qquad f(t) = \frac{1}{2\pi} \int_{-\infty}^{+\infty} d\omega \tilde{f}(\omega) e^{i\omega t}, \tag{A.17}$$

where $f(t)$ and $\tilde{f}(\omega)$ are square integrable functions. Following the same procedure used in deriving Equation (A.15), one has the Kramers-Kronig relations

$$\mathrm{Re}\{\epsilon(\omega)\} = 1 - \frac{2}{\pi} \mathrm{P} \int_0^{\infty} \frac{\omega' \mathrm{Im}\{\epsilon(\omega')\} d\omega'}{\omega'^2 - \omega^2} \tag{A.18}$$

and

$$\Delta\mu_r(\omega) = -\frac{2}{\pi} \mathrm{P} \int_0^{\infty} \frac{\omega' \Delta\mu_i(\omega') d\omega'}{\omega'^2 - \omega^2}. \tag{A.19}$$

As expected, from Equations (A.15) and (A.18), the Kramers-Kronig relation is dependent on the sign convention used in the Fourier transforms. Furthermore, Equations (A.16) and (A.19) reconfirm the conclusion obtained in the first half of this appendix, that the linewidth enhancement factor α indeed depends on the exponential notation representation of the optical field and the displacement.

References

[1] P. Gallion, H. Nakajima, G. Debarge, and C. Chabran, *Electron. Lett.*, **21**, pp. 626-628, 1985.

[2] R. Lang and K. Kobayashi, *IEEE J. Quantum Electron.*, **QE-12**, 194, 1976.

[3] K. Iwashita and K. Nakagawa, *IEEE J. Quantum Electron.*, *QE-18*, 1669, 1982.

[4] Y. Yamamoto and T. Kimura *IEEE J. Quantum Electron.*, **QE-17**, 919, 1981. H. Toba, Y. Kobayashi, and K. Yanagimoto, *Electron. Lett.*, **20**, 370, 1984.

[5] G. Jacobsen, C. J. Nielsen, H. Olesen, and F. Mogensen, in *Proc. IOOC '83*, Tokyo, Japan. pp. 388-389, 1983.

[6] T. Okoshi, K. Emura, K. Kikuchi, and R. T. Kersten, *J. Opt. Commun.*, **2**, 89, 1981.

[7] C. H. Henry, N. A. Olsson, and N. K. Dutta, *IEEE J. Quantum Electron.*, **QE-21**, 1152, 1985.

[8] R. Lang, *IEEE J. Quantum Electron.*, **QE-18**, 976, 1982.

[9] F. Mogensen, H. Olesen, and G. Jacobsen, *IEEE J. Quantum Electron.*, **QE-21**, 784, 1985.

[10] I. Petitbon, P. Gallion, G. Debarge, and C. Chabran, *IEEE J. Quantum Electron.*, **QE-24**, 148, 1988.

[11] K. Otsuka and S. Kobayashi, *Electron. Lett.*, **19**, 262, 1983.

[12] L. Goldberg, H. F. Taylor, and J. F. Weller, *Electron. Lett.*, **18**, 986, 1982.

[13] P. Spano, S. Piazzolla, and M. Tamburrini, *IEEE J. Quantum Electron.*,

QE-22, 427, 1986. K. Otsuka and S. Kobayashi, *Electron. Lett.*, **19**, 262, 1983.

[14] K. Vahala and A. Yariv, *IEEE J. Quantum Electron.*, **QE-19**, 1102, 1983.

[15] C. H. Henry, *IEEE J. Quantum Electron.*, **QE-18**, 259, 1982.

[16] A. Yariv, *Introduction to Optical Electronics*, 2nd ed. p. 114, Holt, New York, 1976.

[17] K. Y. Lau and A. Yariv, in *Semiconductors and Semimetals* **Vol. 22** (W. T. Tsang ed.), Part B. Chap. 2, Academic Press, 1985.

[18] G. R. Hadley, *IEEE J. Quantum Electron.*, **QE-22**, 419, 1986.

[19] C. H. Henry, R. A. Logan, and K. A. Bertness, *J. Appl. Phys.*, **52**, 4457, 1981.

[20] R. Adler, *Proc. IRE*, **34**, 351, 1946.

[21] D. Fye, *IEEE J. Quantum Electron.*, **QE-18**, 1675, 1982.

[22] S. M. Selby, ed., *Standard Mathematical Tables*, The Chemical Rubber Co., Ohio, 1975, p. 105.

[23] I. Petitbon, P. Gallion, G. Debarge, and C. Chabran, *Electron. Lett.*, **22**, 889, 1986.

[24] K. Kobayashi, H. Nishimoto, and R. Lang, *Electron. Lett.*, **18**, 54, 1982.

[25] C. Harder, J. Katz, S. Margalit, J. Shacham, and A. Yariv, *IEEE J. Quantum Electron.*, **QE-18**, 333, 1982.

[26] C. H. Henry, R. A. Logan, and F. R. Merritt, *J. Appl. Phys.*, **51**, 3042, 1980.

[27] D. Welford and A. Mooradian, *Appl. Phys. Lett.*, **40**, 865, 1982.

[28] C. H. Henry, R. A. Logan, H. Temkin, and F. R. Merritt, *IEEE J. Quantum Electron.*, **19**, 941, 1983.

[29] See, for example, J. D. Jackson, *Classical Electrodynamics*, 2nd ed., Wiley, New York, 1975, pp. 306-311.

Chapter 5

Dynamics and Linewidth of Axially Coupled Two-Section Semiconductor Lasers

5.1 Introduction

Axially coupled two-section semiconductor lasers have drawn considerable attention recently [1]. The laser has two sections, with each section having its own current source and being pumped independently. By adjusting the pumping currents separately, the optical coupling between the two cavities can improve the laser's spectral characteristics over the conventional Fabry-Perot semiconductor laser. For example, with one section operating above threshold and another below threshold, an average frequency tuning rate of 26 $\AA$/mA and a total tuning range of 300 $\AA$ were achieved [2]. This laser has been used as an optical source in long-distance transmission experiments [1].

The mode selectivity and stability of this laser have been studied [3] [4]. The dependence of mode discrimination on the coupling junction and cavity length has been examined [5] [6] [7]. Much of this work is built upon an effective mirror formalism [5], which models the coupling from the external cavity as that of the facet facing the external cavity with an effective wavelength-dependent reflectivity. This formalism has been successful in some respects. However, there are characteristics, such as the dynamics and laser linewidth, for which the formalism is inappropriate. As a result, many important and interesting aspects of this laser remain unexplored.

The purpose of this chapter is twofold. The first is to fill the gap in understanding the lasers' behavior such as the current-light characteristics, noise spectra, laser linewidth, and dynamic wavelength chirping. Another is based on the results of this chapter, to demonstrate the usefulness of the theory presented in Chapter 2. Recall that in Chapter 2, the concepts of time-dependent effective reflectivity and time-dependent, complex effective photon lifetime were introduced. Incorporating the time-dependent, complex effective conductivity in Maxwell's equations, a set of two coupled optical field equations for axially coupled two-section semiconductor lasers were derived in the same chapter. The optical field equations will be the basis of this chapter.

In Section 5.2, the steady-state condition and the small-signal equations for the optical fields and the carrier densities will be derived. The previously reported but unexplained light-current data will be examined [1] [2]. In Section 5.3, using the semiclassical theory of laser noise [8], a procedure for obtaining the frequency and relative intensity noise spectra will be outlined. The key intermediate results will be given. Although the complicated final results will not be given, these intermediate results will allow quick access to the final results. Using the method developed in Chapter 3, an analytical expression for the Lorentzian laser linewidth will be derived in Section 5.4. The calculated linewidth will be compared with the experimental results of Boyd et al. [9].

The small-signal current modulation response and the frequency chirping of the laser will be the subject of Section 5.5. Finally, the data of the dynamic wavelength chirping reported by Agrawal et al. [10] will be studied.

5.2 Small-Signal Equations for the Optical Fields and the Carrier Densities

As indicated in Chapter 2, the coupled optical field equations of this laser are complicated. However, as shown in Chapters 3 and 4, in the small-signal regime, the equations can be linearized, and the resulting small-signal equations are indispensable in studying the noise spectra, linewidth, small-signal current modulation response, and dynamic wavelength chirping. Therefore, in this section, the equations describing the optical field and carrier density will be reviewed briefly. Then, the small-signal equations will be derived. The equations governing the steady state of this laser will be given. These equations will then be used to calculate the current-light characteristics, which will be compared with the experimental results.

An axially coupled two-section diode laser is illustrated in Figure 5.1a. It consists of two cavities of lengths l_1 and l_2 with facet reflectivities r_1 on one side and r_4 on the other side of the composite cavity. The coupling between the two cavities is characterized by the transmission and reflection coefficients t_{12}, t_{21}, r_{11}, and r_{22} as indicated in that figure. According to the general formalism developed in Chapter 2, each cavity is equivalent to a solitary laser with one of its two facet mirrors replaced by an effective mirror. As shown in Figure 5.1b, there are two effective mirrors and their time-dependent effective reflectivities $r_{eff}^{(1)}(t)$ and $r_{eff}^{(2)}(t)$ are given by

$$r_{eff}^{(1)}(t) = r_{11} + t_{21}\frac{E_2(t)}{E_1(t)} \tag{5.1a}$$

$$r_{eff}^{(2)}(t) = r_{22} + t_{12}\frac{E_1(t)}{E_2(t)}, \tag{5.1b}$$

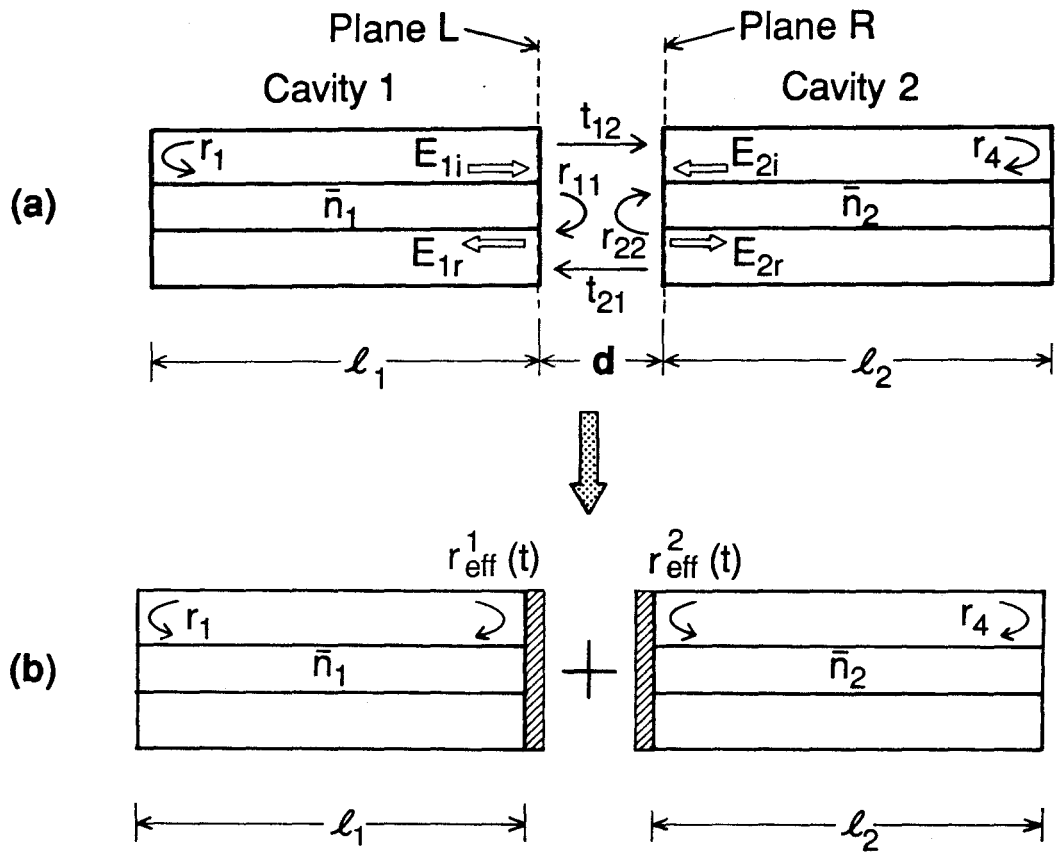

Figure 5.1 (a) Schematic of an axially coupled two-section semiconductor laser. (b) Each cavity of the two-section semiconductor laser is equivalent to a diode laser with an effective mirror.

where $E_j(t)$ is the complex amplitude of the optical field inside the jth cavity. For a single-mode axially coupled two-section diode laser, the optical field equations for cavities 1 and 2 are

$$\frac{d}{dt}E_1(t) - \Big[i\Big(\omega_1 - \Omega - \frac{\Gamma_1\chi_{1r}(n_1)\Omega}{2\bar{\mu}_1^2}\Big) + \frac{1}{2}\Big(\frac{\Gamma_1\chi_{1i}(n_1)\Omega}{\bar{\mu}_1^2} - \alpha_{1o} + \frac{c}{\bar{n}_1 l_1}\ln(r_1 r_{eff}^{(1)}(t))\Big)\Big]E_1(t) = \frac{\Delta_1(t)}{2i\Omega} \quad (5.2a)$$

and

$$\frac{d}{dt}E_2(t) - \Big[i\Big(\omega_2 - \Omega - \frac{\Gamma_2\chi_{2r}(n_2)\Omega}{2\bar{\mu}_2^2}\Big) + \frac{1}{2}\Big(\frac{\Gamma_2\chi_{2i}(n_2)\Omega}{\bar{\mu}_2^2} - \alpha_{2o} + \frac{c}{\bar{n}_2 l_2}\ln(r_4 r_{eff}^{(2)}(t))\Big)\Big]E_2(t) = \frac{\Delta_2(t)}{2i\Omega} \quad (5.2b)$$

respectively. For the jth cavity, Γ_j is the filling factor that represents the fraction of mode energy in the active region; ω_j is the m_jth resonant frequency of the unpumped and lossless cavity; $\chi_j(n_j) = \chi_{jr}(n_j) + i\chi_{ji}(n_j)$ is the susceptibility when the carrier density is n_j; $\bar{\mu}_j$ is the spatially averaged nonresonant refractive index defined in Equation (2.27a); $\alpha_{jo}$is the distributed waveguide loss constant; $\Delta_j(t)$ is the Langevin force originating from spontaneous emission; $\bar{n}_j$ is the real refractive index in the active region; and l_j is the cavity length.

In the jth cavity, the equation for the carrier density n_j is

$$\frac{dn_j}{dt} = -g_j(n_j)p_j - \frac{n_j}{\tau_{js}} + J_j(t) + \eta_j(t), \quad (5.3)$$

with $g_j(n_j) = \frac{\Gamma\chi_{ji}(n_j)\Omega}{\bar{\mu}_j^2}$ and $p_j = \frac{\varepsilon_0\bar{\mu}_j^2}{2\hbar\Omega}|E_j|^2$, where $g_j(n_j)$ is the gain, p_j is the photon density, τ_{js} is the spontaneous lifetime, $J_j(t)$ is the pumping rate of carriers per unit volume, and $\eta_j(t)$ is the Langevin force associated with the discrete nature of the carrier generation and recombination process.

In general, analytical solutions for the coupled Equations (5.2a)-(5.3) are unobtainable. In the following, the small-signal equations for the optical fields and carrier densities will be derived. These equations will then be used to derive analytical expressions for the frequency and relative intensity fluctuation spectra, laser linewidth, small-signal current modulation response, and frequency chirping in Sections 5.3, 5.4, and 5.5 separately.

In the jth cavity, for the small-signal analysis, let

$$E_j(t) = (E_{jo} + E_{j1}(t))e^{i\phi_j(t)}$$

$$n_j = n_{jo} + n_{j1}(t), \qquad J_j(t) = J_{jo} + J_{j1}(t)$$

$$\chi_j(n_j) = \chi_j(n_{jo}) + \xi_j n_{j1}(t), \qquad E_{jo}^2 + 2E_{jo}E_{j1}(t) = I_{jo} + I_{j1}(t),$$

where $E_{j1}(t)$, $\phi_j(t)$, $n_{j1}(t)$, $J_{j1}(t)$ and $I_{j1}(t)$ are real and time-dependent quantities, and their magnitudes are small when compared to E_{jo}, 1, n_{jo}, J_{jo}, and I_{jo}, respectively. $\xi_j = \xi_{jr} + i\xi_{ji}$ is the first order Taylor coefficient in expansion of $\chi_j(n_j) = \chi_{jr}(n_j) + i\chi_{ji}(n_j)$ about the operating-point carrier density n_{jo}. The small terms $E_{j1}(t)$, $\phi_j(t)$, $n_{j1}(t)$, $J_{j1}(t)$, $I_{j1}(t)$, and the Langevin forces $\Delta_j(t)$ and $\eta_j(t)$ are assumed to have zero mean value. It is also assumed that the time variation of these small terms are slow compared to the optical term $\exp(i\Omega t)$.

By neglecting products of small quantities, assuming $|\phi_j(t)| \ll \pi/2$, and using Equations (5.2a) and (5.2b), the distributed losses for cavities 1 and 2 are

$$\alpha_{1o} - \frac{c}{\bar{n}_1 l_1} \ln r_1 r_{eff}^{(1)}(t) = \alpha_{1o} - \frac{c}{\bar{n}_1 l_1} \ln r_1 \bar{r}_{eff}^{(1)} + S_{1r}(t) + iS_{1i}(t) \qquad (5.4a)$$

and

$$\alpha_{2o} - \frac{c}{\bar{n}_2 l_2} \ln r_4 r_{eff}^{(2)}(t) = \alpha_{2o} - \frac{c}{\bar{n}_2 l_2} \ln r_4 \bar{r}_{eff}^{(2)} + S_{2r}(t) + iS_{2i}(t), \qquad (5.4b)$$

respectively, with

$$\bar{r}_{eff}^{(1)} = r_{11} + t_{21}\frac{E_{2o}}{E_{1o}} \tag{5.5a}$$

$$\bar{r}_{eff}^{(2)} = r_{22} + t_{12}\frac{E_{1o}}{E_{2o}} \tag{5.5b}$$

$$S_{1r} = -2T_{1r}\left(\frac{E_{21}(t)}{E_{2o}} - \frac{E_{11}(t)}{E_{1o}}\right) + T_{1i}(\phi_2(t) - \phi_1(t))$$

$$S_{1i} = -T_{1i}\left(\frac{E_{21}(t)}{E_{2o}} - \frac{E_{11}(t)}{E_{1o}}\right) - 2T_{1r}(\phi_2(t) - \phi_1(t))$$

$$S_{2r} = -2T_{2r}\left(\frac{E_{11}(t)}{E_{1o}} - \frac{E_{21}(t)}{E_{2o}}\right) + T_{2i}(\phi_1(t) - \phi_2(t))$$

$$S_{2i} = -T_{2i}\left(\frac{E_{11}(t)}{E_{1o}} - \frac{E_{21}(t)}{E_{2o}}\right) - 2T_{2r}(\phi_1(t) - \phi_2(t)),$$

where the real quantities $2T_{1r}$, $2T_{2r}$, T_{1i}, and T_{2i} are given by

$$2T_{1r} \equiv \mathrm{Re}\left[\frac{c}{\bar{n}_1 l_1}\frac{t_{21}}{\bar{r}_{eff}^{(1)}}\frac{E_{2o}}{E_{1o}}\right], \qquad T_{1i} \equiv \mathrm{Im}\left[\frac{c}{\bar{n}_1 l_1}\frac{t_{21}}{\bar{r}_{eff}^{(1)}}\frac{E_{2o}}{E_{1o}}\right] \tag{5.6a}$$

$$2T_{2r} \equiv \mathrm{Re}\left[\frac{c}{\bar{n}_2 l_2}\frac{t_{12}}{\bar{r}_{eff}^{(2)}}\frac{E_{1o}}{E_{2o}}\right], \qquad T_{2i} \equiv \mathrm{Im}\left[\frac{c}{\bar{n}_2 l_2}\frac{t_{12}}{\bar{r}_{eff}^{(2)}}\frac{E_{1o}}{E_{2o}}\right]; \tag{5.6b}$$

$\bar{r}_{eff}^{(1)}$ and $\bar{r}_{eff}^{(2)}$ are the steady-state effective reflectivities for cavities 1 and 2, respectively.

Similarly, using the results given above and neglecting products of small quantities, Equations (5.2a)-(5.3) are linearized. For the jth cavity, the small-signal equations are

$$\dot{\phi}_j(t) + \frac{1}{2}\alpha_j g_j' n_{j1}(t) + \frac{1}{2}S_{ji}(t) = \frac{-\Delta_{jr}(t)}{2\Omega I_{jo}^{1/2}} \tag{5.7a}$$

$$\dot{I}_{j1}(t) - g_j' I_{jo} n_{j1}(t) + I_{jo} S_{jr}(t) = \frac{\Delta_{ji}(t)}{\Omega} I_{jo}^{1/2} \tag{5.7b}$$

$$\dot{n}_{j1}(t) = -\frac{\Gamma_j \varepsilon_0}{2\hbar}\chi_{ji}(n_{jo}) I_{j1}(t) - \frac{1}{\tau_{jR}} n_{j1}(t) + J_{j1}(t) + \eta_j(t), \tag{5.7c}$$

where

$$\alpha_j \equiv \frac{\xi_{jr}}{\xi_{ji}}, \tag{5.8a}$$

$$g'_j \equiv \frac{\Gamma_j \xi_{ji} \Omega}{\bar{\mu}_j^2}, \tag{5.8b}$$

$$\frac{1}{\tau_{jR}} \equiv \frac{\Gamma_j \varepsilon_o}{2\hbar} \xi_{ji} I_{jo} + \frac{1}{\tau_{js}}. \tag{5.8c}$$

α_j is the ratio of the real to the imaginary part of the refractive index and is commonly referred to as the linewidth enhancement factor [11] [12] [13]. g'_j is the differential optical gain constant, and τ_{jR} is the damping time constant in the relaxation oscillation of solitary semiconductor lasers. $\Delta_{jr}(t)$ and $\Delta_{ji}(t)$ are the real and imaginary parts of $\Delta_j(t)$, respectively.

Clearly, the effects of coupling are included in these equations through the terms $S_{ji}(t)$ and $S_{jr}(t)$. Furthermore, the gain, the lasing frequency, I_{jo}, and n_{jo} for the steady state are determined by the following equations:

$$\alpha_{1o} - \frac{c}{\bar{n}_1 l_1} \ln r_1 \tilde{r}_1 - \frac{\Gamma_1 \chi_{1i}(n_{1o})}{\bar{\mu}_1^2} \Omega = 0 \tag{5.9a}$$

$$\alpha_{2o} - \frac{c}{\bar{n}_2 l_2} \ln r_4 \tilde{r}_2 - \frac{\Gamma_2 \chi_{2i}(n_{2o})}{\bar{\mu}_2^2} \Omega = 0 \tag{5.9b}$$

$$\omega_1 - \Omega - \frac{\Gamma_1 \chi_{1r}(n_{1o})}{2\bar{\mu}_1^2} \Omega + \frac{c}{2\bar{n}_1 l_1} \mathrm{Im}(\ln e^{-i\theta_1}) = 0 \tag{5.9c}$$

$$\omega_2 - \Omega - \frac{\Gamma_2 \chi_{2r}(n_{2o})}{2\bar{\mu}_2^2} \Omega + \frac{c}{2\bar{n}_2 l_2} \mathrm{Im}(\ln e^{-i\theta_2}) = 0 \tag{5.9d}$$

$$-\frac{\Gamma_1 \varepsilon_0}{2\hbar} \chi_{1i}(n_{1o}) I_{1o} - \frac{n_{1o}}{\tau_{1s}} + J_{1o} = 0 \tag{5.9e}$$

$$-\frac{\Gamma_2 \varepsilon_0}{2\hbar} \chi_{2i}(n_{2o}) I_{2o} - \frac{n_{2o}}{\tau_{2s}} + J_{2o} = 0, \tag{5.9f}$$

where the real quantities $\tilde{r}_1$, $\tilde{r}_2$, θ_1 and θ_2 are defined by

$$\bar{r}_{eff}^{(1)} \equiv \tilde{r}_1 e^{-i\theta_1}, \qquad \bar{r}_{eff}^{(2)} \equiv \tilde{r}_2 e^{-i\theta_2}. \tag{5.9g}$$

Equations (5.7a)-(5.7c) are the small-signal equations of the single mode two-section semiconductor laser. The small-signal equations will be used in the following sections. As indicated in Chapter 2, the combined steady-state condition given by Equations (5.9a)-(5.9f) agrees with the eigenvalue equation derived by Henry and Kazarinov [4].

Equations (5.2a) and (5.2b) suggest that each cavity has its own average optical field intensity and, in general, the average photon density in each cavity may not be the same. Since no theory had predicted this interesting feature, the comparison between the experimental results and calculations will be given below.

Since cleaved-coupled-cavity lasers were used in the experiments of References (1) and (2), the analysis will be carried out for this particular class of lasers. Koch and Coldren [5] showed that for the C^3 lasers,

$$r_{11} = r_{22}, \qquad t_{12} = t_{21}; \tag{5.10}$$

and under a single-mode operation, the optimum coupling condition is that t_{12}/r_{11} and t_{21}/r_{22} are real numbers. Consequently, one has

$$T_{1i} = T_{2i} = 0, \tag{5.11a}$$

$$T_{1r} = \frac{c}{2\bar{n}_1 l_1}\left(1 + \frac{r_{11}E_{1o}}{t_{21}E_{2o}}\right)^{-1}, \qquad T_{2r} = \frac{c}{2\bar{n}_2 l_2}\left(1 + \frac{r_{11}E_{2o}}{t_{21}E_{1o}}\right)^{-1}. \tag{5.11b}$$

Parameters used in the calculations are given as follows: $t_{12}/r_{11} = 2.0$; $\bar{n}_1 l_1 = 0.82$ mm; $\bar{n}_2 l_2 = 0.18$ mm; $g_1 = g_2 = 0.5 \times 10^{12} s^{-1}$; $n_{1o} = n_{2o} = 1 \times 10^{18} cm^{-3}$; $\tau_{1s} = \tau_{2s} = 3 \times 10^{-9} sec$; $g_1' = g_2' = 1 \times 10^{-6} cm^3 s^{-1}$; $V_{1c} = 2.47 \times 10^{-10} cm^3$; $V_{2c} = 0.53 \times 10^{-10} cm^3$; $V_1 = 2V_{1c}$; and $V_2 = 2V_{2c}$.

Figure 5.2b shows the DC (or pulsed) light-current characteristic measured from each side of a 1.3 μm InGaAsP/InP laser. With one section pumped, the

(a)

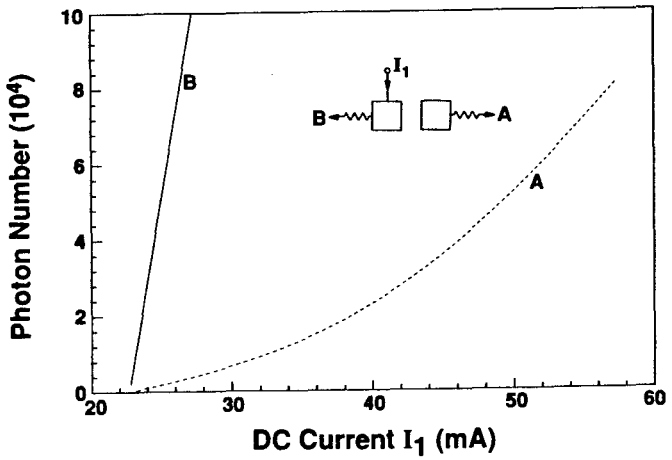

(b)

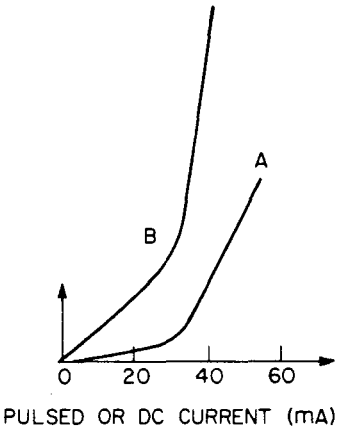

Figure 5.2 (a) Calculated light-current characteristics of two-section lasers when the right section is pumped and the other section is passive. (b) Light-current characteristics measured from each side of a cleaved-couple-cavity laser fabricated from 1.3 μm wavelength InP/InGaAsP crescent laser wafer when the right section is pumped.

optical field generated in the pumped cavity is coupled into the other section. This unequal pumping leads to the asymmetry of the two current-light curves shown in Figure 5.2b. Using Equations (5.8a)-(5.8f), Figure 5.2a shows the calculated light-current curves of a two-section laser with one section pumped and the other section passive. There is a qualitative agreement between the reported data and the calculations. Figure 5.3b shows another experimental light-current characteristic when one section is biased below threshold and another section is biased at a different current level. Again, the experimental data are confirmed qualitatively by the calculations shown in Figure 5.3a.

5.3 Relative-Intensity and Frequency Fluctuation Spectra

As emphasized in previous chapters, the relative intensity and frequency fluctuation spectra of the diode laser are very important characteristics in many practical applications. Therefore, the frequency and the relative intensity fluctuation spectra will be the subject of this section. Despite the cumbersome mathematical procedure, it is necessary to carry out the analysis to some degree. The key intermediate results will be given. Although the complicated final results will not be given, the fluctuation spectra can be obtained from these results with little difficulty. In addition, the noise-driven phase deviations obtained in this section will be used in the next section for deriving the laser linewidth.

Let $\delta_{\phi_j}(t)$, $\delta_{I_j}(t)$, and $\delta_{n_j}(t)$ be the noise-driven deviations of phase and intensity of the electric field and carrier density, respectively, from their steady-state values. When $J_{j1}(t) = 0$ in Equation (5.7c), Equations (5.7a)-(5.7c) become the noise-driven equations of $\delta_{\phi_j}(t)$, $\delta_{I_j}(t)$ and $\delta_{n_j}(t)$. These equations are:

$$\dot{\delta}_{\phi_1}(t) + \frac{\alpha_1}{2} g_1' \delta_{n_1}(t) + \frac{1}{2} S_{1i}(t) = \frac{-\Delta_{1r}(t)}{2\Omega I_{1o}^{1/2}} \qquad (5.12a)$$

(a)

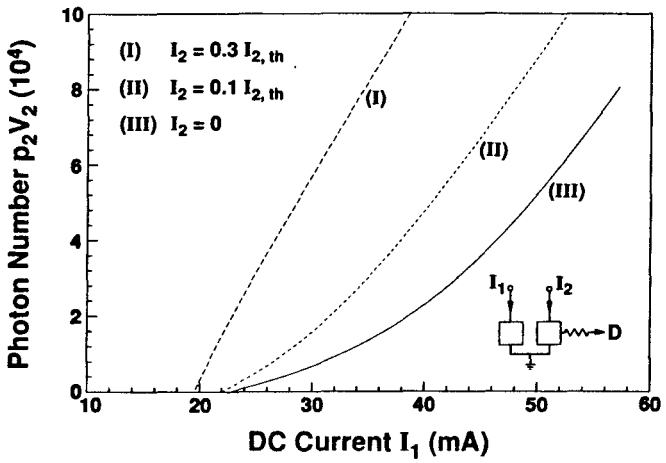

(b)

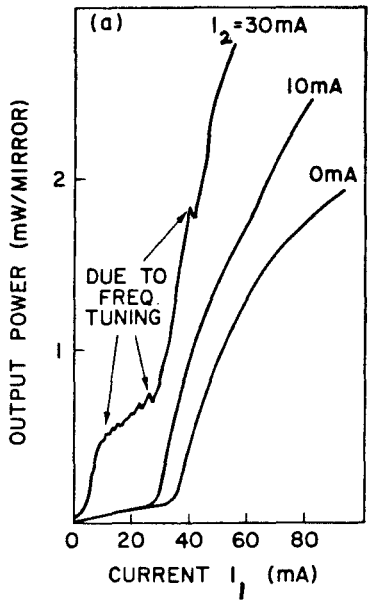

Figure 5.3 (a) Calculated light-current characteristics of two-section lasers when the right section is pumped and the other section is biased at different current levels. (b) Light-current characteristics measured from the right side of a cleaved-couple-cavity laser fabricated from 1.5 μm wavelength InP/InGaAsP crescent laser wafer when the left section is pumped and the right section is biased at different current levels.

$$\dot{\delta}_{\phi_2}(t) + \frac{\alpha_2}{2} g_2' \delta_{n_2}(t) + \frac{1}{2} S_{2i}(t) = \frac{-\Delta_{2r}(t)}{2\Omega I_{2o}^{1/2}} \tag{5.12b}$$

$$\dot{\delta}_{I_1}(t) - g_1' I_{1o} \delta_{n_1}(t) + I_{1o} S_{1r}(t) = \frac{\Delta_{1i}(t)}{\Omega} I_{1o}^{1/2} \tag{5.12c}$$

$$\dot{\delta}_{I_2}(t) - g_2' I_{2o} \delta_{n_2}(t) + I_{2o} S_{2r}(t) = \frac{\Delta_{2i}(t)}{\Omega} I_{2o}^{1/2} \tag{5.12d}$$

$$\dot{\delta}_{n_1}(t) = -\frac{\Gamma_1 \varepsilon_0}{2\hbar} \chi_{1i}(n_{1o}) \delta_{I_1}(t) - \frac{1}{\tau_{1R}} \delta_{n_1}(t) + \eta_1(t) \tag{5.12e}$$

$$\dot{\delta}_{n_2}(t) = -\frac{\Gamma_2 \varepsilon_0}{2\hbar} \chi_{2i}(n_{2o}) \delta_{I_2}(t) - \frac{1}{\tau_{2R}} \delta_{n_2}(t) + \eta_2(t). \tag{5.12f}$$

For the jth cavity, the Langevin force correlations are given as follows [8] [14]:

$$< \Delta_{ji}(t) \Delta_{ji}(t') > = < \Delta_{jr}(t) \Delta_{jr}(t') > = W_{jo} \delta(t - t') \tag{5.13a}$$

$$< \eta_j(t) \eta_j(t') > = W_{j2} \delta(t - t'), \qquad < \eta_j(t) \Delta_{ji}(t') > = W_{j1} \delta(t - t') \tag{5.13b}$$

$$< \eta_j(t) \Delta_{jr}(t') > = 0, \qquad < \Delta_{ji}(t) \Delta_{jr}(t') > = 0, \tag{5.13c}$$

with

$$\frac{W_{jo}}{\Omega^2 I_{jo}} = 2 n_{j,sp} \frac{g_j}{p_{jo} V_j}, \qquad \frac{W_{j1}}{\Omega I_{jo}^{1/2}} = -(2 n_{j,sp} - 1) \frac{g}{V_{jc}},$$

$$W_{j2} = (2 n_{j,sp} - 1) \frac{g_j p_{jo} V_j}{V_{jc}^2} + \frac{n_{jo}}{V_{jc} \tau_{js}}, \tag{5.14}$$

where $n_{j,sp}$ is the ratio of the spontaneous emission rate into the lasing mode to the gain of that same mode [15] [16] [17], p_{jo} is the steady-state photon number density; V_{jc} is the volume occupied by the carriers; <> denotes ensemble average; and V_j is the average mode volume such that $p_{jo} V_j$ is the total photon number inside the jth diode cavity. It is assumed that the correlations between the Langevin forces of different cavities are zero.

It was shown in Chapters 3 and 4 that the Fourier transform method is a powerful technique in deriving the spectral density function and the linewidth formula. Therefore, a similar procedure will be applied in the following. For a square integrable function f(t), the Fourier transforms are defined by

$$\tilde{f}(\omega) = \int_{-\infty}^{+\infty} dt f(t) e^{-i\omega t}, \qquad f(t) = \frac{1}{2\pi} \int_{-\infty}^{+\infty} d\omega \tilde{f}(\omega) e^{i\omega t}.$$

Taking the Fourier transforms of Equations (5.12a)-(5.12f), one has

$$\begin{pmatrix} i\omega + T_{1r} & -T_{1r} & \frac{T_{1i}}{4} - \frac{\alpha_1 \omega_{1R}^2}{2(i\omega + 1/\tau_{1R})} & -\frac{T_{1i}}{4} \\ -T_{1i} & T_{1i} & i\omega + T_{1r} + \frac{\omega_{1R}^2}{i\omega + 1/\tau_{1R}} & -T_{1r} \\ -T_{2r} & i\omega + T_{2r} & -\frac{T_{2i}}{4} & \frac{T_{2i}}{4} - \frac{\alpha_2 \omega_{2R}^2}{2(i\omega + 1/\tau_{2R})} \\ T_{2i} & -T_{2i} & -T_{2r} & i\omega + T_{2r} + \frac{\omega_{2R}^2}{i\omega + 1/\tau_{2R}} \end{pmatrix}$$

$$\times \begin{pmatrix} \tilde{\delta}_{\phi_1}(\omega) \\ \tilde{\delta}_{\phi_2}(\omega) \\ \frac{\tilde{\delta}_{I_1}(\omega)}{I_{1o}} \\ \frac{\tilde{\delta}_{I_2}(\omega)}{I_{2o}} \end{pmatrix} = \begin{pmatrix} -\frac{\tilde{\Delta}_{1r}(\omega)}{2\Omega I_{1o}^{1/2}} - \frac{\alpha_1 g_1' \tilde{\eta}_1(\omega)}{2(i\omega + 1/\tau_{1R})} \\ \frac{\tilde{\Delta}_{1i}(\omega)}{\Omega I_{1o}^{1/2}} + \frac{g_1' \tilde{\eta}_1(\omega)}{i\omega + 1/\tau_{1R}} \\ -\frac{\tilde{\Delta}_{2r}(\omega)}{2\Omega I_{2o}^{1/2}} - \frac{\alpha_2 g_2' \tilde{\eta}_2(\omega)}{2(i\omega + 1/\tau_{2R})} \\ \frac{\tilde{\Delta}_{2i}(\omega)}{\Omega I_{2o}^{1/2}} + \frac{g_2' \tilde{\eta}_2(\omega)}{i\omega + 1/\tau_{2R}} \end{pmatrix} \tag{5.15a}$$

$$\tilde{\delta}_{n_1}(\omega) = \frac{1}{i\omega + 1/\tau_{1R}} [-\frac{\varepsilon_o}{2\hbar} \chi_{1i}(n_{1o}) \tilde{\delta}_{I_1}(\omega) + \tilde{\eta}_1(\omega)] \tag{5.15b}$$

$$\tilde{\delta}_{n_2}(\omega) = \frac{1}{i\omega + 1/\tau_{2R}} [-\frac{\varepsilon_o}{2\hbar} \chi_{2i}(n_{2o}) \tilde{\delta}_{I_2}(\omega) + \tilde{\eta}_2(\omega)], \tag{5.15c}$$

where

$$\omega_{1R}^2 \equiv \frac{\Gamma_1^2 \xi_{1i} \Omega I_{1o} \varepsilon_o \chi_{1i}(n_{1o})}{2\hbar \bar{\mu}_1^2} = g_1 g_1' p_{1o}$$

$$\omega_{2R}^2 \equiv \frac{\Gamma_2^2 \xi_{2i} \Omega I_{2o} \varepsilon_0 \chi_{2i}(n_{2o})}{2\hbar \bar{\mu}_2^2} = g_2 g_2' p_{2o}.$$

For the jth cavity, $\omega_{jR}/2\pi$ is referred to as the relaxation oscillation frequency. In deriving Equation (5.15a), the relations among $\tilde{\delta}_{I_1}(\omega)$, $\tilde{\delta}_{I_2}(\omega)$, $\tilde{\delta}_{\phi_1}(\omega)$, and $\tilde{\delta}_{\phi_2}(\omega)$ given in Equations (5.15b)-(5.15c) were used.

From Equation (5.15a), one obtains solutions for $\tilde{\delta}_{\phi_1}(\omega)$, $\tilde{\delta}_{\phi_2}(\omega)$, $\tilde{\delta}_{I_1}(\omega)$, and $\tilde{\delta}_{I_1}(\omega)$ given by

$$\tilde{\delta}_{\phi_1}(\omega) = \frac{1}{i\omega \mathrm{D}} \times \begin{vmatrix} -\frac{\tilde{\Delta}_{1r}(\omega)}{2\Omega I_{1o}^{1/2}} - \frac{\alpha_1 g_1' \tilde{\eta}_1(\omega)}{2(i\omega+1/\tau_{1R})} & -T_{1r} & \frac{T_{1i}}{4} - \frac{\alpha_1}{2}a(\omega) & -\frac{T_{1i}}{4} \\ \frac{\tilde{\Delta}_{1i}(\omega)}{\Omega I_{1o}^{1/2}} + \frac{g_1' \tilde{\eta}_1(\omega)}{i\omega+1/\tau_{1R}} & T_{1i} & i\omega + T_{1r} + a(\omega) & -T_{1r} \\ -\frac{\tilde{\Delta}_{2r}(\omega)}{2\Omega I_{2o}^{1/2}} - \frac{\alpha_2 g_2' \tilde{\eta}_2(\omega)}{2(i\omega+1/\tau_{2R})} & i\omega + T_{2r} & -\frac{T_{2i}}{4} & \frac{T_{2i}}{4} - \frac{\alpha_2}{2}b(\omega) \\ \frac{\tilde{\Delta}_{2i}(\omega)}{\Omega I_{2o}^{1/2}} + \frac{g_2' \tilde{\eta}_2(\omega)}{i\omega+1/\tau_{2R}} & -T_{2i} & -T_{2r} & i\omega + T_{2r} + b(\omega) \end{vmatrix} \quad (5.16a)$$

$$\tilde{\delta}_{\phi_2}(\omega) = \frac{1}{i\omega \mathrm{D}} \times \begin{vmatrix} i\omega + T_{1r} & -\frac{\tilde{\Delta}_{1r}(\omega)}{2\Omega I_{1o}^{1/2}} - \frac{\alpha_1 g_1' \tilde{\eta}_1(\omega)}{2(i\omega+1/\tau_{1R})} & \frac{T_{1i}}{4} - \frac{\alpha_1}{2}a(\omega) & -\frac{T_{1i}}{4} \\ -T_{1i} & \frac{\tilde{\Delta}_{1i}(\omega)}{\Omega I_{1o}^{1/2}} + \frac{g_1' \tilde{\eta}_1(\omega)}{i\omega+1/\tau_{1R}} & i\omega + T_{1r} + a(\omega) & -T_{1r} \\ -T_{2r} & -\frac{\tilde{\Delta}_{2r}(\omega)}{2\Omega I_{2o}^{1/2}} - \frac{\alpha_2 g_2' \tilde{\eta}_2(\omega)}{2(i\omega+1/\tau_{2R})} & -\frac{T_{2i}}{4} & \frac{T_{2i}}{4} - \frac{\alpha_2}{2}b(\omega) \\ T_{2i} & \frac{\tilde{\Delta}_{2i}(\omega)}{\Omega I_{2o}^{1/2}} + \frac{g_2' \tilde{\eta}_2(\omega)}{i\omega+1/\tau_{2R}} & -T_{2r} & i\omega + T_{2r} + b(\omega) \end{vmatrix} \quad (5.16b)$$

$$\frac{\tilde{\delta}_{I_1}(\omega)}{I_{1o}} = \frac{1}{\mathrm{D}} \begin{vmatrix} 1 & -T_{1r} & -\frac{\tilde{\Delta}_{1r}(\omega)}{2\Omega I_{1o}^{1/2}} - \frac{\alpha_1 g_1' \tilde{\eta}_1(\omega)}{2(i\omega+1/\tau_{1R})} & -\frac{T_{1i}}{4} \\ 0 & T_{1i} & \frac{\tilde{\Delta}_{1i}(\omega)}{\Omega I_{1o}^{1/2}} + \frac{g_1' \tilde{\eta}_1(\omega)}{i\omega+1/\tau_{1R}} & -T_{1r} \\ 1 & i\omega + T_{2r} & -\frac{\tilde{\Delta}_{2r}(\omega)}{2\Omega I_{2o}^{1/2}} - \frac{\alpha_2 g_2' \tilde{\eta}_2(\omega)}{2(i\omega+1/\tau_{2R})} & \frac{T_{2i}}{4} - \frac{\alpha_2}{2}b(\omega) \\ 0 & -T_{2i} & \frac{\tilde{\Delta}_{2i}(\omega)}{\Omega I_{2o}^{1/2}} + \frac{g_2' \tilde{\eta}_2(\omega)}{i\omega+1/\tau_{2R}} & i\omega + T_{2r} + b(\omega) \end{vmatrix} \quad (5.16c)$$

$$\frac{\tilde{\delta}_{I_2}(\omega)}{I_{2o}} = \frac{1}{\mathrm{D}} \begin{vmatrix} 1 & -T_{1r} & \frac{T_{1i}}{4} - \frac{\alpha_1}{2}a(\omega) & -\frac{\tilde{\Delta}_{1r}(\omega)}{2\Omega I_{1o}^{1/2}} - \frac{\alpha_1 g_1' \tilde{\eta}_1(\omega)}{2(i\omega+1/\tau_{1R})} \\ 0 & T_{1i} & i\omega + T_{1r} + a(\omega) & \frac{\tilde{\Delta}_{1i}(\omega)}{\Omega I_{1o}^{1/2}} + \frac{g_1' \tilde{\eta}_1(\omega)}{i\omega+1/\tau_{1R}} \\ 1 & i\omega + T_{2r} & -\frac{T_{2i}}{4} & -\frac{\tilde{\Delta}_{2r}(\omega)}{2\Omega I_{2o}^{1/2}} - \frac{\alpha_2 g_2' \tilde{\eta}_2(\omega)}{2(i\omega+1/\tau_{2R})} \\ 0 & -T_{2i} & -T_{2r} & \frac{\tilde{\Delta}_{2i}(\omega)}{\Omega I_{2o}^{1/2}} + \frac{g_2' \tilde{\eta}_2(\omega)}{i\omega+1/\tau_{2R}} \end{vmatrix}, \quad (5.16d)$$

with

$$D = \begin{vmatrix} T_{1i} & i\omega + T_{1r} + \frac{\omega_{1R}^2}{i\omega+1/\tau_{1R}} & -T_{1r} \\ i\omega + T_{2r} & -\frac{T_{2i}}{4} & \frac{T_{2i}}{4} - \frac{\alpha_2 \omega_{2R}^2}{2(i\omega+1/\tau_{2R})} \\ -T_{2i} & -T_{2r} & i\omega + T_{2r} + \frac{\omega_{2R}^2}{i\omega+1/\tau_{2R}} \end{vmatrix}$$

$$+\begin{vmatrix} -T_{1r} & \frac{T_{1i}}{4} - \frac{\alpha_1 \omega_{1R}^2}{2(i\omega+1/\tau_{1R})} & -\frac{T_{1i}}{4} \\ T_{1i} & i\omega + T_{1r} + \frac{\omega_{1R}^2}{i\omega+1/\tau_{1R}} & -T_{1r} \\ -T_{2i} & -T_{2r} & i\omega + T_{2r} + \frac{\omega_{2R}^2}{i\omega+1/\tau_{2R}} \end{vmatrix}$$

where

$$a(\omega) = \frac{\omega_{1R}^2}{i\omega + 1/\tau_{1R}}, \qquad b(\omega) = \frac{\omega_{2R}^2}{i\omega + 1/\tau_{2R}}.$$

The spectral density for stationary random functions f(t) and g(t) is defined by the Wiener-Khintchine relation as:

$$W_{fg}(\omega) = \int_{-\infty}^{+\infty} ds < f^*(t)g(t+s) > e^{-i\omega s},$$

As shown in Chapter 3, the spectral density function can be expressed in terms of $\tilde{f}(\omega)$ and $\tilde{g}(\omega)$ as

$$W_{fg}(\omega) = \frac{\delta\omega}{2\pi} < \tilde{f}^*(\omega)\tilde{g}(\omega) >, \tag{5.17}$$

where $\delta\omega/2\pi$ is the resolution bandwidth of the instrument used in the ensemble averaging. Accordingly, the relative intensity fluctuation spectrum is given by

$$W_{\Delta I_j}(\omega) = \frac{\delta\omega}{2\pi}\frac{1}{I_{j\circ}^2} < \tilde{\delta}_{I_j}^*(\omega)\tilde{\delta}_{I_j}(\omega) >, \tag{5.18}$$

and the frequency fluctuation spectrum by

$$W_{\Delta\omega}(\omega) = \frac{\delta\omega}{2\pi} < \tilde{\delta}_{\phi_j}^*(\omega)\tilde{\delta}_{\phi_j}(\omega) > . \tag{5.19}$$

Similarly, the correlations (5.13a)-(5.13c) can be rewritten as

$$< \tilde{\Delta}_{ji}^*(\omega)\tilde{\Delta}_{ji}(\omega) > = < \tilde{\Delta}_{jr}^*(\omega)\tilde{\Delta}_{jr}(\omega) > = \frac{2\pi}{\delta\omega} W_{j\circ} \tag{5.20a}$$

$$< \tilde{\eta}_j^*(\omega)\tilde{\eta}_j(\omega) > = \frac{2\pi}{\delta\omega} W_{j2}, \qquad < \tilde{\eta}_j^*(\omega)\tilde{\Delta}_{ji}(\omega) > = \frac{2\pi}{\delta\omega} W_{j1} \tag{5.20b}$$

$$< \tilde{\eta}_j^*(\omega)\tilde{\Delta}_{jr}(\omega) > = 0, \qquad < \tilde{\Delta}_{ji}^*(\omega)\tilde{\Delta}_{jr}(\omega) > = 0. \tag{5.20c}$$

With results given in Equations (5.16a)-(5.16d), (5.17), (5.20a)-(5.20c), (5.18), and (5.19), it is straightforward to obtain $W_{\Delta I}(\omega)$ and $W_{\Delta\omega}(\omega)$. Since the final results are complicated, these two spectra will not be given here.

5.4 Laser Linewidth

In a coherent optical communication system, the frequency or phase noise of the optical source such as a semiconductor laser is very critical to the system's performance. The linewidth is just a macroscopic effect of the phase fluctuation inside the laser. Because of the carrier density dependence of the refractive index and the strong amplitude-phase coupling, the solitary diode laser linewidth is typically on the order of 10 MHz. This excessively large laser linewidth has been explained by the theories of References [8] and [11]. These theories also predict that the linewidth is inversely proportional to output power or the total photon number inside the cavity. However, an unexpected power-independent component first reported by Welford and Mooradian [18] has attracted attention, and different theories have been proposed [18] [19] [20]. Recently, Derry et al. [21] reported the same finding in quantum well AlGaAs/GaAs lasers.

For the two-section lasers, Boyd et al. [9] reported that the linewidth is roughly inversely proportional to power. The linewidth they obtained is typically on the order of 10 MHz. They also observed the power-independent linewidth. However, when compared to solitary lasers, the magnitude of this power-independent component is about two or more times larger. Since no linewidth formula has been reported for two-section lasers, the semiclassical theory of laser noise [8] and the method of Chapter 3 will be applied to derive the linewidth formula. Then, the numerical results of this formula will be compared

to the experimental data of Boyd et al. [9], and the physical mechanism involved will be explained. It will be shown that, to a certain degree, the linewidth formula derived in this section predicts the power-independent component of a two-section laser.

The spectral density function of the laser field $\mathcal{E}(t)$ is

$$W_{EE}(\omega) = \int_{-\infty}^{+\infty} dt' < \mathcal{E}^*(t)\mathcal{E}(t+t') > e^{-i\omega t'},$$

If the correlation between phase and amplitude fluctuations is neglected, the field spectrum is given by

$$W_{E_jE_j}(\omega) = E_{j0}^2 \int_{-\infty}^{+\infty} dt' \exp[-i(\omega-\Omega)t' - \frac{1}{2} < (\delta_{\phi_j}(t+t') - \delta_{\phi_j}(t))^2 >],$$

with

$$< (\delta_{\phi_j}(t+t') - \delta_{\phi_j}(t))^2 >= \frac{\delta\omega}{2\pi}\frac{1}{\pi}\Big| \int_{-\infty}^{+\infty} d\omega < \tilde{\delta}_\phi^*(\omega)\tilde{\delta}_\phi(\omega) > (1 - e^{i\omega t'})\Big|.$$

As pointed out in Chapter 3, when the weak sidemode structure in the field spectrum can be neglected, the Lorentzian laser linewidth $\Delta\nu_j$ for the optical field inside the jth cavity is given by

$$\Delta\nu_j = \frac{1}{2\pi}\Big|\frac{1}{t'}\mathrm{Res}(0)\Big|, \tag{5.21}$$

where Res(0) is the residue of the integrand

$$\frac{\delta\omega}{2\pi} < \tilde{\delta}_{\phi_j}^*(\omega)\tilde{\delta}_{\phi_j}(\omega) > (1 - e^{i\omega t'})$$

at the simple pole $\omega = 0$.

To derive the linewidth formula, one needs to know the asymptotic behavior of function $\tilde{\delta}_\phi(\omega)$ as $\omega \to 0$. From Equation (5.16a), one obtains

$$\lim_{\omega\to 0}\tilde{\delta}_{\phi_1}(\omega) = \frac{1}{i\omega D_0}$$
$$\times \begin{vmatrix} -\frac{\tilde{\Delta}_{1r}(\omega)}{2\Omega I_{1o}^{1/2}} - \frac{\alpha_1 g_1'\tilde{\eta}_1(\omega)}{2(i\omega+1/\tau_{1R})} & -T_{1r} & \frac{T_{1i}}{4} - \frac{\alpha_1}{2}\omega_{1R}^2\tau_{1R} & -\frac{T_{1i}}{4} \\ \frac{\tilde{\Delta}_{1i}(\omega)}{\Omega I_{1o}^{1/2}} + \frac{g_1'\tilde{\eta}_1(\omega)}{i\omega+1/\tau_{1R}} & T_{1i} & +T_{1r}+\omega_{1R}^2\tau_{1R} & -T_{1r} \\ -\frac{\tilde{\Delta}_{2r}(\omega)}{2\Omega I_{2o}^{1/2}} - \frac{\alpha_2 g_2'\tilde{\eta}_2(\omega)}{2(i\omega+1/\tau_{2R})} & +T_{2r} & -\frac{T_{2i}}{4} & \frac{T_{2i}}{4} - \frac{\alpha_2}{2}\omega_{2R}^2\tau_{2R} \\ \frac{\tilde{\Delta}_{2i}(\omega)}{\Omega I_{2o}^{1/2}} + \frac{g_2'\tilde{\eta}_2(\omega)}{i\omega+1/\tau_{2R}} & -T_{2i} & -T_{2r} & T_{2r}+\omega_{2R}^2\tau_{2R} \end{vmatrix} \quad (5.22)$$

with

$$D_0 = \begin{vmatrix} T_{1i} & T_{1r}+\omega_{1R}^2\tau_{1R} & -T_{1r} \\ T_{2r} & -\frac{T_{2i}}{4} & \frac{T_{2i}}{4} - \frac{\alpha_2}{2}\omega_{2R}^2\tau_{2R} \\ -T_{2i} & -T_{2r} & T_{2r}+\omega_{2R}^2\tau_{2R} \end{vmatrix}$$
$$+ \begin{vmatrix} -T_{1r} & \frac{T_{1i}}{4} - \frac{\alpha_1}{2}\omega_{1R}^2\tau_{1R} & -\frac{T_{1i}}{4} \\ T_{1i} & T_{1r}+\omega_{1R}^2\tau_{1R} & -T_{1r} \\ -T_{2i} & -T_{2r} & T_{2r}+\omega_{2R}^2\tau_{2R} \end{vmatrix}.$$

Clearly, Res(0) exists, and the linewidth formula can be obtained after some algebraic manipulations.

To show the usefulness of the results given above, a detailed analysis will be carried out for cleaved-couple-cavity (C^3) lasers, which have drawn considerable attention in the past five years. Using the results of (5.10)-(5.11b), Equation (5.22) is simplified, and one obtains

$$\lim_{\omega\to 0}\Big\{\frac{\delta\omega}{2\pi} < \tilde{\delta}_{\phi_1}^*(\omega)\tilde{\delta}_{\phi_1}(\omega) > (1-e^{i\omega t'})\Big\}$$
$$= -\frac{it'}{\omega}\Big\{(1+\alpha^2)\Big[\Big(\frac{T_{1r}}{T_{1r}+T_{2r}}\Big)^2\frac{W_{2o}}{4\Omega^2 I_{2o}} + \Big(\frac{T_{2r}}{T_{1r}+T_{2r}}\Big)^2\frac{W_{1o}}{4\Omega^2 I_{1o}}\Big]$$
$$+\frac{\alpha^2}{2}\Big[\Big(\frac{T_{1r}}{T_{1r}+T_{2r}}\Big)^2\frac{g_2'^2 W_{22}}{(1/\tau_{2R})^2} + \Big(\frac{T_{2r}}{T_{1r}+T_{2r}}\Big)^2\frac{g_1'^2 W_{12}}{(1/\tau_{1R})^2}\Big]$$
$$+\Big(\frac{\alpha^2}{2}+\alpha\Big)\Big[\Big(\frac{T_{1r}}{T_{1r}+T_{2r}}\Big)^2\frac{g_2' W_{21}}{\Omega I_{2o}^{1/2}(1/\tau_{2R})} + \Big(\frac{T_{2r}}{T_{1r}+T_{2r}}\Big)^2\frac{g_1' W_{11}}{\Omega I_{1o}^{1/2}(1/\tau_{1R})}\Big]\Big\} \quad (5.23)$$

In deriving Equation (5.23), it is assumed that

$$\alpha_1 = \alpha_2 \equiv \alpha,$$

where α_1 and α_2 are defined in Equation (5.8a).

Using the result of Equation (5.23), and according to Equation (5.21), the linewidth $\Delta\mu_1$ is given by

$$\begin{aligned}\Delta\nu_1 = \frac{1}{2\pi}\Big\{&(1+\alpha^2)\Big[\Big(\frac{T_{1r}}{T_{1r}+T_{2r}}\Big)^2\frac{W_{2o}}{4\Omega^2 I_{2o}} + \Big(\frac{T_{2r}}{T_{1r}+T_{2r}}\Big)^2\frac{W_{1o}}{4\Omega^2 I_{1o}}\Big] \\ &+\frac{\alpha^2}{2}\Big[\Big(\frac{T_{1r}}{T_{1r}+T_{2r}}\Big)^2\frac{g_2'^2 W_{22}}{(1/\tau_{2R})^2} + \Big(\frac{T_{2r}}{T_{1r}+T_{2r}}\Big)^2\frac{g_1'^2 W_{12}}{(1/\tau_{1R})^2}\Big] \\ +\Big(\frac{\alpha^2}{2}+\alpha\Big)&\Big[\Big(\frac{T_{1r}}{T_{1r}+T_{2r}}\Big)^2\frac{g_2' W_{21}}{\Omega I_{2o}^{1/2}(1/\tau_{2R})} + \Big(\frac{T_{2r}}{T_{1r}+T_{2r}}\Big)^2\frac{g_1' W_{11}}{\Omega I_{1o}^{1/2}(1/\tau_{1R})}\Big]\Big\}\end{aligned} \quad (5.24)$$

Following the same procedure, one can obtain the linewidth $\Delta\nu_2$ for the optical field in the other cavity. For the first subscripts 1 and 2, the symmetric characteristic of Equation (5.24) indicates that

$$\Delta\nu_1 = \Delta\nu_2.$$

As expected, the optical field of two-section lasers is characterized by one linewidth.

From Equation (5.24), the linewidth has contributions from both cavities with weighting factors $T_{1r}^2/(T_{1r}+T_{2r})^2$ and $T_{2r}^2/(T_{1r}+T_{2r})^2$. The factor $T_{1r}^2/(T_{1r}+T_{2r})^2$ is just a measure of the contribution from Cavity 2. Similarly, the factor $T_{2r}^2/(T_{1r}+T_{2r})^2$ is measuring the contribution from Cavity 1. The T_{1r} and T_{2r} given by Equation (5.11b) are directly linked to the optical coupling coefficients between the two cavities.

In order to understand fully the physical meaning of the terms given in the linewidth formula, a brief revisit to the semiclassical theory of laser noise [8] is

essential. For the jth cavity, W_{j0} is directly proportional to the average rate of events that change the photon number, W_{j2} is directly proportional to the average rate of events that change the carrier number, and W_{j1} is directly proportional to the average rate of events that change photon number and carrier number simultaneously. For the jth solitary diode laser, the linewidth is solely proportional to W_{j0}. On the other hand, the two-section laser linewidth is composed of contributions from all three different average rates. Apparently, this unique feature arises from the optical coupling between the two cavities.

As shown in (5.24), there is no simple relation between the output power (or the photon number) and the linewidth. In order to have a better understanding, numerical evaluation is necessary. Figure 5.4b shows linewidth as a function of the photon number for three different paths of current injections. As shown in Figure 5.4b, Curve (I) is under the condition that one section is biased at $0.1I_{1,th}$, and that another section is injected with a variable current level. Similarly, Curve (II) is obtained when the current path is as shown in Curve (II) of Figure 5.4a. Other parameters used in Figures 5.4a and 5.4b are given as follows: $t_{12}/r_{11} = 2.0$; $\bar{n}_1 l_1 = 0.82$ mm; $\bar{n}_2 l_2 = .18$ mm; $\alpha = -5$; $g_1 = g_2 = 0.5 \times 10^{12} s^{-1}$; $\Gamma_1 = \Gamma_2 = 0.5$; $n_{1o} = n_{2o} = 1 \times 10^{18} cm^{-3}$; $\tau_{1s} = \tau_{2s} = 3 \times 10^{-9} sec$; $g_1' = g_2' = 1 \times 10^{-6} cm^3 s^{-1}$; $V_{1c} = 2.47 \times 10^{-10} cm^3$; $V_{2c} = 0.53 \times 10^{-10} cm^3$; $V_1 = 2V_{1c}$; $V_2 = 2V_{2c}$; and $n_{sp} = 1.8$.

Figure 5.4b shows the general trend that the laser linewidth is roughly inversely proportional to the output power with nonzero intercept. It also shows that the linewidth depends on the current path. With the same output power or photon number, the linewidth obtained from current path (I) is larger than that from current path (II). The calculated linewidth is also typically on the

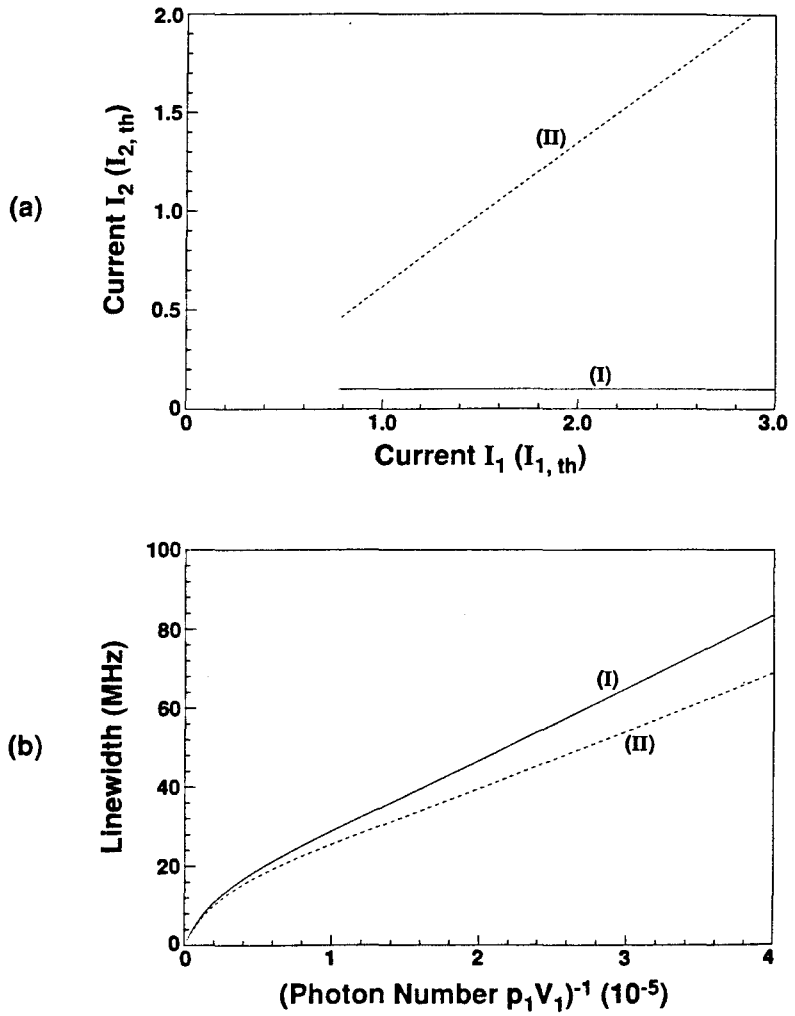

Figure 5.4 (a) Two different current paths used in calculating the linewidth of a two-section laser. (b) Calculated laser linewidth as a function of reciprocal photon number $(p_1V_1)^{-1}$ for two different current paths shown in (a).

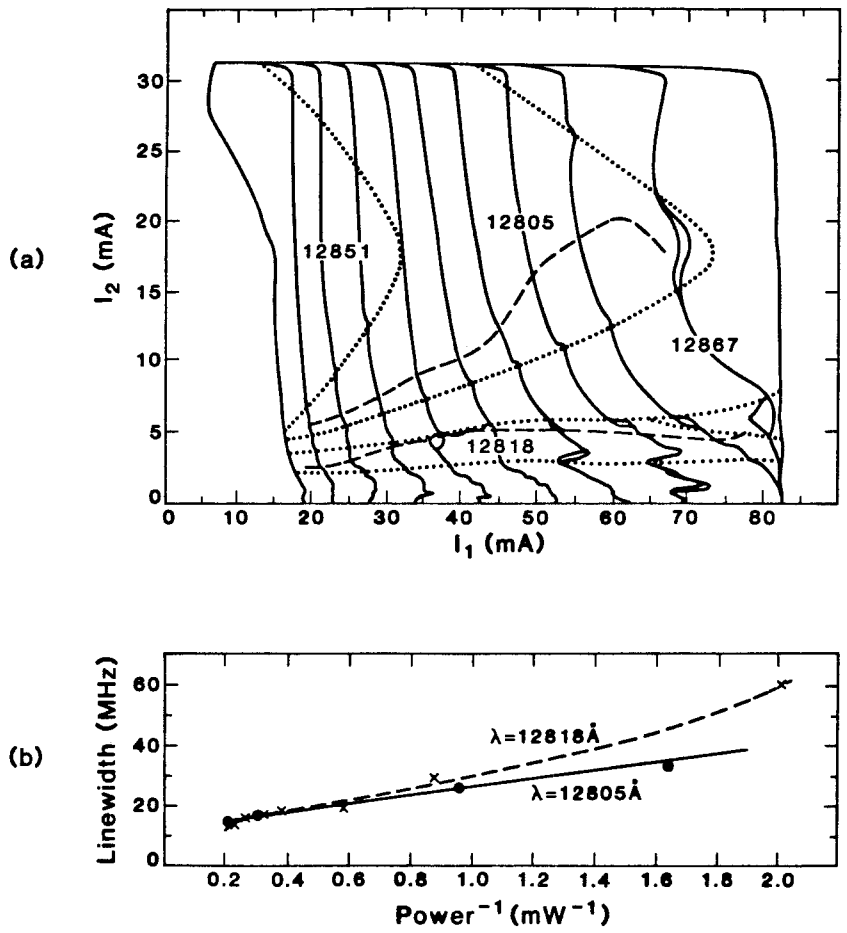

Figure 5.5 (a) Constant-power contours (solid lines) and mode hop boundaries (dotted line) for a C^3 laser. Broken lines indicate the path of minimum linewidth as the power is reduced along an approximate radius. The cavity lengths and threshold are $l_1 = 191\ \mu m$, $l_2 = 41\ \mu m$, $I_1(th) = 16\ mA$ and $I_2(th) = 66\ mA$, respectively [9]. (b) Linewidth against inverse power for two distinct modes as indicated in (a) [9].

order of 10 MHz. Although, in the limit of infinite photon number, the linewidth eventually narrows to zero, the power required would be too high to allow the experimental observations of such behavior. Therefore, in reality, one would like to conclude that there is a power independent component. All the above-mentioned features agree with Boyd et al.'s experimental observations shown in Figure 5.5b.

With regard to the power independent component of the total linewidth of solitary semiconductor lasers, several theories have been proposed [18] [19] [20]. However, in this section, the semiclassical theory of laser noise [8] alone predicts that limited by the finite attainable output power, extrapolating the experimental data of two-section lasers will give the power independent component of the total linewidth. Therefore, in general, the discussion given above and the theories proposed in [18], [19], and [20] suggest that there may be more than one mechnism contributing to the power independent linewidth of two-section lasers.

5.5 Small-Signal Current Modulation Response and Frequency Chirping

Since the refractive index depends on the carrier density, under high speed modulation, the periodic carrier density variation shifts the wavelength of the emitted optical field. This dynamic wavelength shifting is called frequency chirping, which limits the maximum data transmission rate in optical communication systems. Comparing the two-section laser with the conventional diode laser, Agrawal et al. [10] reported that the frequency chirping in a two-section laser is reduced typically by a factor of 2. In this section, the small-signal equations derived in Section 5.2 will be used to derive the small-signal modulation response

and to evaluate the frequency chirping. Cases with both cavities DC-biased and only one cavity modulated with a small sinusoidal current will be considered.

From Equations (5.7a)-(5.7c), the small-signal equations for the deterministic component $I_{11}(t)$, $I_{21}(t)$, $n_{11}(t)$, $n_{21}(t)$, $\phi_1(t)$ and $\phi_2(t)$ caused by the modulation source $J_{11}(t)$ are

$$\dot{\phi}_1(t) + \frac{\alpha_1 g_1'}{2} n_{11}(t) + \frac{1}{2} S_{1i}(t) = 0 \tag{5.26a}$$

$$\dot{\phi}_2(t) + \frac{\alpha_2 g_2'}{2} n_{21}(t) + \frac{1}{2} S_{2i}(t) = 0 \tag{5.26b}$$

$$\dot{I}_{11}(t) - g_1' I_{1o} n_{11}(t) + I_{1o} S_{1r}(t) = 0 \tag{5.26c}$$

$$\dot{I}_{21}(t) - g_2' I_{2o} n_{21}(t) + I_{2o} S_{2r}(t) = 0 \tag{5.26d}$$

$$\dot{n}_{11}(t) = -\frac{\Gamma_1 \varepsilon_o}{2\hbar} \chi_i(n_{1o}) I_{11}(t) - \frac{1}{\tau_{1R}} n_{11}(t) + J_{11}(t) \tag{5.26e}$$

$$\dot{n}_{21}(t) = -\frac{\Gamma_2 \varepsilon_o}{2\hbar} \chi_i(n_{2o}) I_{21}(t) - \frac{1}{\tau_{2R}} n_{21}(t). \tag{5.26f}$$

Let

$$J_{11}(t) = \tilde{J}_{11}(\Omega_m) e^{i\Omega_m t}$$

$$I_{11}(t) = \tilde{I}_{11}(\Omega_m) e^{i\Omega_m t} \qquad I_{21}(t) = \tilde{I}_{21}(\Omega_m) e^{i\Omega_m t}$$

$$n_{11}(t) = \tilde{n}_{11}(\Omega_m) e^{i\Omega_m t} \qquad n_{21}(t) = \tilde{n}_{21}(\Omega_m) e^{i\Omega_m t}$$

$$\phi_1(t) = \tilde{\phi}_1(\Omega_m) e^{i\Omega_m t} \qquad \phi_2(t) = \tilde{\phi}_2(\Omega_m) e^{i\Omega_m t},$$

where Ω_m is the frequency of the modulation current. Taking the Fourier transforms of Equations (5.26a)-(5.26f) yields

$$\begin{pmatrix} i\Omega_m + T_{1r} & -T_{1r} & \frac{T_{1i}}{4} - -\frac{\alpha_1}{2} a(\omega) & -\frac{T_{1i}}{4} \\ -T_{1i} & T_{1i} & i\Omega_m + T_{1r} + a(\omega) & -T_{1r} \\ -T_{2r} & i\Omega_m + T_{2r} & -\frac{T_{2i}}{4} & \frac{T_{2i}}{4} - \frac{\alpha_2}{2} b(\omega) \\ T_{2i} & -T_{2i} & -T_{2r} & i\Omega_m + T_{2r} + b(\omega) \end{pmatrix}$$

$$\times \begin{pmatrix} \tilde{\phi}_1(\Omega_m) \\ \tilde{\phi}_2(\Omega_m) \\ \tilde{I}_{11}(\Omega_m)/I_{1o} \\ \tilde{I}_{21}(\Omega_m)/I_{2o} \end{pmatrix} = \begin{pmatrix} -\frac{\alpha_1 g_1' \tilde{J}_{11}(\Omega_m)}{2(i\Omega_m + 1/\tau_{1R})} \\ \frac{g_1' \tilde{J}_{11}(\Omega_m)}{i\Omega_m + 1/\tau_{1R}} \\ 0 \\ 0 \end{pmatrix} \tag{5.27a}$$

$$\tilde{n}_{11}(\Omega_m) = \frac{-1}{i\Omega_m + 1/\tau_{1R}} \Big[\frac{\Gamma_1 \varepsilon_o}{2\hbar} \chi_{1i}(n_{1o}) \tilde{I}_{11}(\Omega_m) + \tilde{J}_{11}(\Omega_m) \Big] \tag{5.27b}$$

$$\tilde{n}_{21}(\Omega_m) = \frac{-1}{i\Omega_m + 1/\tau_{2R}} \Big(\frac{\Gamma_2 \varepsilon_o}{2\hbar} \Big) \chi_{2i}(n_{2o}) \tilde{I}_{21}(\Omega_m). \tag{5.27c}$$

From Equation (5.27a), the solutions for the frequency components $\tilde{\phi}_1(\Omega_m)$, $\tilde{\phi}_2(\Omega_m)$, $\tilde{I}_{11}(\Omega_m)$, and $\tilde{I}_{21}(\Omega_m)$ are

$$\tilde{\phi}_1(\Omega_m) = \frac{1}{i\Omega_m \mathrm{D_m}} \times \begin{vmatrix} -\frac{\alpha_1 g_1' \tilde{J}_{11}(\Omega_m)}{2(i\Omega_m + 1/\tau_{1R})} & -T_{1r} & \frac{T_{1i}}{4} - \frac{\alpha_1}{2} a(\omega) & -\frac{T_{1i}}{4} \\ \frac{g_1' \tilde{J}_{11}(\Omega_m)}{i\Omega_m + 1/\tau_{1R}} & T_{1i} & i\Omega_m + T_{1r} + a(\omega) & -T_{1r} \\ 0 & i\Omega_m + T_{2r} & -\frac{T_{2i}}{4} & \frac{T_{2i}}{4} - \frac{\alpha_2}{2} b(\omega) \\ 0 & -T_{2i} & -T_{2r} & i\Omega_m + T_{2r} + b(\omega) \end{vmatrix} \tag{5.28a}$$

$$\tilde{\phi}_2(\Omega_m) = \frac{1}{i\Omega_m \mathrm{D_m}} \times \begin{vmatrix} i\Omega_m + T_{1r} & -\frac{\alpha_1 g_1' \tilde{J}_{11}(\Omega_m)}{2(i\Omega_m + 1/\tau_{1R})} & \frac{T_{1i}}{4} - \frac{\alpha_1}{2} a(\omega) & -\frac{T_{1i}}{4} \\ -T_{1i} & \frac{g_1' \tilde{J}_{11}(\Omega_m)}{i\Omega_m + 1/\tau_{1R}} & i\Omega_m + T_{1r} + a(\omega) & -T_{1r} \\ -T_{2r} & 0 & -\frac{T_{2i}}{4} & \frac{T_{2i}}{4} - \frac{\alpha_2}{2} b(\omega) \\ T_{2i} & 0 & -T_{2r} & i\Omega_m + T_{2r} + b(\omega) \end{vmatrix} \tag{5.28b}$$

$$\tilde{I}_{11}(\Omega_m) = \frac{I_{1o}}{\mathrm{D_m}} \begin{vmatrix} 1 & -T_{1r} & -\frac{\alpha_1 g_1' \tilde{J}_{11}(\Omega_m)}{2(i\Omega_m + 1/\tau_{1R})} & -\frac{T_{1i}}{4} \\ 0 & T_{1i} & \frac{g_1' \tilde{J}_{11}(\Omega_m)}{i\Omega_m + 1/\tau_{1R}} & -T_{1r} \\ 1 & i\Omega_m + T_{2r} & 0 & \frac{T_{2i}}{4} - \frac{\alpha_2}{2} b(\omega) \\ 0 & -T_{2i} & 0 & i\Omega_m + T_{2r} + b(\omega) \end{vmatrix} \tag{5.28c}$$

$$\tilde{I}_{21}(\Omega_m) = \frac{I_{2o}}{\mathrm{D_m}} \begin{vmatrix} 1 & -T_{1r} & \frac{T_{1i}}{4} - \frac{\alpha_1}{2} a(\omega) & -\frac{\alpha_1 g_1' \tilde{J}_{11}(\Omega_m)}{2(i\Omega_m + 1/\tau_{1R})} \\ 0 & T_{1i} & i\Omega_m + T_{1r} + a(\omega) & \frac{g_1' \tilde{J}_{11}(\Omega_m)}{i\Omega_m + 1/\tau_{1R}} \\ 1 & i\Omega_m + T_{2r} & -\frac{T_{2i}}{4} & 0 \\ 0 & -T_{2i} & -T_{2r} & 0 \end{vmatrix} \tag{5.28d}$$

with

$$D_m = \begin{vmatrix} T_{1i} & i\Omega_m + T_{1r} + \frac{\omega_{1R}^2}{i\Omega_m + 1/\tau_{1R}} & -T_{1r} \\ i\Omega_m + T_{2r} & -\frac{T_{2i}}{4} & \frac{T_{2i}}{4} - \frac{\alpha_2 \omega_{2R}^2}{2(i\Omega_m + 1/\tau_{2R})} \\ -T_{2i} & -T_{2r} & i\Omega_m + T_{2r} + \frac{\omega_{2R}^2}{i\Omega_m + 1/\tau_{2R}} \end{vmatrix}$$

$$+ \begin{vmatrix} -T_{1r} & \frac{T_{1i}}{4} - \frac{\alpha_1 \omega_{1R}^2}{2(i\Omega_m + 1/\tau_{1R})} & -\frac{T_{1i}}{4} \\ T_{1i} & i\Omega_m + T_{1r} + \frac{\omega_{1R}^2}{i\Omega_m + 1/\tau_{1R}} & -T_{1r} \\ -T_{2i} & -T_{2r} & i\Omega_m + T_{2r} + \frac{\omega_{2R}^2}{i\Omega_m + 1/\tau_{2R}} \end{vmatrix}. \qquad (5.28e)$$

Next, to simplify the situation, lasers used in the paper by Agrawal et al. [10] will be considered. Thus, after substituting Equations (5.10)-(5.11b) and (5.28e) into Equations (5.28a)-(5.28d), one obtains

$$\tilde{\phi}_1(\Omega_m) = \frac{-\frac{\alpha}{2}\left(i\Omega_m + T_{2r} + \frac{\omega_{2R}^2}{i\Omega_m + 1/\tau_{2R}}\right)\frac{g_1' \tilde{J}_{11}(\Omega_m)}{i\Omega_m + 1/\tau_{1R}}}{\left[\left(i\Omega_m + T_{1r} + \frac{\omega_{1R}^2}{i\Omega_m + 1/\tau_{1R}}\right)\left(i\Omega_m + T_{2r} + \frac{\omega_{2R}^2}{i\Omega_m + 1/\tau_{2R}}\right) - T_{1r}T_{2r}\right]} \qquad (5.29a)$$

$$\tilde{\phi}_2(\Omega_m) = \frac{-\left(\frac{\alpha}{2}\right)T_{2r}\frac{g_1' \tilde{J}_{11}(\Omega_m)}{i\Omega_m + 1/\tau_{1R}}}{\left[\left(i\Omega_m + T_{1r} + \frac{\omega_{1R}^2}{i\Omega_m + 1/\tau_{1R}}\right)\left(i\Omega_m + T_{2r} + \frac{\omega_{2R}^2}{i\Omega_m + 1/\tau_{2R}}\right) - T_{1r}T_{2r}\right]} \qquad (5.29b)$$

$$\frac{\tilde{I}_{11}(\Omega_m)}{I_{1o}} = \frac{\left(i\Omega_m + T_{2r} + \frac{\omega_{2R}^2}{i\Omega_m + 1/\tau_{2R}}\right)\frac{g_1' \tilde{J}_{11}(\Omega_m)}{i\Omega_m + 1/\tau_{1R}}}{\left[\left(i\Omega_m + T_{1r} + \frac{\omega_{1R}^2}{i\Omega_m + 1/\tau_{1R}}\right)\left(i\Omega_m + T_{2r} + \frac{\omega_{2R}^2}{i\Omega_m + 1/\tau_{2R}}\right) - T_{1r}T_{2r}\right]} \qquad (5.29c)$$

$$\frac{\tilde{I}_{21}(\Omega_m)}{I_{2o}} = \frac{T_{2r}\frac{g_1' \tilde{J}_{11}(\Omega_m)}{i\Omega_m + 1/\tau_{1R}}}{\left[\left(i\Omega_m + T_{1r} + \frac{\omega_{1R}^2}{i\Omega_m + 1/\tau_{1R}}\right)\left(i\Omega_m + T_{2r} + \frac{\omega_{2R}^2}{i\Omega_m + 1/\tau_{2R}}\right) - T_{1r}T_{2r}\right]}. \qquad (5.29d)$$

As shown in Equations (5.29a)-(5.29d), the modulation response for each cavity is slightly different. Because each cavity has its own current source and the two cavities are coupled only optically, this is expected. Similarly, for a solitary diode laser under the same current modulation, one has

$$\tilde{\phi}_{sl}(\Omega_m) = -\frac{\alpha_{sl}}{2}\frac{\frac{g_{sl}' \tilde{J}_{11}(\Omega_m)}{i\Omega_m + 1/\tau_{sl,R}}}{i\Omega_m + \frac{\omega_{sl,R}^2}{i\Omega_m + 1/\tau_{sl,R}}}.$$

In order to study the experimental results, a new quantity will be defined here. This is the frequency chirping ratio, which is given by

$$\text{Chirping Ratio} = \frac{\Delta\Omega}{(\Delta\Omega)_{sl}} = \left|\frac{\phi_{11}(\Omega_m)}{\phi_{sl}(\Omega_m)}\right|, \tag{5.30}$$

where $\Delta\Omega$ and $(\Delta\Omega)_{sl}$ are the frequency chirpings for a two-section semiconductor laser and a solitary semiconductor laser, respectively. Considering cases with

$$\alpha_{sl} = \alpha, \qquad g'_{sl} = g'_1, \qquad \tau_{sl,R} = \tau_{1R}, \qquad \omega_{1R}^2 = \omega_{sl,R}^2,$$

the chirping ratio defined by (5.30) becomes

$$\text{Chirping Ratio} = \left|\frac{\left(i\Omega_m + T_{2r} + \frac{\omega_{2R}^2}{i\Omega_m + 1/\tau_{2R}}\right)\left(i\Omega_m + \frac{\omega_{1R}^2}{i\Omega_m + 1/\tau_{1R}}\right)}{\left[\left(i\Omega_m + T_{1r} + \frac{\omega_{1R}^2}{i\Omega_m + 1/\tau_{1R}}\right)\left(i\Omega_m + T_{2r} + \frac{\omega_{2R}^2}{i\Omega_m + 1/\tau_{2R}}\right) - T_{1r}T_{2r}\right]}\right|.$$

Figure 5.6a shows the calculated results for the wavelength chirping as a function of the ac current level. Since the calculated results are valid only in the small-signal regime, the large ac current range shown in Figure 5.6a is solely for the purpose of comparing this figure with the reported results shown in Figure 5.6b. The calculated wavelength chirpings are in good agreement with the experimental results.

In addition, numerical results of the chirping ratio are shown in Figures 5.7 and 5.8 as a function of the coupling strength t_{21}/r_{11}. When there is no coupling, the modulated cavity becomes a solitary laser and the chirping ratio is 1. As the coupling strength increases, the chirping ratio decreases and eventually becomes a constant. The chirping ratio at 1 MHz is larger than the chirping ratio at 1 GHz. For coupling strength $t_{21}/r_{11} > 0.4$, the chirping ratio shown in Figure

(a)

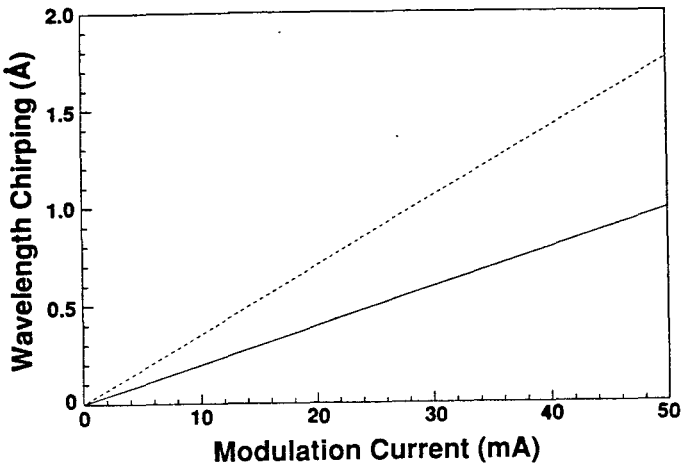

(b)

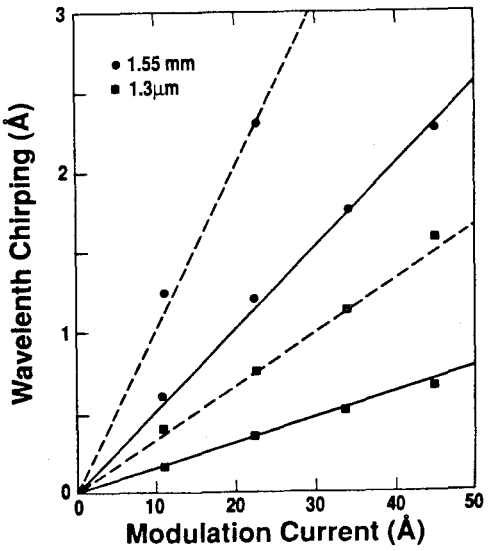

Figure 5.6 (a) Calculated wavelength chirpings as a function of the modulation current at 100 MHz for 1.3 μm lasers. Inside each cavity of the two-section laser, the photon densities are $p_{1o} = p_{2o} = 1 \times 10^{14} cm^{-3}$. The cavity lengths are given by $\bar{n}_1 l_1 = \bar{n}_2 l_2 = 0.5\ mm$. (b) Measured wavelength chirpings vs modulation current at 100 MHz for 1.3 and 1.55 μm lasers [10]. For both (a) and (b), dashed and full lines correspond to a conventional and a cleaved-coupled-cavity laser, respectively.

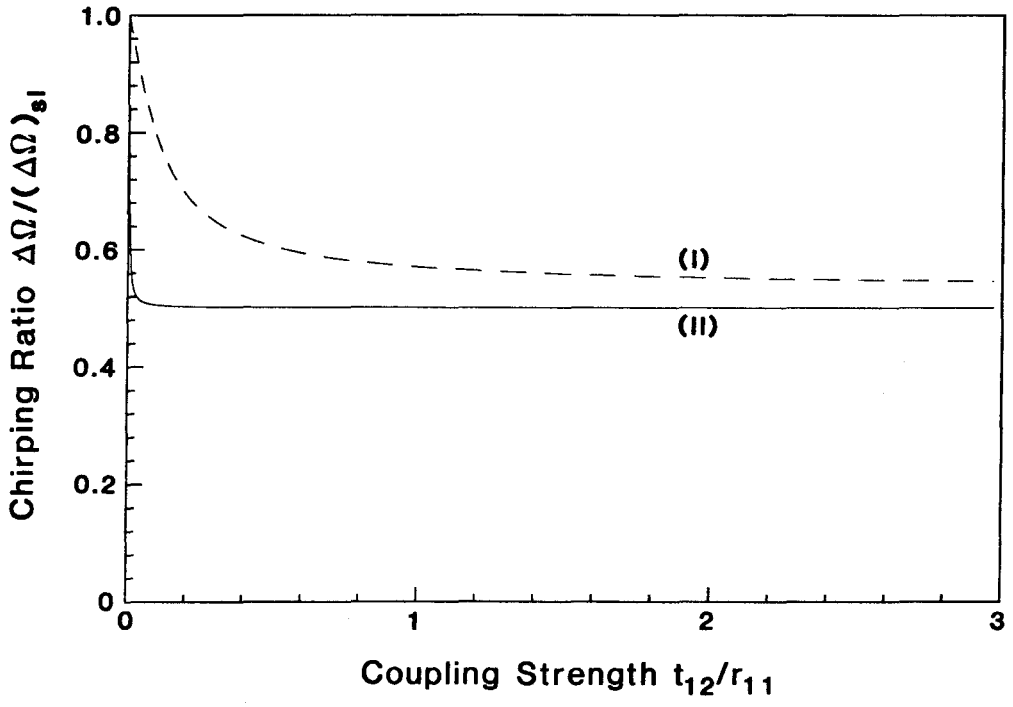

Figure 5.7 Calculated chirping ratio $\Delta\Omega/(\Delta\Omega)_{sl}$ as a function of the coupling strength t_{21}/r_{11}. $\Delta\Omega$ and $(\Delta\Omega)_{sl}$ are the frequency chirpings for a two-section semiconductor laser and a solitary semiconductor laser, respectively. Inside each cavity of the two-section laser, the photon densities are $p_{1o} = p_{2o} = 1 \times 10^{14} cm^{-3}$. The cavity lengths are given by $\bar{n}_1 l_1 = \bar{n}_2 l_2 = 0.5\ mm$. The modulating frequencies are (I) 100 MHz and (II) 1 GHz.

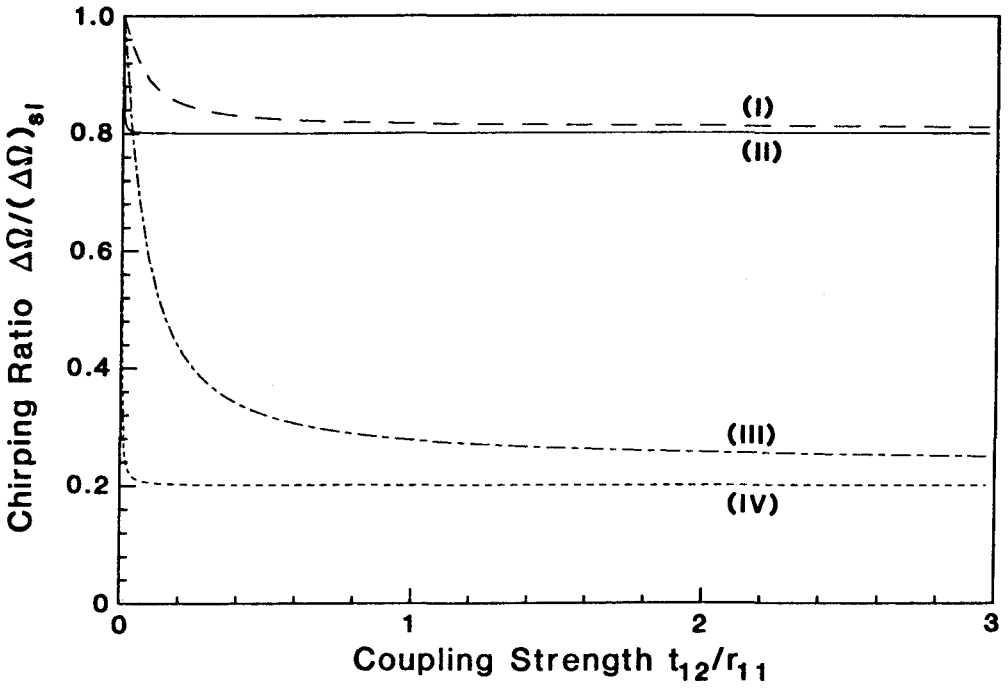

Figure 5.8 Calculated chirping ratio $\Delta\Omega/(\Delta\Omega)_{sl}$ as a function of the coupling strength t_{21}/r_{11} with $p_{1o} = p_{2o} = 1 \times 10^{14} cm^{-3}$. Other parameters are (I) $\bar{n}_1 l_1 = 0.8$ mm, $\bar{n}_2 l_2 = 0.2$ mm, $\Omega_m = 100$ MHz; (II) $\bar{n}_1 l_1 = 0.8$ mm, $\bar{n}_2 l_2 = 0.2$ mm, $\Omega_m = 1$ GHz; (III) $\bar{n}_1 l_1 = 0.2$ mm, $\bar{n}_2 l_2 = 0.8$ mm, $\Omega_m = 100$ MHz; and (IV) $\bar{n}_1 l_1 = 0.2$ mm, $\bar{n}_2 l_2 = 0.8$ mm, $\Omega_m = 1$ GHz.

5.7 is on the order of 0.5. This agrees with Agrawal et al.'s experimental results shown in Figure 5.6b.

Figure 5.8 shows the chirping ratio for different cavity lengths. With the same photon density in each cavity, modulating the longer cavity gives a larger chirping ratio, and vice versa. Since the current is modulated in only one cavity, the other cavity acts as a buffer to resist the carrier density variation induced by the incoming modulated optical field. The unmodulated cavity will also emit an unmodulated optical field to the other cavity to smooth out the carrier density variation induced by the direct current modulation. Therefore, the larger the photon number in the unmodulated cavity with respect to the photon number in the modulated cavity, the lower the frequency chirping, and vice versa.

5.6 Conclusion

Using the optical field equations derived in Chapter 2, the dynamics, noise spectra, and laser linewidth of an axially coupled two-section semiconductor laser have been studied. The small-signal equations for the optical fields and carrier densities were first derived. The semiclassical noise theory was employed in deriving the frequency and relative intensity fluctuation spectra. Although the complicated final results were not given, the spectra can be obtained with difficulty from the intermediate results given in this chapter.

An analytical expression for the laser linewidth has been derived. The contribution from each cavity to the linewidth is characterized by the weighting factors $T_{1r}^2/(T_{1r}+T_{2r})^2$ and $T_{2r}^2/(T_{1r}+T_{2r})^2$. The solitary laser linewidth is due solely to the random events that change photon number. However, the two-section laser linewidth is caused by three different kinds of random events. The

three different kinds of random events are events that change photon number, events that change carrier number, and events that change the photon number and carrier number simultaneously.

The linewidth is dependent on the path of the current injection, and the general trend is that the linewidth is inversely proportional to the output power. Although the theory does not predict the power independent component, the calculations show that because of the finite output power, extrapolating the experimental data leads to a power independent component. The theoretical results agree quantitatively with the experimental results of Boyd et al. [9].

In Section 5.5, the small-signal current modulation response and the frequency chirping have been studied. The experimental results of Agrawal et al. [10] have been explained. Generally speaking, when the laser is directly modulated in only one cavity, the larger the photon number in the unmodulated cavity, the smaller the frequency chirping, and vice versa. Similarly, the larger the photon number in the modulated cavity, the larger the frequency chirping, and vice versa. Finally, the usefulness of the general theory established in Chapter 2 is demonstrated.

References

[1] For a review, see W. T. Tsang, *Semiconductors and Semimetals* **Vol.22**, Part B, Academic Press, 1985, pp. 257-373.

[2] W. T. Tsang, N. A. Olsson, R. A. Linke and R. A. Logan, *Electron. Lett.*, **19**, 415, 1983.

[3] R. J. Lang and A. Yariv, *IEEE J. Quantum Electron.*, **QE-22**, 631, 1986.

[4] C. H. Henry and R. F. Kazarinov, *IEEE J. Quantum Electron.*, **QE-20**, 733, 1984.

[5] T. L. Koch and L. A. Coldren, *J. Appl. Phys.* **57**, 740, 1985.

[6] L. A. Codren and T. L. Koch, *IEEE J. Quantum Electron.*, **QE-20**, 659, 1984.

[7] L. A. Codren and T. L. Koch, *IEEE J. Quantum Electron.*, **QE-20**, 671, 1984.

[8] K. Vahala and A. Yariv, *IEEE J. Quantum Electron.*, **QE-19**, 1102, 1983.

[9] G. D. Boyd, C. E. Soccolich, J. E. Bowers, T. L. Koch, C. A. Burrus, and R. M. Jopson, *Electron. Lett.*, **21**, 1129, 1985.

[10] G. P. Agrawal, N. A. Olsson, and N. K. Dutta, *Appl. Phys. Lett.* **45**, 119, 1984.

[11] C. H. Henry, *IEEE J. Quantum Electron.*, **QE-18**, 259, 1982.

[12] C. Harder, K. Vahala, and A. Yariv, *Appl. Phys. Lett.*, **42**, 328, 1983.

[13] K. Vahala, L. C. Chiu, S. Margalit, and A. Yariv, *Appl. Phys. Lett.*, **42**, 631, 1983.

[14] C. Harder, J. Katz, S. Margalit, J. Shacham, and A. Yariv, *IEEE J. Quan-*

tum Electron., **QE-18**, 333, 1982.

[15] C. H. Henry, R. A. Logan, and F. R. Merritt, *J. Appl. Phys.*, **51**, 3042, 1980.

[16] D. Welford and A. Mooradian, *Appl. Phys. Lett.*, **40**, 865, 1982.

[17] C. H. Henry, R. A. Logan, H. Temkin, and F. R. Merritt, *IEEE J. Quantum Electron.*, **19**, 941, 1983.

[18] D. Welford and A. Mooradian, *Appl. Phys. Lett.*, **40**, 560, 1982.

[19] R. J. Lang, K. J. Vahala, and A. Yariv, *IEEE J. Quantum Electron.*, **21**, 443, 1985.

[20] K. Vahala and A. Yariv, *Appl. Phys. Lett.*, **43**, 140, 1983.

[21] P. L. Derry, T. R. Chen, Y. H. Zhuang, J. Paslaski, M. Mittelstein, K. Vahala, and A. Yariv, "Spectral and dynamic characteristics of buried heterostructure single quantum well (Al, Ga)As lasers," to be published.